

Power Quality Impact of Photovoltaic Systems on Residential Distribution  
Networks

by

Qingxin Shi

A thesis submitted in partial fulfillment of the requirements for the degree of

Master of Science

in

Energy Systems

Department of Electrical and Computer Engineering  
University of Alberta

© Qingxin Shi, 2014

# Abstract

The rapid proliferation of distributed photovoltaic (PV) panels results in some power quality concerns of residential distributed networks. Therefore a thorough study is highly needed on evaluating the severity of such concerns, which includes the harmonic distortion and the voltage rise.

In order to study the power quality impact, the fundamental and harmonic models are proposed to represent the detailed power electronics circuit of the PV inverter. The model is verified by a simulation study and a lab experiment. Based on the model, the thesis investigates how serious the harmonic impacts become when multiple PV inverters are integrated to the residential distribution network. In particular, the harmonic resonance concern caused by the PV inverter filter is analyzed.

In addition, a Monte Carlo simulation platform has been developed for studying the low voltage networks. The platform incorporates the behavior and electrical models of the PV inverter and residential loads. It can support several power-quality-related studies in regard to residential distribution networks.

# Acknowledgement

First and foremost, I would like to express my most sincere gratitude to my supervisor, Dr. Wilsun Xu for his tireless guidance and supervision during my M.Sc. program. In the thousands of hours he devoted to my research, he showed me how to think like a researcher and how to organize the study in a logical and clear manner, which will significantly benefit my future careers. It has been my great honor to be a student under his supervision.

I'd like to show my special appreciation to Dr. Jing Yong. Her patient guidance and insightful suggestions have contributed greatly to this thesis, especially to Chapter 2 and 3.

I would like to thank all my colleagues for their friendship, and it was a great pleasure to work with them. I should express my special appreciation to Haitao Hu, Ricardo Torquato, Ming Dong, Pengfei Gao, Jinwei He, Tyrone Ding, Ramiar Alaei and Hesam Yazdanpanahi, for their selfless help during various stages of this project.

Finally, I would also like to express my gratitude to the love and support from my parents, Mr. Yunxing Shi and Mrs. Yuzhi Liang. I dedicate this thesis to them all.

# Contents

|                  |  |           |
|------------------|--|-----------|
| <b>Chapter 1</b> | <b>Introduction.....</b>   | <b>1</b>  |
| 1.1              | Overview.....  | 1         |
| 1.2              | Harmonic Impact of PV Inverters.....                                 | 3         |
| 1.2.1            | <i>Significance of the Harmonic Issue of PV Inverters.....</i>       | <i>3</i>  |
| 1.2.2            | <i>Traditional Harmonic Modeling Method of PV Inverters.....</i>     | <i>5</i>  |
| 1.2.3            | <i>Harmonic Impact of PV Inverters on Distribution Networks.....</i> | <i>7</i>  |
| 1.3              | Thesis Scope and Outline.....  | 10        |
| <b>Chapter 2</b> | <b>Harmonic Characteristics and Models of PV Inverters.....</b>      | <b>13</b> |
| 2.1              | Description of the PV System.....                                    | 13        |
| 2.1.1            | <i>Configuration and Electric Feature of PV Arrays.....</i>          | <i>13</i> |
| 2.1.2            | <i>Configuration and Function of Grid-tied PV Inverters.....</i>     | <i>17</i> |
| 2.2              | Modeling of PV Inverters at the Fundamental Frequency.....           | 23        |
| 2.2.1            | <i>Fundamental Frequency Model of PV.....</i>                        | <i>23</i> |
| 2.2.2            | <i>Verification of the Fundamental Frequency Model.....</i>          | <i>25</i> |
| 2.3              | Modeling of PV Inverters at the Harmonic Frequency.....              | 29        |
| 2.3.1            | <i>The Switching Function of the Single-Phase PWM Inverter.....</i>  | <i>30</i> |
| 2.3.2            | <i>The Characteristic of the DC-link Voltage.....</i>                | <i>34</i> |
| 2.3.3            | <i>Harmonic Model of PV.....</i>                                     | <i>37</i> |
| 2.3.4            | <i>Discussion on the Harmonic Model.....</i>                         | <i>39</i> |
| 2.4              | Verification Study on the PV Inverter Model - Simulation.....        | 41        |
| 2.4.1            | <i>Simulation System.....</i>  | <i>41</i> |
| 2.4.2            | <i>Simulation Results and Analysis.....</i>                          | <i>43</i> |
| 2.5              | Verification Study on the PV Inverter Model – Lab Experiment.....    | 45        |
| 2.5.1            | <i>Description of the Experimental PV Inverter.....</i>              | <i>45</i> |
| 2.5.2            | <i>Experiment Principle and Procedure.....</i>                       | <i>46</i> |
| 2.5.3            | <i>Experiment Implementation.....</i>                                | <i>48</i> |
| 2.5.4            | <i>Experiment Result and Analysis.....</i>                           | <i>50</i> |
| 2.6              | Characteristics of the PV Harmonic Model.....                        | 52        |

|                  |  |           |
|------------------|--|-----------|
| 2.6.1            | <i>Harmonic Source Characteristics</i> .....   | 53        |
| 2.6.2            | <i>Harmonic Impedance Characteristics</i> .....  | 55        |
| 2.7              | Summary.....   | 56        |
| <b>Chapter 3</b> | <b>Harmonic Impact of PV Inverters on Secondary Distribution Systems</b> .....               | <b>58</b> |
| 3.1              | Description of Secondary Distribution System Model .....                                     | 58        |
| 3.2              | Harmonic Impact of PVs on the System – Simulation Study.....                                 | 61        |
| 3.2.1            | <i>Simulation Study Method</i> .....   | 61        |
| 3.2.2            | <i>Simulation Results and Analysis</i> .....   | 63        |
| 3.3              | Harmonic Impact of PVs on the System – Analytical Study.....                                 | 67        |
| 3.3.1            | <i>Simplification of the Secondary System</i> .....  | 67        |
| 3.3.2            | <i>Harmonic Resonance Analysis</i> .....   | 71        |
| 3.3.3            | <i>Sensitivity Study on the Harmonic Resonance</i> .....                                     | 73        |
| 3.4              | Summary.....   | 78        |
| <b>Chapter 4</b> | <b>A Monte Carlo Simulation Platform for Studying Low Voltage Residential Networks</b> ..... | <b>80</b> |
| 4.1              | The Proposed Simulation Platform.....  | 82        |
| 4.1.1            | <i>General Requirements on the Simulation Platform</i> .....                                 | 83        |
| 4.1.2            | <i>Electric Model</i> .....  | 84        |
| 4.1.3            | <i>Behavior Model</i> .....  | 86        |
| 4.1.4            | <i>Sequential Monte Carlo Simulation</i> .....   | 86        |
| 4.2              | Load Behavior Modeling Technique .....   | 87        |
| 4.2.1            | <i>Home Appliance Time-of-use Probabilistic Behavior</i> .....                               | 87        |
| 4.2.2            | <i>Electric Vehicle Charging Behavior</i> .....  | 89        |
| 4.2.3            | <i>Solar Irradiance Level Behavior</i> .....   | 90        |
| 4.2.4            | <i>Deterministic device behavior</i> .....   | 93        |
| 4.3              | Residential Network Modeling Technique .....   | 94        |
| 4.3.1            | <i>Fundamental Power Flow Calculation</i> .....  | 94        |
| 4.3.2            | <i>Harmonic power flow Calculation</i> .....   | 100       |
| 4.3.3            | <i>Electromechanical Transients Simulation of Motor Starting</i> .....                       | 102       |

|                  |   |            |
|------------------|---|------------|
| 4.3.4            | <i>Simulation of Home Appliances Dynamic Behavior</i> .....                                     | 106        |
| 4.4              | Summary of Simulation Platform .....  | 111        |
| 4.4.1            | <i>Structure of the Simulation Platform</i> .....   | 111        |
| 4.4.2            | <i>Examples of the Simulation Result</i> .....  | 113        |
| 4.5              | Case Studies .....  | 115        |
| 4.5.1            | <i>Power Quality Impact of PV Inverter Integration</i> .....                                    | 116        |
| 4.5.2            | <i>Neutral-to-earth Voltage Incidence</i> .....   | 117        |
| 4.5.3            | <i>Residential load Identification</i> .....  | 118        |
| 4.5.4            | <i>Demand Response Analysis</i> .....   | 120        |
| 4.6              | Summary .....   | 122        |
| <b>Chapter 5</b> | <b>Conclusions and Future Works</b> .....   | <b>123</b> |
| 5.1              | Thesis Conclusions and Contributions.....   | 123        |
| 5.2              | Suggestion for Future Works .....   | 124        |
|                  | <b>References</b> .....   | <b>126</b> |
|                  | <b>Appendix A PV Inverter Filter Parameters</b> .....   | <b>131</b> |
|                  | <b>Appendix B Modeling of Multiphase Network Components</b> .....                               | <b>132</b> |
| B.1              | Modeling of the Multiphase Coupled Line .....   | 132        |
| B.2              | Modeling of Single-Phase Three-Winding Transformers .....                                       | 135        |
|                  | <b>Appendix C Single-phase Induction Motor Parameters</b> .....                                 | <b>137</b> |
|                  | <b>Appendix D Input Data Summary of Monte Carlo Simulation Platform ...</b>                     | <b>139</b> |
|                  | <b>Appendix E Cloud Transient Impact on Distribution Systems with High PV Penetration</b> ..... | <b>145</b> |
| E.1              | Characteristics of Solar Irradiance Variability – Temporal Distribution .                       | 146        |
| E.2              | Characteristics of Solar Irradiance Variability – Spatial Distribution.....                     | 153        |
|                  | <b>Appendix F Method of Detecting the Cloud Transient Event</b> .....                           | <b>157</b> |

# List of Tables

|  |     |
|--|-----|
| Table 2.1 Comparisons of different types of PV module .....                          | 15  |
| Table 2.2 PV module temperature coefficient .....                                    | 17  |
| Table 2.3 An example of PV inverter technical data .....                             | 21  |
| Table 2.4 Summary of the major standard dealing with integrations of PV system ..... | 22  |
| Table 2.5 Parameter of the PV system.....  | 42  |
| Table 2.6 Typical grid harmonic voltage spectrum .....                               | 42  |
| Table 2.7 Electrical specification of GT3.0-NA-DS-240 .....                          | 46  |
| Table 2.8 Parameter and function of the experiment instruments .....                 | 49  |
| Table 2.9 Parameter of the PV inverter .....   | 53  |
| Table 2.10 Comparing harmonic impact of the PV inverter and home appliances .....    | 55  |
| Table 3.1 Secondary distribution system parameters .....                             | 60  |
| Table 3.2 PV inverter parameters .....   | 61  |
| Table 3.3 Description of daily time period for simulation.....                       | 62  |
| Table 3.4 Residential load specifications.....                                       | 73  |
| Table 4.1 Cloud Coverage Level Probability for Different Day-types.....              | 91  |
| Table 4.2 Network branch information.....  | 96  |
| Table 4.3 List of power trend signatures .....                                       | 107 |
| Table 4.4 Example of LCD TV as a falling spike model.....                            | 108 |
| Table 4.5 Example of stove as a pulses model .....                                   | 109 |
| Table 4.6 Example of furnace as a multi-level, multi-stage model .....               | 109 |
| Table 4.7 Example of freezer as a fluctuation model .....                            | 110 |
| Table 4.8 Input / built-in parameters.....   | 115 |
| Table 4.9 Home appliance parameters.....   | 115 |
| Table 4.10 95%-index of NEV for Different Neutral Conditions .....                   | 118 |
| Table 4.11 Identification accuracy summary.....                                      | 119 |
| Table 4.12 Time-of-use electricity price in Ontario .....                            | 121 |
| Table 4.13 Daily Expense Saving with Demand Response Strategy Application .....      | 121 |
| Table A.1 A summary of typical filter parameters .....                               | 131 |
| Table C.1 Typical parameters of the single phase induction motor .....               | 137 |
| Table D.1 Harmonic spectrum of home appliance – Part I.....                          | 140 |
| Table D.2 Harmonic spectrum of home appliance – Part II .....                        | 140 |
| Table D.3 Household activity classification .....                                    | 142 |
| Table D.4 Input data file 3 - appliance general information.....                     | 143 |
| Table D.5 Checklist of home appliance codes.....                                     | 144 |
| Table F.1 An example of detected data segment .....                                  | 158 |

# List of Figures

|   |    |
|---|----|
| Figure 1.1 Solar power global capacity 1995-2012 .....  | 1  |
| Figure 1.2 Global energy use by source in the 21 <sup>st</sup> century .....                    | 2  |
| Figure 1.3 Residential distribution system with PV system integrated (rotate 90 deg) .....      | 2  |
| Figure 1.4 Grid-tied PV inverter .....  | 4  |
| Figure 1.5 Harmonic current spectrum of PV inverter .....                                       | 4  |
| Figure 1.6 Norton equivalent of the PV inverter .....   | 5  |
| Figure 1.7 Harmonic model of grid-integrated PV inverter .....                                  | 6  |
| Figure 1.8 Secondary distribution network with its supply system .....                          | 8  |
| Figure 1.9 Residential distribution network model.....  | 9  |
| Figure 1.10 Procedure of harmonic impact study of PV inverters .....                            | 9  |
| Figure 2.1 The structure of a PV array .....  | 14 |
| Figure 2.2 Basic PV module equivalent circuit .....   | 16 |
| Figure 2.3 Electrical feature of a PV module .....  | 16 |
| Figure 2.4 Solar irradiance at various PV panel orientations .....                              | 17 |
| Figure 2.5 The general configuration of a PV system .....                                       | 18 |
| Figure 2.6 The function components of PV inverter .....   | 18 |
| Figure 2.7 A 60 Hz, transformer-based, three-phase inverter circuit .....                       | 19 |
| Figure 2.8 A high frequency, transformer-based, single-phase inverter circuit ...               | 20 |
| Figure 2.9 A single-stage transformerless inverter .....  | 20 |
| Figure 2.10 A two-stage transformerless inverter.....   | 21 |
| Figure 2.11 Fundamental model of PV inverter .....  | 23 |
| Figure 2.12 PV output power (measured in Edmonton, June 24, 2013).....                          | 25 |
| Figure 2.13 PV output power and PCC voltage (measured in Edmonton, June 28, 2013).....          | 26 |
| Figure 2.14 Correlation power and voltage changing rate.....                                    | 28 |
| Figure 2.15 Single-phase PWM inverter .....   | 29 |
| Figure 2.16 Sampling method and the resultant PWM switching function.....                       | 30 |
| Figure 2.17 Sampling method and PWM switching function.....                                     | 31 |
| Figure 2.18 Harmonic spectrum of the switching function .....                                   | 32 |
| Figure 2.19 Harmonic spectrum of the switching function with different switching frequency..... | 33 |
| Figure 2.20 Measured DC-link voltage waveform [27].....   | 34 |
| Figure 2.21 Input power and output power for a single-phase PV inverter.....                    | 35 |
| Figure 2.22 Harmonic spectrum of inverter terminal voltage.....                                 | 37 |
| Figure 2.23 Harmonic model of PV inverter .....   | 38 |
| Figure 2.24 Modulation process using enhanced sampling for two-level PWM inverter .....         | 33 |
| Figure 2.25 Constant power control for PV inverter .....  | 39 |
| Figure 2.26 Part of the power control block with harmonic compensation.....                     | 40 |
| Figure 2.27 Simulated grid-connected PV inverter .....  | 41 |
| Figure 2.28 Harmonic spectrum of $I_{pcc}$ (under sinusoidal grid voltage).....                 | 43 |
| Figure 2.29 Harmonic spectrum of $I_{pcc}$ (under grid harmonic voltage).....                   | 43 |



|   |     |
|---|-----|
| Figure 2.30 Simulated DC-link voltage waveform.....   | 44  |
| Figure 2.31 Picture of Xantrex inverter .....   | 46  |
| Figure 2.32 Experiment circuit topology .....   | 47  |
| Figure 2.33 PV inverter circuit topology .....  | 47  |
| Figure 2.34 The experiment system of PV integration .....                                     | 49  |
| Figure 2.35 Transient DC input voltage of PV inverter.....                                    | 50  |
| Figure 2.36 Inverter output power under two scenarios .....                                   | 51  |
| Figure 2.37 Harmonic spectrum of PCC voltage $V_{pcc}$ (directly measured) .....              | 52  |
| Figure 2.38 Harmonic spectrum of inverter bridge voltage $V_{pwm}$ (indirectly measured)..... | 52  |
| Figure 2.39 Equivalent circuit of PV inverter integration .....                               | 53  |
| Figure 2.40 Harmonic spectrum of the output current $I_{pcc}$ .....                           | 54  |
| Figure 2.41 Frequency response of the filter impedance .....                                  | 56  |
| Figure 3.1 Secondary distribution system with PV integration .....                            | 59  |
| Figure 3.2 Residential house model with PV inverter .....                                     | 62  |
| Figure 3.3 Phase B harmonic voltage and current trend at the service panel (7:30~7:50) .....  | 64  |
| Figure 3.4 Harmonic voltage and current spectrum at the service panel.....                    | 66  |
| Figure 3.5 Harmonic model of PV inverter (neglecting the harmonic source) ....                | 68  |
| Figure 3.6 Simplification method of the secondary system (at harmonic frequency) .....        | 68  |
| Figure 3.7 Simplification method of multi-house circuit (at harmonic frequency) .....         | 70  |
| Figure 3.8 Frequency response of $Z_{pcc}$ with different $R_c$ .....                         | 74  |
| Figure 3.9 Frequency response of $Z_{pcc}$ with different PV inverter number .....            | 74  |
| Figure 3.10 Harmonic voltage spectrums under different damping resistance ....                | 76  |
| Figure 3.11 PV inverter harmonic model .....  | 76  |
| Figure 3.12 The power loss and resonance amplification with different $R_c$ .....             | 77  |
| Figure 4.1 Generic multiphase low-voltage residential distribution network.....               | 85  |
| Figure 4.2 Single-house detailed circuit .....  | 85  |
| Figure 4.3 Sample household load behavior profile. ....                                       | 86  |
| Figure 4.4 Example of time-of-use probability profile for household activities ..             | 88  |
| Figure 4.5 Charging profile for three EVs using different charging strategies ....            | 90  |
| Figure 4.6 Solar irradiance level prediction for a clear day.....                             | 93  |
| Figure 4.7 Multiphase secondary distribution network .....                                    | 95  |
| Figure 4.8 Single room equivalent circuit.....  | 98  |
| Figure 4.9 PV inverter model for harmonic power flow calculation.....                         | 101 |
| Figure 4.10 Capacitor-start, capacitor run induction motor.....                               | 103 |
| Figure 4.11 Equivalent circuit of single-phase motor we being standstill.....                 | 103 |
| Figure 4.12 Measurement results during fridge starting transient .....                        | 106 |
| Figure 4.13 Simulation results during a fridge starting transient.....                        | 106 |
| Figure 4.14 Rising spike signature.....   | 107 |
| Figure 4.15 Falling spike signature.....  | 108 |
| Figure 4.16 Duty cycle of pulses .....  | 108 |
| Figure 4.17 Multi-stage appliances.....   | 109 |
| Figure 4.18 Fluctuation signature .....   | 110 |

|   |     |
|---|-----|
| Figure 4.19 Multi-stage appliances.....   | 110 |
| Figure 4.20 Standard noise for simulating the random load behavior.....                     | 111 |
| Figure 4.21 Overall LV network simulation platform flowchart.....                           | 112 |
| Figure 4.22 Sample power demand and third harmonic simulation results.....                  | 114 |
| Figure 4.23 PV array integration impact on service panel voltages.....                      | 116 |
| Figure 4.24 Impact of neutral condition on neutral-to-earth voltage level.....              | 118 |
| Figure 4.25 Neutral-to-earth voltage at the service panel side (House #9).....              | 118 |
| Figure 4.26 Identification of home appliances.....  | 120 |
| Figure 4.27 Demand response technique evaluation on LV simulator.....                       | 121 |
| Figure A.1 Filter topology of Xantrex Grid-tied inverter GT3.0-NA-DS-240...                 | 131 |
| Figure B.1 Three-phase conductor.....   | 132 |
| Figure B.2 Equivalent circuit of three-phase conductor.....                                 | 133 |
| Figure B.3 Equivalent circuit of three-phase conductor (with parameters).....               | 135 |
| Figure B.4 Single-phase three-winding transformer.....                                      | 135 |
| Figure D.1 Input data file 1 – system and appliance electric data.....                      | 139 |
| Figure D.2 Input data file 2 – appliance usage probability data.....                        | 141 |
| Figure D.3 Example of time-of-use probability curves for household activities               | 141 |
| Figure E.1 Distributions of the irradiance fluctuations registered at Cintruenigo site..... | 147 |
| Figure E.2 Power output fluctuation induced by moving cloud.....                            | 148 |
| Figure E.3 Cloud transient event.....   | 148 |
| Figure E.4 Example of cloud transient event.....  | 150 |
| Figure E.5 Cloud transient event.....   | 150 |
| Figure E.6 Probability density of cloud approaching/leaving duration.....                   | 151 |
| Figure E.7 Probability density of cloud staying duration.....                               | 152 |
| Figure E.8 Probability density of PV output fluctuation magnitude.....                      | 153 |
| Figure E.9 The moving cloud passing a PV site.....  | 154 |
| Figure E.10 Global irradiance ( <i>GHI</i> ) and clear-sky global irradiance.....           | 154 |
| Figure E.11 Comparison of results to geographic diversity study.....                        | 155 |
| Figure E.12 Zero correlation crossover distance as a function of time scale.....            | 156 |
| Figure F.1 The recorded data of a cloud transient event.....                                | 157 |
| Figure F.2 Flowchart of the detecting method.....   | 158 |

# List of Abbreviations

|      |                                |
|------|--------------------------------|
| CFL  | Compact Fluorescent Lamp       |
| DG   | Distributed Generation         |
| FFT  | Fast Fourier Transformation    |
| IDD  | Individual Demand Distortion   |
| IHD  | Individual Harmonic Distortion |
| LV   | Low Voltage                    |
| MPP  | Maximal Power Point            |
| MPPT | Maximal Power Point Tracking   |
| NEV  | Neutral-to-Earth Voltage       |
| NILM | Non-Intrusive Load Monitoring  |
| PCC  | Point of Common Coupling       |
| PEV  | Plug-in Electric Vehicle       |
| PV   | Photovoltaic                   |
| PWM  | Pulse Width Modulation         |
| SMC  | Sequential Monte Carlo         |

# Chapter 1

## Introduction

Photovoltaic (PV) is a method of generating electrical power by converting solar radiation into direct current (DC) electricity using semiconductors that exhibit the photovoltaic effect. Compared with other types of renewable power generation, the PV generation has no rotation components, no mechanical loss or noise. It is relatively easy to build and relocate. The maintaining cost is low. In this chapter, the application background and the motivation of this research topics is introduced. A literature review is presented on the modeling of PV inverter and its harmonic impact studies. In addition, the thesis scopes and outline are presented.

### 1.1 Overview

In recent years, the solar power global capacity is experiencing a rapid development, as is shown in Figure 1.1. As predicted by [1], the solar power will provide up to 20% of the total electricity demand worldwide by the year of 2050 and 64% by 2100 (in Figure 1.2).

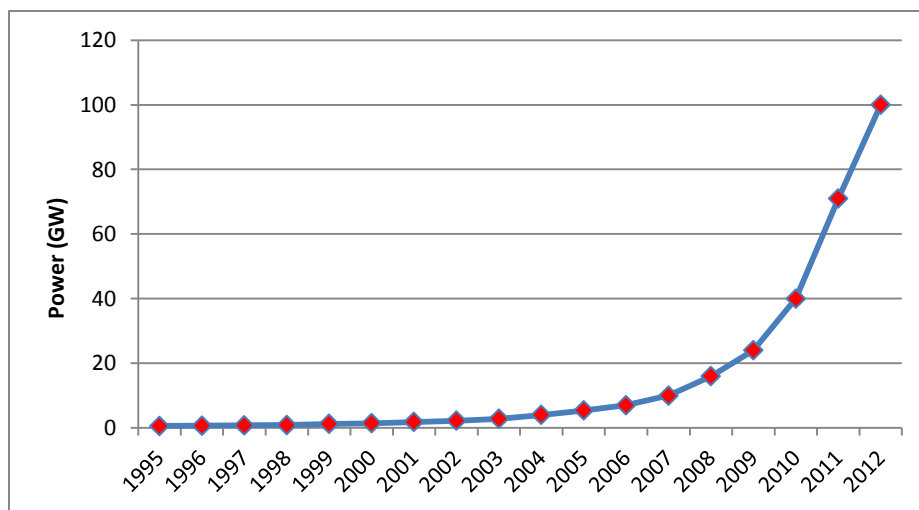


Figure 1.1 Solar power global capacity 1995-2012

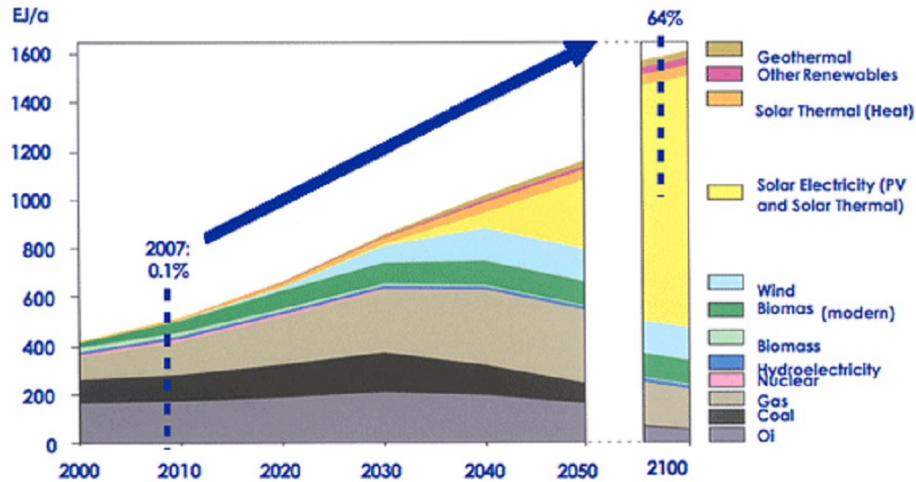


Figure 1.2 Global energy use by source in the 21<sup>st</sup> century

The application of PV generation includes two aspects: large-scale PV plants in wild area and small-scale rooftop PV systems in the city. Figure 1.3 shows a general single-line topology of the North American residential distribution network (secondary side) with PV systems integrated. The PV system mainly consists of a PV array that converts the solar irradiance into DC power, and a PV inverter that converts the DC power into AC power.

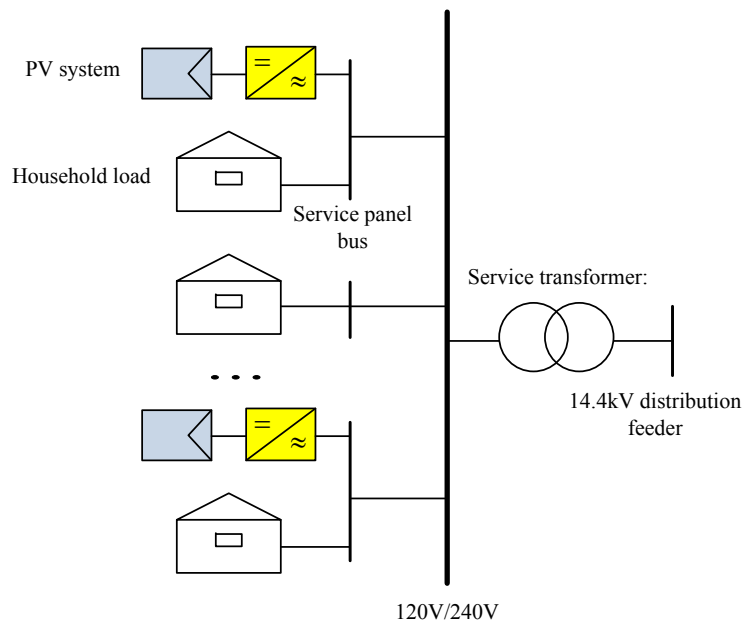


Figure 1.3 Residential distribution system with PV system integrated

The rooftop PV system is an important type of distributed generator. It is installed where electricity is used and therefore reduces the stress on electricity distribution networks, especially during peak demand hours. However, it is claimed that several power quality problems arise due to the high penetration of PV system, such as harmonic distortion, voltage rise and voltage fluctuation problems [5]~[7]. The severity of these problems should be evaluated when planning and managing the distribution system.

This thesis is concentrated on modeling distributed PV systems and evaluating their power quality impacts on the residential distribution system. In addition, since only the PV inverter interface the secondary system (shown in Figure 1.3), the term “PV inverter modeling” is equivalent to “PV system modeling” in the thesis.

## **1.2 Harmonic Impact of PV Inverters**

In this subsection a literature review is presented about the harmonic modeling of the distributed PV inverters and its harmonic impact on the low voltage network.

### ***1.2.1 Significance of the Harmonic Issue of PV Inverters***

The PWM inverter is widely used in modern grid-tied PV inverters to convert DC power into AC power. The overall structure of a grid-tied PV inverter is shown in Figure 1.4. Figure 1.5 shows the harmonic spectrum of a PV inverter output current ( $I_{pcc}$ ). It is measured by Yokugawa DL850 with a high sampling frequency of 1MHz. As this figure reveals, both low order harmonic (<2kHz or 30<sup>th</sup> order) and high order harmonic (equals to or multiples of switching frequency) components exist in the PV output current. Traditionally, the PV inverter was usually considered a harmonic source. Its low-order harmonic feature and harmonic impact on the distribution system received a great deal of attention [7]-[15]. However, few detailed studies were done to explain the mechanism of the harmonic current generation: that is, whether the harmonic is generated by the inverter itself or by the grid background harmonic. Furthermore, since the low-

pass filter displays capacitive characteristic at a specified frequency band, it can interact with the system impedance and result in additional resonance in the system [11].

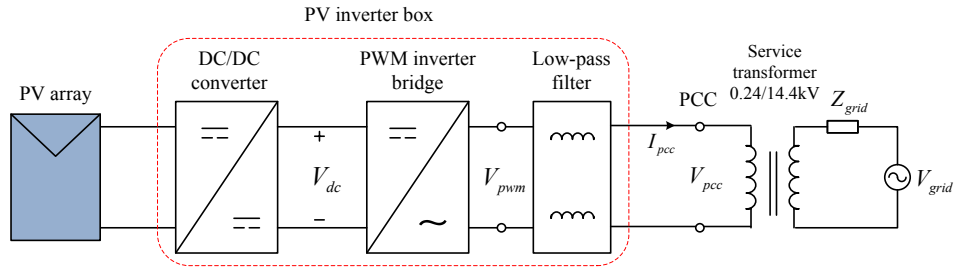


Figure 1.4 Grid-tied PV inverter

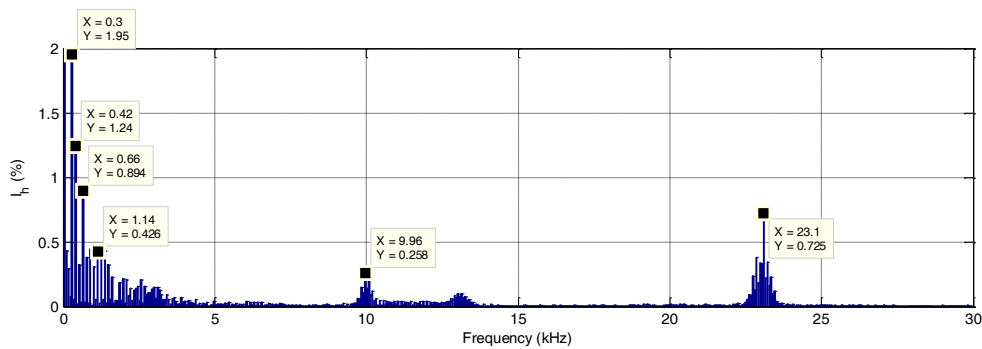


Figure 1.5 Harmonic current spectrum of PV inverter

Therefore, it is quite essential to investigate and clarify the low order harmonic impact of PV inverters on the supply systems. The harmonic impact consists of two aspects:

- On the one hand, the PV inverter acts as a harmonic source. We need to determine its harmonic current injection to the system;
- On the other hand, the PV inverter acts as a harmonic impedance. We need to investigate its harmonic interaction with the system impedance and potential resonance problem.

Obviously, the harmonic source characteristic is shared by all kinds of nonlinear loads, while the harmonic impedance characteristic is unique for filter-based power converters and should be studied in depth.

### 1.2.2 Traditional Harmonic Modeling Method of PV Inverters

In order to investigate the aggregated harmonic impact of PV inverters on distribution systems, a simplified and accurate harmonic model should be built up. The existing harmonic models of the PV inverters can be classified into three categories.

#### A. Current Source Model

Reference [7] suggested that the PV inverter can be modeled as a current source, on the basis that the low order harmonic current was measured at the PV output side. Reference [15] studied the allowable penetration of distributed resources by considering the harmonic limits and other power quality constraints. And the PV inverter was also modeled as current source.

However, such references lack a detailed and convincing study on the harmonic characteristic of the PV inverter: they failed to explain how the harmonic current is generated and to verify whether it remains constant under different background harmonic voltages. Therefore this model is inadequate for power system harmonic studies.

#### B. Norton/Impedance Model

The Norton model was proposed in [8]-[10]. These references assumed that the harmonic current output of a PV inverter consists of two parts. As is shown in Figure 1.6, the Norton current source  $I_{inv}(h)$  represents the PV output harmonic current  $I_{pcc}(h)$  when the grid voltage is sinusoidal. The Norton impedance  $Z_{inv}(h)$  represents the impact of grid harmonic voltage  $V_{pcc}(h)$  on  $I_{pcc}(h)$ .

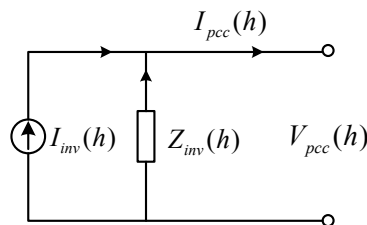


Figure 1.6 Norton equivalent of the PV inverter



Reference [8] proposed an active measurement-based method for determining  $I_{inv}(h)$  and  $Z_{inv}(h)$ . The PV inverter is connected to a programmable voltage source, which can modify the harmonic voltage  $V_{pcc}(h)$ . Then  $I_{pcc}(h)$  is also modified. The Norton impedance and current source are estimated by (1.1):

$$\begin{aligned} Z_{inv}(h) &= \frac{V_{pcc-2}(h) - V_{pcc-1}(h)}{I_{pcc-2}(h) - I_{pcc-1}(h)}, \quad 2 \leq h \leq 50 \\ I_{inv}(h) &= I_{pcc-1} - \frac{V_{pcc-1}(h)}{Z_{inv}(h)} \end{aligned} \quad (1.1)$$

Reference [9]-[10] proposed the dynamic frequency-domain Norton model which incorporates the general control strategy of the PWM inverter. To some degree the model explained the cause of harmonic current emission. However, control block parameters are required to implement this model and it is not convenient to apply this model to harmonic impact studies.

### **C. Full Circuit Model**

Reference [11] analyzed the mechanism of the PV inverter's harmonic current generation in 2011. The equivalent circuit of the PV inverter is presented in Figure 1.7. In the steady state condition, the inverter bridge output terminal is represented by an independent voltage source  $V_s$  at both the fundamental and the harmonic frequencies. The harmonic spectrum of  $V_s$  is obtained by the lab measurement.  $Z_{Lf}$  and  $Z_{Cf}$  represent the filter inductance and capacitance and  $Z_{Lg}$  represents the combination of filter inductance and grid impedance.

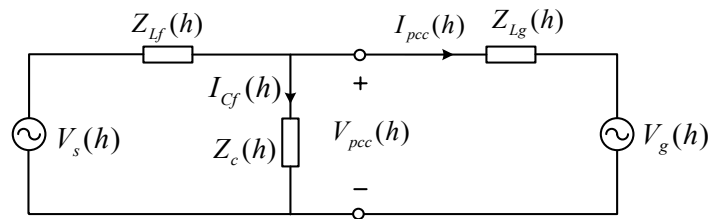


Figure 1.7 Harmonic model of grid-integrated PV inverter

This topology clearly indicates that both the inverter harmonic voltage and grid background harmonic voltage contribute to the PV inverter harmonic current

$I_{pcc}(h)$ . However, there is still room for improvement in this model: no verification study was done to prove that the inverter bridge output can be modeled as a voltage source at each harmonic order, which is the theoretical basis of the harmonic modeling.

In summary, the contributions of traditional studies are as follow: 1) the low-order harmonic feature of the PV inverter is partially explained; and 2) the measurement-based model is proposed to quantify the low-order harmonic feature of the PV inverter. However, an analytical model needs to be proposed and validated so that we can analyze the potential harmonic impact of aggregated PV inverters on the power system.

### ***1.2.3 Harmonic Impact of PV Inverters on Distribution Networks***

Low order harmonics are presented in the PV output current. These currents, flowing through the impedances of the distribution system, result in additional harmonic voltage distortion. The harmonic impact of a single PV inverter is probably not significant. However, the number of grid-tied PV inverters may increase very quickly in the low voltage networks. This phenomenon creates a concern whether the grid harmonic voltage will increase obviously [13].

The secondary distribution system model is presented in Figure 1.8 [12]. It indicates that North American structures and European structure are quite different, which may lead to differences in the harmonic impact study.

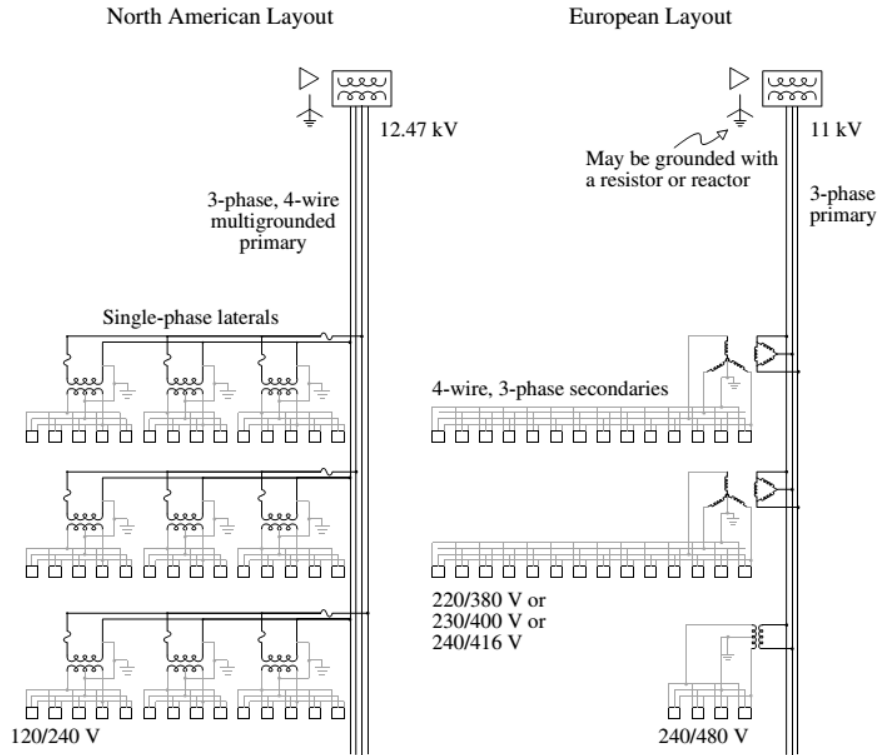


Figure 1.8 Secondary distribution network with its supply system

Traditional harmonic impact studies usually regarded the PV inverter as a harmonic current source whose spectrum was based on the measurement. Reference [13]-[15] proposed the measurement-based method for investigating the harmonic impact of rooftop PV panels or small-scale PV plants on the residential distribution network in Europe. In these studies, the simplified European secondary system model is applied (shown in Figure 1.9). The PV inverter is modeled as a current source at harmonic frequency and its harmonic spectrum is extracted from field measurement data. Then, sensitivity studies are conducted to estimate the harmonic voltage distortion under different grid operating conditions, for example: 1) how the harmonic voltage changes with the total PV installation capacity; and 2) how the harmonic voltage changes with solar irradiance. The study procedures of these three references are quite similar and are summarized in Figure 1.10.

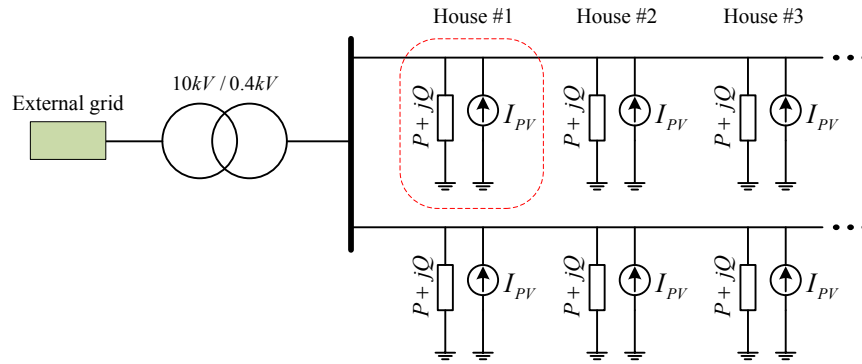


Figure 1.9 Residential distribution network model

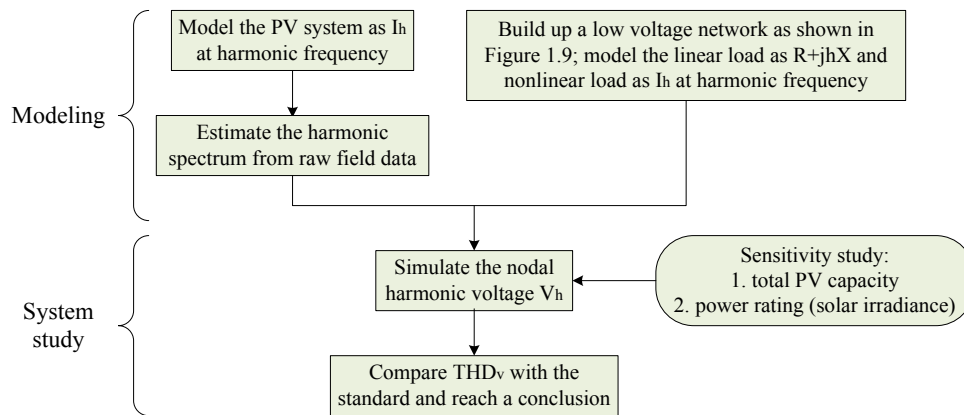


Figure 1.10 Procedure of harmonic impact study of PV inverters

Reference [16] also presented a harmonic impact study of the PV inverter. This paper made a difference in that it investigated the potential harmonic resonance problem caused by the filter of the PV inverters.

In summary, although the traditional studies demonstrated the harmonic impact of PV inverters by providing sufficient field data, there still exist three shortages:

- **About the PV inverter model:** these studies failed to explain the harmonic characteristic of a PV inverter in an analytical manner. Reference [13] suggested that the PV output harmonic current might change with system harmonic voltage but didn't investigate the problem in detail.

- **About the residential load model:** The residential load parameters are hypothetical and cannot represent the general operating conditions of a practical residential distribution network.
- **About the network topology:** The network topology is only applicable to European networks and is sometimes oversimplified. In North America, however, the secondary distribution network is quite different. Therefore more studies are needed to estimate how the PV inverter affects harmonic power flow in typical North American low-voltage networks.

### 1.3 Thesis Scope and Outline

This thesis is mainly focused on the collective power quality impact of PV inverters on residential distribution networks. Two topics are discussed in this research work.

The first topic is the harmonic characteristics and modeling of the PV inverter. With the harmonic model, we can estimate the harmonic impact of the PV inverter. This study will try to answer the following two questions:

- Why does the PV inverter generate low order harmonic current and how to quantify it? If this is done, we can decide whether it causes significant harmonic impact on the distribution system.
- How does the inverter filter interact with the system impedance, and can it cause a serious resonance problem in the power system?

The second topic is a Monte Carlo simulation platform for studying the electric features of a low voltage residential network. The platform incorporates the behavior model and electric model of residential loads (developed by [3]) and those models of PV inverter (developed in this thesis). It is able to simulate the random loading behavior of the residential distribution network. Therefore it is an effective tool for studying the power quality impact of PV inverter on residential distribution systems.

In addition, another project related to power quality impact of PV is presented in Appendix E. It is a survey and a fundamental study on the statistical pattern of the cloud transient behavior, which is the basis for studying the cloud transient impact on the distribution systems with large PV penetration.

The thesis is organized as follows:

Chapter 2 proposes the steady-state model of the PV inverter at both fundamental and harmonic frequency, based on the operating principle of the PV panel and PV inverter. The fundamental model is verified by field measurement data. The harmonic model is verified by the simulation study and the PV integration experiment.

Based on the PV model in Chapter 2, Chapter 3 presents a harmonic impact study of the PV inverter on residential distribution networks. Firstly a detailed simulation study is made in order to demonstrate how the PV inverter affects the harmonic voltage and harmonic current at the house entrance point. Besides, an analytical study is conducted to demonstrate the mechanism of harmonic resonance problem caused by the PV inverter.

Chapter 4 presents a Matlab-based program that can simulate the electric parameters of a residential distribution network over an extended period of 24 hours. The program takes into consideration the random loading behavior of home appliances and PV panels. Therefore it can support not only comprehensive PV integration studies, but also several demand side studies such as *non-intrusive load monitoring (NILM)*, demand response and other power quality problems.

Chapter 5 concludes this thesis and provides suggestions for future research.

Appendix A summarizes the typical parameters of the PV inverter filter.

Appendix B presents the modeling of the multiphase coupled line and the single-phase three-winding transformer for secondary system power flow calculation.

Appendix C documents the typical parameters of a single-phase induction motor.

Appendix D documents the input data structure of the Monte Carlo simulation platform introduced in Chapter 4.

Appendix E presents a statistic pattern of cloud transient indices. The result can be used to study the impact of the solar irradiance variability on the voltage regulation of the distribution systems with large PV penetration.

Appendix F presents the computer programming method for automatically counting the cloud transient indices from the raw field data.

## Chapter 2

### Harmonic Characteristics and Models of PV Inverters

Large PV penetration may result in several power quality problems in the distribution systems such as harmonic distortion and overvoltage. In order to estimate the severity of these problems, a PV inverter model at both fundamental and harmonic frequency is required.

This chapter explains the configuration of practical PV inverters and conducts theoretical analysis on the harmonic characteristics of the PV inverter during the steady-state operation. An analytical harmonic model of PV inverter is proposed. Section 2.1 presents a survey of the configuration and electric feature of the distributed PV array and PV inverter. In Section 2.2, a fundamental frequency model of the PV inverter is proposed. Also, in Section 2.3, the harmonic characteristic of PV inverter is analyzed and the harmonic frequency model is proposed. The model is further verified by simulation study and lab experiment in Section 2.4 and 2.5 respectively. The characteristic of the harmonic model is further analyzed in Section 2.6, which is followed by a summary in Section 2.7.

#### 2.1 Description of the PV System

This section presents a survey of the typical circuit topology of an authentic PV system and its technical parameters, which is quite essential for the later modeling studies.

##### *2.1.1 Configuration and Electric Feature of PV Arrays*

###### *A. Configuration of PV Array*

The configuration of a rooftop PV array is shown in Figure 2.1. Each part of the PV array is described as follows [19]:



- **Solar (PV) cell:** an electronic device that converts solar energy into direct current electricity through the PV effect. Assembly of cells is used to make PV modules.
- **PV module:** A group of PV cells connected in series to provide a significant output voltage (typically larger than 20V) is called a PV module. A module typically consists of 48, 60 or 72 cells.
- **PV string:** Group of series-connected solar PV string to obtain a higher output voltage.
- **PV array:** Group of parallel-connected solar PV string to allow the system to produce more current.

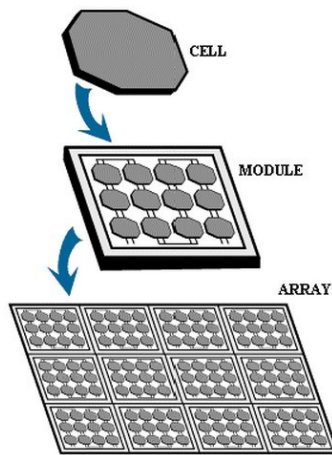
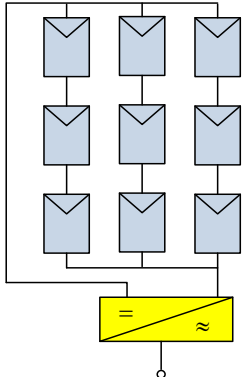
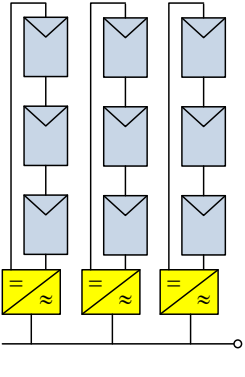
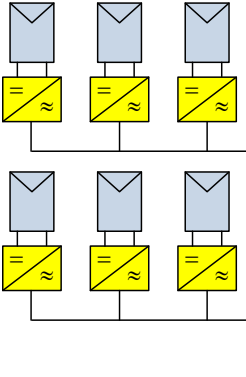


Figure 2.1 The structure of a PV array

A number of PV modules are connected together to build up a PV array. There are mainly three different ways of connecting the PV module circuit, shown in Table 2.1 [25].

Table 2.1 Comparisons of different types of PV module

| Type             | Central  | String   | Module  |
|------------------|--|--|---|
| Circuit topology |   |      |                                |
| DC bus           | High voltage, high current   | High voltage, low current  | Low voltage, low current  |
| Feature          | - Higher power losses,<br>- Mismatch losses between PV modules,<br>- Nonflexible design for enlargement,<br>- Low power quality. | - Separate MPPT for each string,<br>- Higher overall efficiency than central inverter. | - Higher installation cost,<br>- No mismatch losses due to individual MPPT,<br>- Flexible design for enlargement. |
| Usage situation  | This topology is widely used in the past and less used nowadays  | This topology is most widely used nowadays   | This topology is widely used nowadays   |

### **B. Electric Feature of PV Module**

The basic PV module equivalent circuit is presented in Figure 2.2. The brochure usually provides four main technical parameters [17]: open-circuit voltage ( $V_{oc}$ ), short-circuit current ( $I_{st}$ ), maximum power voltage ( $V_{mp}$ ) and maximum power current ( $I_{mp}$ ). The electric feature of a practical PV module product is shown in Figure 2.3 [17]. The following conclusions can be drawn from the figure:

- The maximum power voltage  $V_{mp}$  almost remain constant under different solar irradiance;
- The maximum power  $P_{mp}$  is proportional to the solar irradiance.

Besides, the technical parameters are based on the **Standard Test Condition** (STC) (solar irradiance  $1000\text{W}/\text{m}^2$  and a cell temperature of  $25^\circ\text{C}$ ). Therefore the rated  $P_{mp}$  of PV module is reached under  $1000\text{W}/\text{m}^2$  irradiance.

Because of its I-V and P-V characteristics, **maximum power point tracking** (MPPT) is required to harvest the maximum energy that the PV module can produce. In practical, this is achieved by the MPPT controller inside the PV inverter.

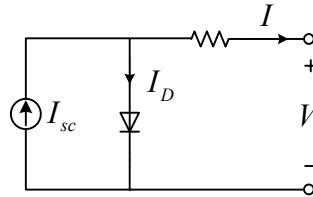
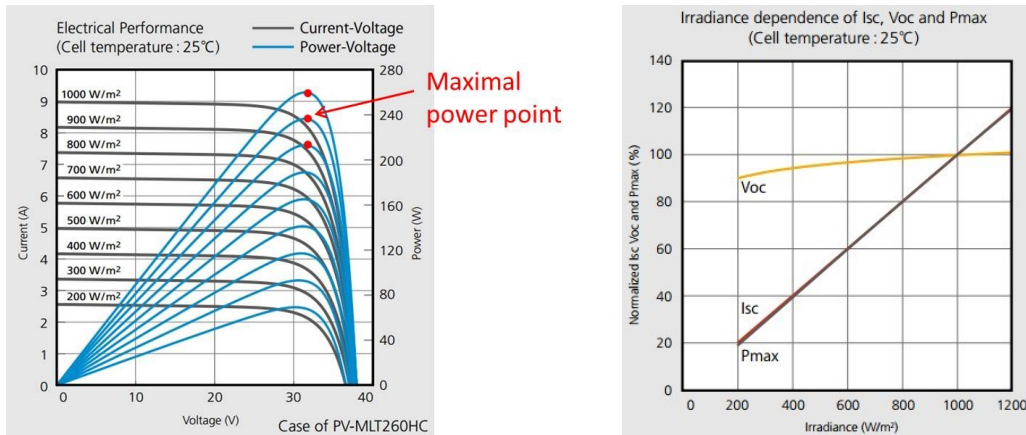


Figure 2.2 Basic PV module equivalent circuit



(a) V-I curve under different irradiance

(b) Maximal power with irradiance

Figure 2.3 Electrical feature of a PV module

In practical, the PV module cannot always operate in the temperature of 25°C. Under a fixed solar irradiance, the relation between PV maximal output power and temperature is:

$$P_{MPP(p.u.)}(T) = 1 + \lambda(T - 25) \quad (2.1)$$

where  $T$  is the PV cell temperature (°C),  $P_{MPP(p.u.)}$  is the per-unit of maximal power under temperature  $T$ , and  $\lambda$  is the temperature coefficient (%/°C).

Table 2.2 lists several coefficients for different PV module products.

Table 2.2 PV module temperature coefficient

| Product                    | Rated MPP power (W) | Operation temperature (°C) | Coefficient $\lambda$ (%/°C) |
|----------------------------|---------------------|----------------------------|------------------------------|
| Mitsubishi: PV MTL260-HC   | 260                 | -30 ~ +80                  | -0.45                        |
| Canadian solar: CS6X-300P  | 300                 | -40 ~ +85                  | -0.43                        |
| SunTech: STP250S-20        | 250                 | -40 ~ +85                  | -0.44                        |
| General Electric: GEPVP200 | 200                 | N/A                        | -0.5                         |

Therefore we select the average value  $\lambda = -0.45\%$  as the temperature coefficient for the general PV module. Then, equation (2.1) can be expressed as:

$$P_{MPP(p.u.)}(T) = 1 - 0.0045(T - 25) \quad (2.2)$$

### C. PV Panel Orientation

There are three kinds of PV panel orientation: horizontal, latitude tile and 2-axis tracking. One example of the field data is presented in Figure 2.4 [18]. In large-scale PV plant, the 2-axis tracking is sometimes applied. The tracking greatly promotes the solar energy harvesting efficiency but increases the expense. Therefore the latitude tile is widely applied in rooftop PV panel. In areas of different latitude, an optimal tilt angle is decided for the PV panel installation. In this thesis, the solar irradiance profile of interest is based on the **latitude tile** type.

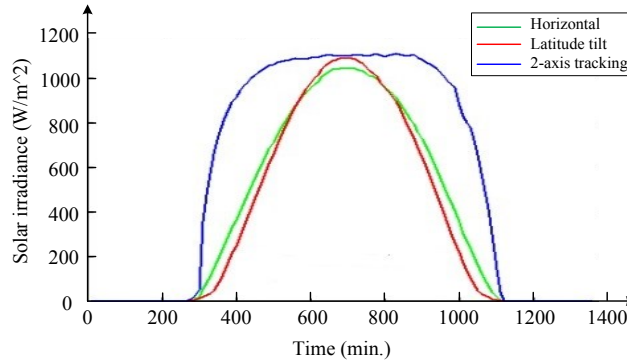


Figure 2.4 Solar irradiance at various PV panel orientations

#### **2.1.2 Configuration and Function of Grid-tied PV Inverters**

Grid-tied PV inverter is a packaged box which mainly includes a DC/DC converter, a PWM inverter bridge and a low-pass filter. The topology and general

control scheme of a grid-tied PV inverter is summarized in Figure 2.5. The major components of a PV inverter are summarized as Figure 2.6 [10], [22], [25], [32].

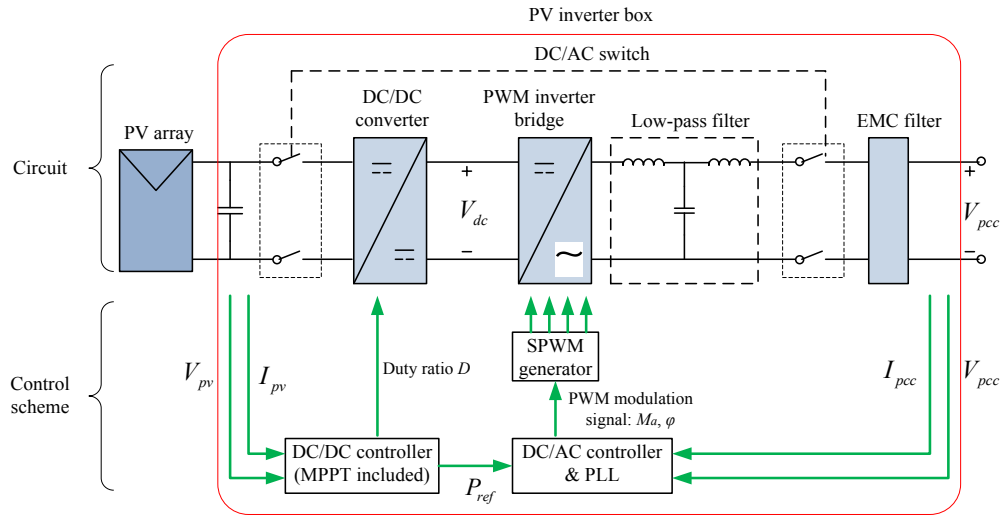


Figure 2.5 The general configuration of a PV system

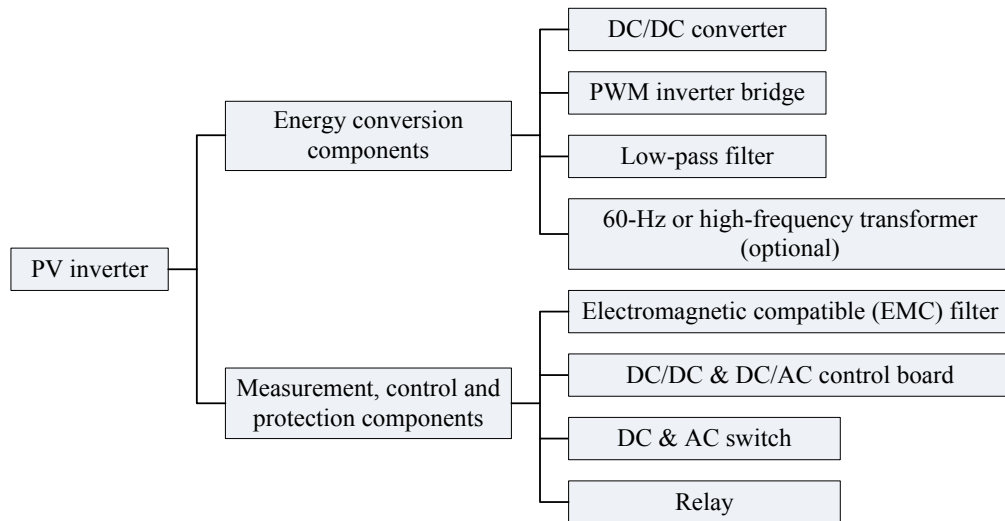


Figure 2.6 The function components of PV inverter

A grid-tied PV inverter is required to realize three functions [22]:

- **Power conversion:** the PV inverter converts the DC current generated by PV array into AC current (almost sinusoidal) that is in phase with the grid voltage. Therefore a phase lock loop (PLL) element is included in the PWM control board for detecting the grid voltage phase angle.

- **Maximum power point tracking (MPPT):** MPPT is the control method that a PV inverter uses to remain close to the ever-moving maximum power point (MPP) of a PV array. The PV inverter is able to track the MPP under the varying solar irradiance level by adjusting the terminal voltage of PV array. Nowadays the MPPT efficiency of a commercial PV inverter can be as high as 99.5%, according to the user manuals [19]-[21].
- **Grid disconnection and protection:** As required by IEEE-1547 [29], all grid-tied inverters must disconnect from the grid if the AC line voltage or frequency exceeds the limits prescribed in the standard.

A variety of PV inverter topologies are applied in the industry. One general classification is to divide them into two types: insulated (transformer-based) type and non-insulated (transformerless) type [25]. Below is a review of four common types of topology.

#### **A. Insulated type (transformer-based type)**

The transformer in the PV converter has two functions: 1) regulate the voltage level and 2) insulate the DC component from the grid.

**Power frequency transformer inverters:** As is shown in Figure 2.7, a 60-Hz transformer is installed between the LC filter and the PCC. The 60-Hz transformer can insulate the DC current components from the grid. However, it makes the inverter quite bulky. This type is applicable to high power level PV systems (generally larger than 30kW).

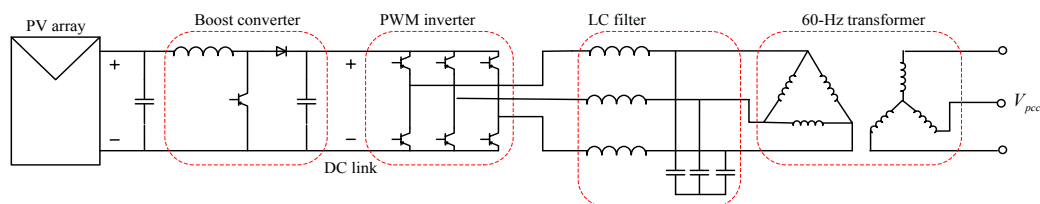


Figure 2.7 A 60 Hz, transformer-based, three-phase inverter circuit

**High-frequency transformer inverters:** Many of the grid-tied inverters available in North America today utilize high frequency transformers [22]. This type has

the low weight advantage over power frequency transformer-based inverters. As is shown in Figure 2.8, a high-frequency transformer is installed between the H-bridge and the LC filter. The transformer provides isolation and boosts the voltage for grid interconnection. This type is more applicable to low capacity situation (several kW).

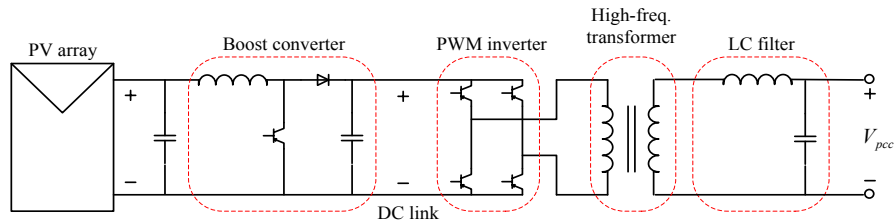


Figure 2.8 A high frequency, transformer-based, single-phase inverter circuit

### **B. Non-insulated type (Transformerless type)**

Transformerless PV inverter is popular in Europe, especially for string inverters and increasingly for 3-phase central inverters. The basic premise is that since a building or utility transformer is down the line anyway, another transformer right in or alongside the PV inverter is not needed [22]. Eliminating the transformer not only reduces cost, size and weight but also reduces the power loss associated with the transformer, increasing inverter efficiency.

**Single-stage transformerless inverter:** the single-stage inverter realizes two functions, MPPT and DC/AC conversion, with the same device. Figure 2.9 is a typical topology of single-stage inverter. However, since there is no voltage boost component in single-stage inverter, there must be a number of (at least 10) PV modules connected in series to obtain a required DC voltage for the inverter. This makes the PV array less flexible to build.

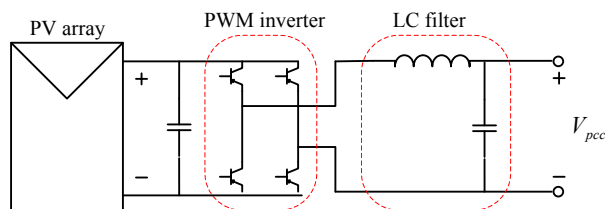


Figure 2.9 A single-stage transformerless inverter

**Two-stage transformerless inverter:** the first stage is DC/DC converter, realizing the function of voltage boost and MPPT; and the second stage is DC/AC inverter, realizing the function of voltage conversion (in Figure 2.10). In the industry, this topology is the most widely used topology for small-scale PV panels (<10kW) [22].

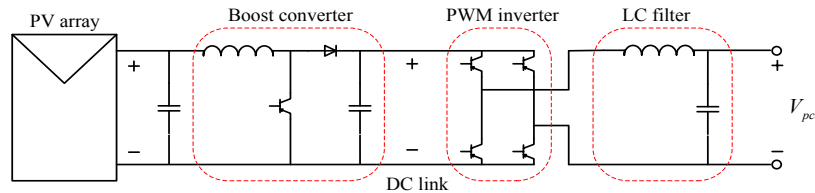


Figure 2.10 A two-stage transformerless inverter

In summary, the 60-Hz transformer is only used in large capacity, 3-phase inverters [19]-[21]. Since this project is focused on the residential PV system, the single-phase, two-stage, transformerless PV inverter will be considered as the typical topology of interest. In addition, the LC/LCL type filter is widely adopted in the commercial inverter. The technical data of a typical single-phase, two-stage PV inverter is presented in Table 2.3 [21].

Table 2.3 An example of PV inverter technical data

Manufacture: Canadian solar CSI-150

0TLD-GW

| Item                              | Value    | Remarks                                    |
|-----------------------------------|----------|--|
| DC input data                     |          |  |
| Max. PV-generator power (W)       | 1800     |  |
| Max. DC voltage (V)               | 450      |  |
| MPPT voltage range (V)            | 120~450  |  |
| Turn on DC voltage (V)            | 125      |  |
| Max. DC work current (A)          | 12       |  |
| Number of inputs/MPPT trackers    | 1/1      |  |
| Standby power consumption (W)     | 5        |  |
| AC output data                    |          |  |
| Nominal AC power (W)              | 1500     |  |
| Max. AC power (W)                 | 1650     |  |
| Nominal output voltage range (V)  | 110~260V |  |
| Max. AC current (A)               | 18       |  |
| THD <sub>1</sub> (at rated power) | <1.5%    | THD <sub>1</sub> ranges 1~5% for different |



|                 |                    |  |
|-----------------|--------------------|--|
|                 |                    | products   |
| Power factor    | ~1 (nominal power) |  |
| AC connector    | Single phase       |  |
| Efficiency      |                    |  |
| Max. efficiency | 97.6%              | When the PV module reaches about 30%P <sub>rated</sub> , the efficiency almost reaches the maximal. Usually it is between 95~98% for different products. |
| MPPT efficiency | >99.5%             | 99.5% is the typical value for almost all PV inverters   |

The grid-tied PV inverter should obey standards given by the utility companies. In particular, the IEC-61727 [23] and the IEEE-1547 [29] are worth considering. These standards deal with issues like power quality, detection of islanding operation, grounding, etc. in regard to the integration of distributed energy resources (DER). Summaries are listed in Table 2.4.

Table 2.4 Summary of the major standard dealing with integrations of PV system

| Issue   | IEC61727   | IEEE1547  |
|---|--|---|
| Nominal power                                 | 10kW   | 30kW  |
| Harmonic current Limits in percent of $I_L^*$ | (3-9) 4.0%<br>(11-15) 2.0%<br>(17-21) 1.5%<br>(23-33) 0.6%                               | (2-10) 4.0%<br>(11-16) 2.0%<br>(17-22) 1.5%<br>(23-34) 0.6%<br>(>35) 0.3% |
|   | Even harmonics in these ranges shall be less than 25% of the odd harmonic limits listed. |   |
| Maximum current THD                           | 5%   |   |
| Power factor at 50% of rated power            | 0.9  |   |
| DC current injection                          | Less than 1.0% of rated output current.  | Less than 0.5% of rated output current.                                   |
| Voltage range for normal operation            | 85 ~ 110%  | 88 ~ 110%   |
| Frequency range for normal operations         | 50 ± 1Hz   | 59.3 ~ 60.5 Hz  |

\*  $I_L = \max(I_{load}, I_{PV})$  where  $I_{load}$  is the Local maximum load current integrated demand without the DER unit, and  $I_{PV}$  is the DER unit rated current capacity.

## 2.2 Modeling of PV Inverters at the Fundamental Frequency

In the power flow calculation, the distributed PV inverter is different from the large-scale power plant that can be modeled as a PV (power-voltage) node. The main reason is that no constant-voltage control method is applied to the PV inverter.

### 2.2.1 Fundamental Frequency Model of PV

#### A. Real Power Calculation

In references [6]-[7], the PV system is modeled as a current source at the fundamental frequency. However, it can be concluded from PV inverter manuals that the MPPT efficiency of commercial inverters is as high as 99%. Furthermore, the efficiency of PV inverter is usually above 95% when its output power is larger than 0.25 p.u. [19]-[20]. Therefore it is reasonable to assume that under the same solar irradiance and same temperature, the PV inverter can keep constant output power no matter how the PCC voltage fluctuates. Then the PV inverter can be modeled as a **negative** P-Q load at the fundamental frequency (see Figure 2.11), where  $P$  is a function of the solar irradiance  $Irr$  and temperature  $T$ :  $P = f(Irr, T)$ .

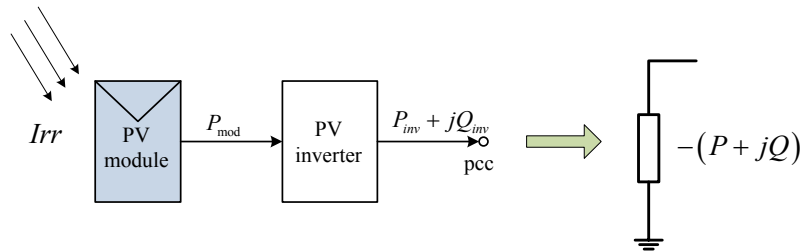


Figure 2.11 Fundamental model of PV inverter

Recall equation (2.2) in Section 2.1.1, the PV array output power is,

$$P_{\max}(T) = P_{\max\_STC} [1 - 0.0045(T - 25)] \quad (2.3)$$

where:

$T$  is the PV cell temperature ( $^{\circ}\text{C}$ );

$Irr$  is the projection of solar irradiance ( $W/m^2$ ) into the normal vector direction of the PV module;

$P_{max\_STC}$  is the maximal power under the Standard Test Condition ( $Irr = 1000W/m^2$ ,  $T = 25^\circ C$ ).

According to the discussion in Section 2.1.1 and the field measurement result in [24], the maximal DC power produced by the PV module is proportional to the solar irradiance it received. However, if the DC power exceeds the maximal power rating, the exceeding part is “cut off” by the PV inverter,

$$P_{mod}(T) = \min\left(\frac{Irr}{1000 W/m^2} \times P_{max}(T), P_{max}(T)\right) \quad (2.4)$$

Based on the operation efficiency of the PV inverter (set 0.96 as a typical value), the AC power transmitted to the grid is,

$$P(T) = P_{inv}(T) = \eta_{inv} P_{mod}(T) = 0.96 \min\left(\frac{Irr}{1000 W/m^2} \times P_{max}(T), P_{max}(T)\right) \quad (2.5)$$

In addition, the PV cell temperature  $T$  can be replaced by the atmosphere temperature  $T'$  if  $T$  value is unavailable.

### **B. Reactive Power Calculation**

Figure 2.12 shows the 24-hour measurement data of a practical PV inverter on a cloudy day. The following electrical features can be concluded accordingly:

- During the night, the PV inverter doesn't generate real power. The inverter acts as a small-capacity STATCOM because its filter capacitor and controller still generates the reactive power. The PV inverter cannot be regarded as open circuit.
- The value of  $Q$  keeps roughly constant no matter how  $P$  fluctuates during the day.

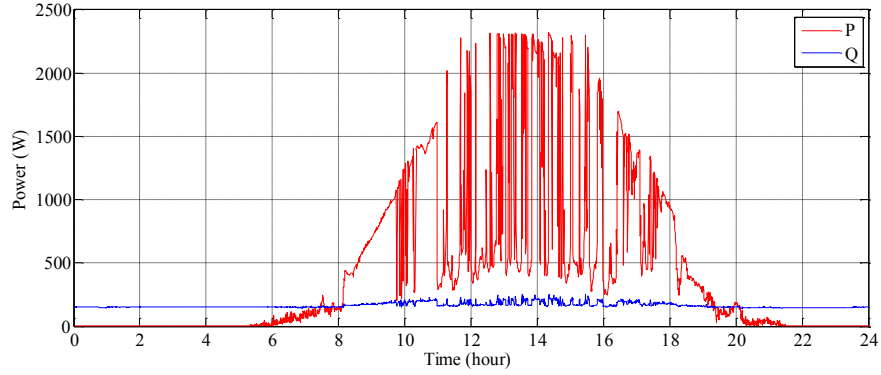


Figure 2.12 PV output power (measured in Edmonton, June 24, 2013)

Generally  $Q$  is much smaller than  $P$ . Therefore  $Q$  can be assumed zero for simplification and the PV inverter is modeled as a constant power element at the fundamental frequency (under constant solar irradiance).

### 2.2.2 Verification of the Fundamental Frequency Model

In this subsection, we will verify the constant power model by studying the statistical correlation between PV power and voltage from the measurement data. According to the definition of load classification:

$$\frac{P}{P_{rated}} = \left( \frac{V}{V_{rated}} \right)^\alpha \quad (2.6)$$

If  $\alpha = 2$ , the element is a constant impedance;

If  $\alpha = 1$ , the element is a constant current source;

If  $\alpha = 0$ , the element is a constant power.

Figure 2.13 (a) shows the measured output power and voltage profile of a PV inverter during a whole day (the time interval of the data is 0.5 minutes). A 30-min partial amplitude is presented in Figure 2.13 (b). When a voltage step change happens, from 247.0V to 252.5V, the power almost remains constant at this time step. Due to some dynamic process inside the PV inverter, the output power cannot keep exactly constant and  $\alpha$  cannot be exactly 0. Therefore a statistical

method is proposed to verify whether the PV inverter can be approximated as a constant power model under the constant solar irradiance condition.

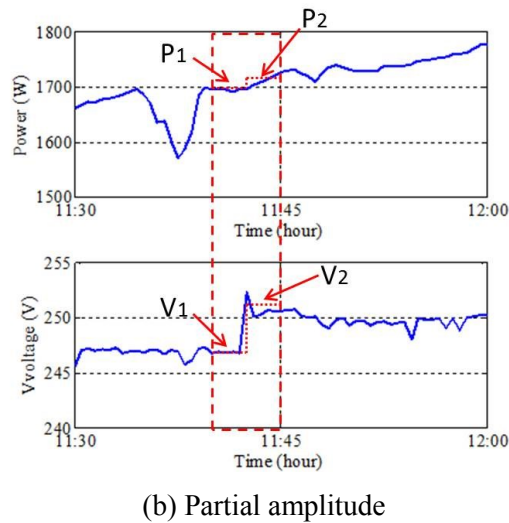
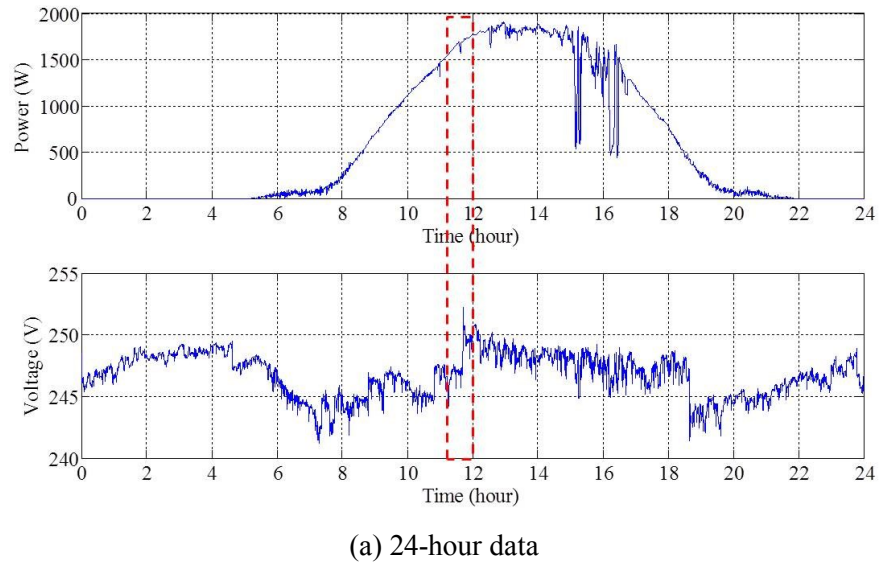


Figure 2.13 PV output power and PCC voltage (measured in Edmonton, June 28, 2013)

**Step 1:** From the multi-day PV measurement data, select the 4-minute data segment containing the voltage rising or falling edge ( $|\Delta V| > 1V$ ), as shown in Figure 2.13 (a). Define  $t_1$  and  $t_2$  as the snapshot before and after the voltage change. Note: if a data segment contains both a voltage step change and a large power step change (say,  $|\Delta P| > 0.1P_{rated}$ ), this segment cannot be selected because

the “constant solar irradiance” condition is not satisfied (the big power change is caused by the solar irradiance transient).

**Step 2:** Calculate the moving average of the voltage and power segment near the voltage rising/falling edge, as shown in Figure 2.13 (b).

$$V_1 = \frac{V(t_1 - 3) + V(t_1 - 2) + V(t_1 - 1) + V(t_1)}{4}$$

$$V_2 = \frac{V(t_2) + V(t_2 + 1) + V(t_2 + 2) + V(t_2 + 3)}{4}$$

The calculation of  $P_1$  and  $P_2$  are similar to  $V_1$  and  $V_2$ . Since the data resolution is 0.5 minutes, the duration of  $V_1$  segment and  $V_2$  segment is 4 minutes, during which the solar irradiance can be regarded as constant.

**Step 3:** Calculate the power and voltage increment  $\Delta P$  and  $\Delta V$  respectively; then the  $\alpha$  index is obtained. If  $\alpha < 0.5$ , it is reasonable to consider the PV inverter as a constant power model.

$$\begin{aligned} \Delta P &= P_2 - P_1 \\ \Delta V &= V_2 - V_1 \end{aligned} \quad (2.7)$$

The following is a method for calculating the  $\alpha$  index:

$$\begin{cases} \frac{P_1}{P_{rated}} = \left( \frac{V_1}{V_{rated}} \right)^\alpha \\ \frac{P_2}{P_{rated}} = \left( \frac{V_2}{V_{rated}} \right)^\alpha \end{cases} \quad (2.8)$$

Formula (2.8) is simplified to:

$$\frac{P_2}{P_1} = \left( \frac{V_2}{V_1} \right)^\alpha \quad (2.9)$$

$$\alpha = \ln \left( \frac{P_2}{P_1} \right) / \ln \left( \frac{V_2}{V_1} \right) \quad (2.10)$$

Since  $\frac{\Delta P}{P_1}$  and  $\frac{\Delta V}{V_1}$  are basically less than 2%,  $\alpha$  is expressed as:

$$\alpha = \frac{\ln\left(\frac{P_1 + \Delta P}{P_1}\right)}{\ln\left(\frac{V_1 + \Delta V}{V_1}\right)} = \frac{\ln\left(1 + \frac{\Delta P}{P_1}\right)}{\ln\left(1 + \frac{\Delta V}{V_1}\right)} \approx \frac{\frac{\Delta P}{P_1}}{\frac{\Delta V}{V_1}} \triangleq \Delta P_{pu} \quad (2.11)$$

Formula (2.11) indicates that the index  $\alpha$  approximate to the ratio between power changing rate and voltage changing rate.

According to the proposed method, 9 suitable data segments are selected from the two-week measurement data and processed according to the above method, the correlation between  $\Delta P_{pu}$  and  $\Delta V_{pu}$  is shown in Figure 2.14.

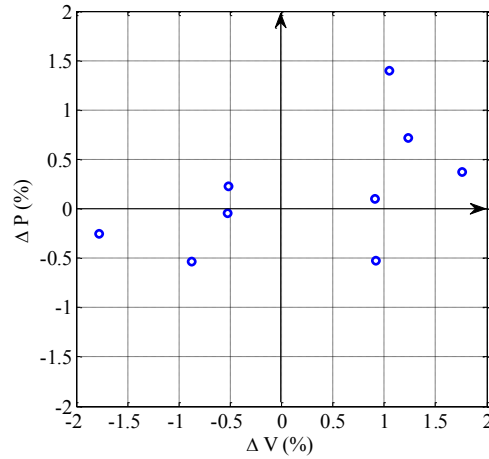


Figure 2.14 Correlation power and voltage changing rate

Then the average  $\alpha$  is:

$$\bar{\alpha} = \sqrt{\frac{\sum_{i=1}^9 \alpha_i^2}{9}} = 0.41$$

The field data analysis indicates that the power change caused by the voltage step change is quite small and the PV output power is not obviously affected by the PCC voltage. Therefore it is accurate to model the PV system as a negative  $P$  load for power flow calculation.

### 2.3 Modeling of PV Inverters at the Harmonic Frequency

According to the general circuit topology of the PV inverter (shown in Figure 2.15), the low order harmonic modeling consists of two steps:

- 1) Properly model the inverter bridge output terminal that has a harmonic source characteristic;
- 2) Model the low-pass filter that has a harmonic impedance characteristic.

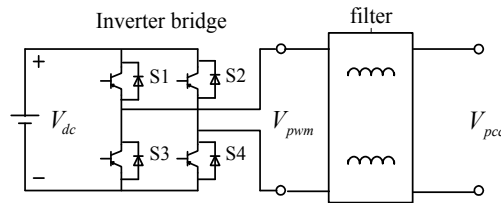


Figure 2.15 Single-phase PWM inverter

Step 2 can be achieved when the filter topology and parameters are obtained. The following is a discussion on how to implement Step 1. For a PWM inverter, the inverter bridge output can be expressed as a deterministic voltage source  $V_{pwm}(t)$  in the steady-state operation:

$$V_{pwm}(t) = V_{dc} \times S(t) \quad (2.12)$$

where,

$S(t)$  is the time-domain representation of the switching function,  $S(t)$  equals to 0 or 1 depending on the switch-on state of the device;

$V_{dc}$  is the DC-link voltage.

Equation (2.12) indicates that the DC-link voltage and PWM switching function are two factors for determining the harmonic spectrum of inverter bridge output voltage  $V_{pwm}(t)$ . Therefore, in the next two subsections, the harmonic characteristic of the switching function and the DC-link voltage will be discussed in detail, providing the PV inverter modeling with theoretical basis.



### 2.3.1 The Switching Function of the Single-Phase PWM Inverter

Figure 2.16 shows the PWM modulation principle. During the positive half cycle, when the reference signal is higher than the carrier signal ( $m(t) > V_{cr}(t)$ ), the switches (S1, S4) are on; otherwise the switches are off. During the negative half cycle, the switches (S2, S3) work in a similar way. Using this technique, the magnitude and phase angle of the inverter output voltage can be directly controlled by adjusting the magnitude  $M_a$  and phase angle  $\varphi$  of the reference signal.

$$m(t) = M_a \cos(\omega t - \varphi) \quad (2.13)$$

$$m(t) \xrightarrow{\text{sampling method}} S(t)$$

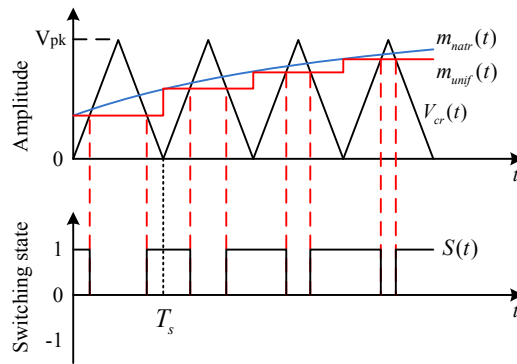


Figure 2.16 Sampling method and the resultant PWM switching function

There are two kinds of PWM implementation: **natural sampling** (the reference signal is represented by  $m_{natr}(t)$ ) and **uniform sampling** (the reference signal is represented by  $m_{unif}(t)$ ), shown in Figure 2.16. For the uniform sampling, the reference signal update is performed only at the beginning of each modulation period  $T_s$  [11]. It is expected that if the switching frequency is higher,  $m_{unif}(t)$  is closer to  $m_{natr}(t)$ .

Figure 2.17 shows an example of the PWM switching function  $S(t)$  based on the uniform sampling implementation. In this example, the modulation index  $M_a = 0.9$ , and the switching frequency is 3600Hz (60<sup>th</sup> order). The FFT calculation is done to the function  $S(t)$  with a very high sampling rate of 8333 point/cycle

( $=5 \cdot 10^5 / 60$ , to simulate the 500kHz sampling frequency). The numerical harmonic spectrum is expressed by (2.14).

$$S(t) = \sum_{h=1}^H |S_h| \cos(h\omega t + \varphi_h) \quad (2.14)$$

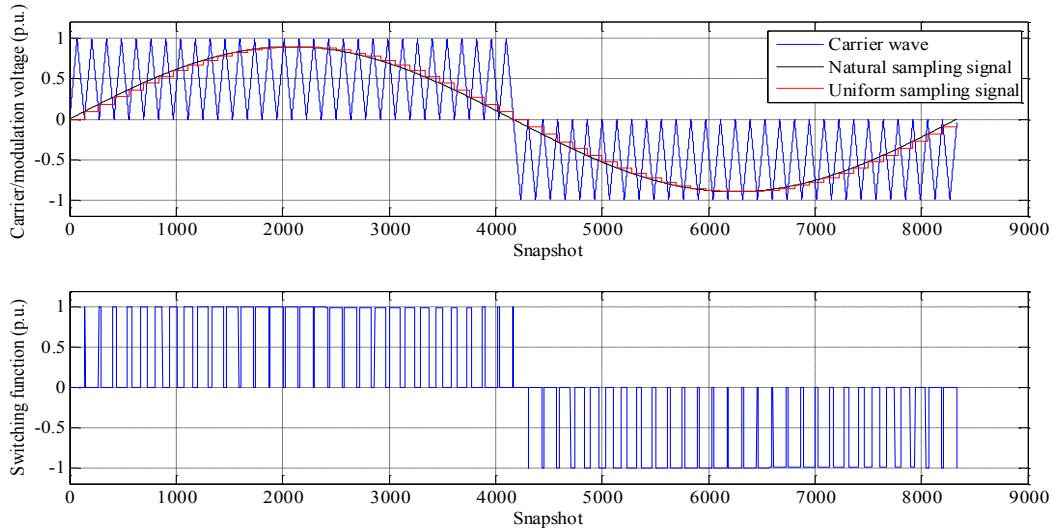
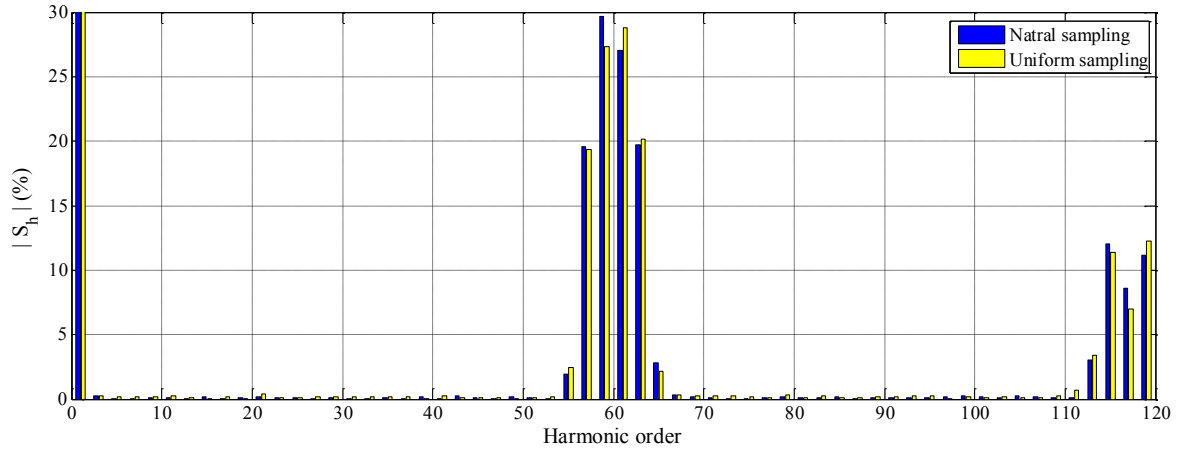


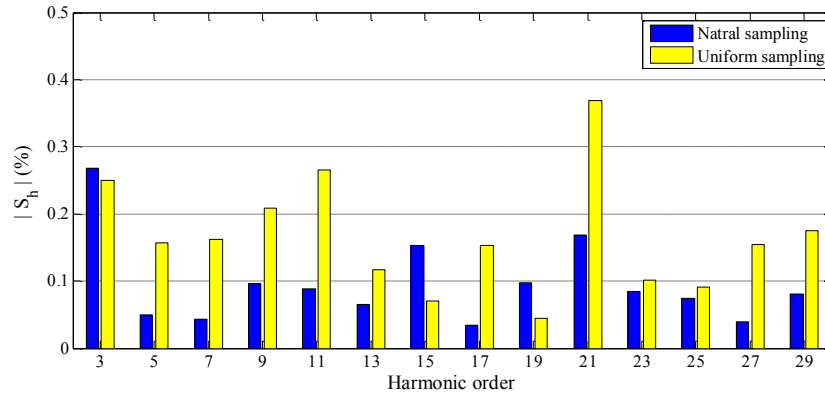
Figure 2.17 Sampling method and PWM switching function

Then the harmonic spectrum of the switching function is obtained. The magnitude of the harmonic spectrum  $|S_h|$  ( $h = 1, 3, 5 \dots$ ) is presented in Figure 2.18 (the even-order harmonics are not shown because their magnitudes are much less than that of odd-order harmonics). The following conclusions can be made:

- The low-order harmonics still exist in the switching function even if the reference signal is purely sinusoidal. However, the low-order harmonics are much smaller than the switching frequency harmonics.
- Compared with the natural sampling, the uniform sampling leads to a higher low-order harmonic component. Besides, the sampling method has little impact on the switching frequency harmonics.



(a) Full spectrum



(b) Partial amplitude

Figure 2.18 Harmonic spectrum of the switching function

The switching frequency of a practical PV inverter is fixed. However, for various types of PV inverters, the switching frequency is different. Figure 2.19 presents the harmonic spectrum of switching functions with three switching frequencies. In this sensitivity study the uniform sampling method is applied. As the figure reveals, the low-order harmonic spectrum is quite arbitrary: there is no deterministic relation between the low-order harmonic magnitude and the switching frequency. However, the IHD of the low-order harmonic is typically less than 0.5%.

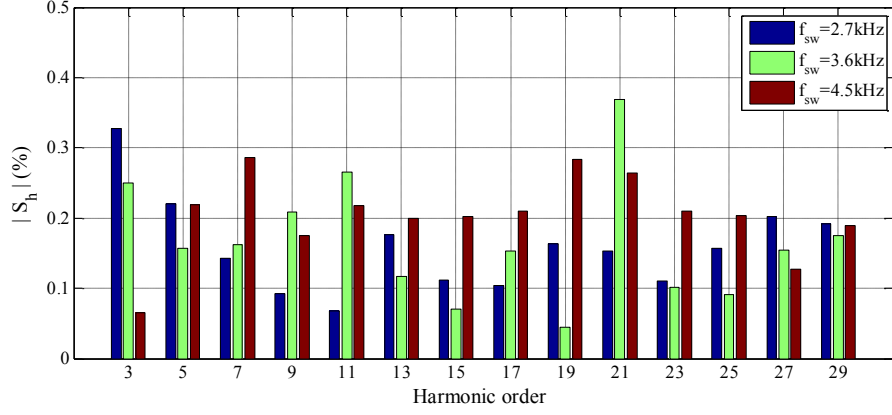


Figure 2.19 Harmonic spectrum of the switching function with different switching frequency

Furthermore, the low-order harmonic spectrum of the PWM switching function can be analyzed through complex deduction. Reference [30] proposed a double-Fourier time-domain switching function of PWM inverter:

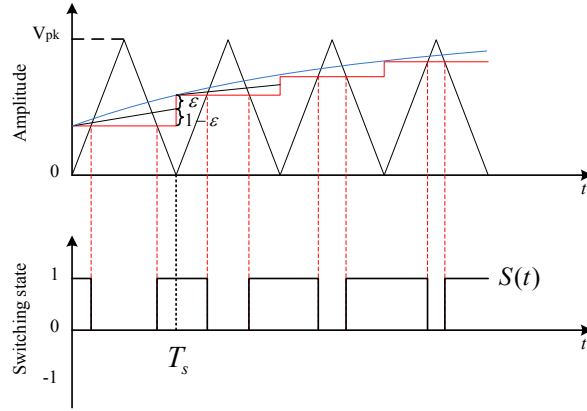


Figure 2.20 Modulation process using enhanced sampling for two-level PWM inverter

$$\begin{aligned}
 S(t) = & \sum_{h=1,3,\dots}^{\infty} \frac{4J_h\left(\frac{hp\varepsilon M_a \pi}{2}\right)}{hp\varepsilon\pi} \sin\left(h\omega_f t - \frac{hp\varepsilon\pi}{2}\right) + \\
 & \sum_{m=1,2,\dots}^{\infty} \sum_{\dots}^{\pm\infty} (-1)^{\frac{m+1}{2}} \frac{4J_0\left(\frac{mM_r \pi}{2}\right)}{m\pi} \sin\left((m\omega_c t + h\omega_f t) - \frac{hp\varepsilon\pi}{2}\right)
 \end{aligned} \tag{2.15}$$

where:

$\omega_f$  is the modulation frequency, which equals to the grid voltage frequency;

$\omega_c$  is the carrier wave frequency;

$$p = \frac{1}{M_R}, \text{ and } M_R \text{ is the modulation ratio } M_R = \frac{\omega_c}{\omega_f};$$

$\varepsilon$  is the sampling factor, the definition is shown in Figure 2.20. “ $\varepsilon = 1$ ” represents the uniform sampling;

$M_a$  is the modulation index, the magnitude of the PWM reference signal;

$J_h(x)$  is the Bessel function of the first kind, order  $h$ ;

Note: The first term on the right-hand side of (2.15) includes low-order odd harmonics  $h\omega_m$  for  $h = 1, 3, 5, \dots$ . The second term represents switch-frequency harmonics  $m\omega_c + h\omega_m$ , for  $m = 1, 2, \dots$  and  $h = \pm 1, \pm 3, \pm 5, \dots$

Formula (2.15) indicates that the switching function contains characterized low-order harmonic components. Furthermore, the low-order harmonic spectrum mainly depends on the carrier wave frequency  $\omega_c$  and the sampling factor  $\varepsilon$ .

### 2.3.2 The Characteristic of the DC-link Voltage

This subsection discusses whether the DC-link voltage can be regarded as a constant DC voltage source. If it can be, the harmonic analysis of the inverter is greatly simplified.

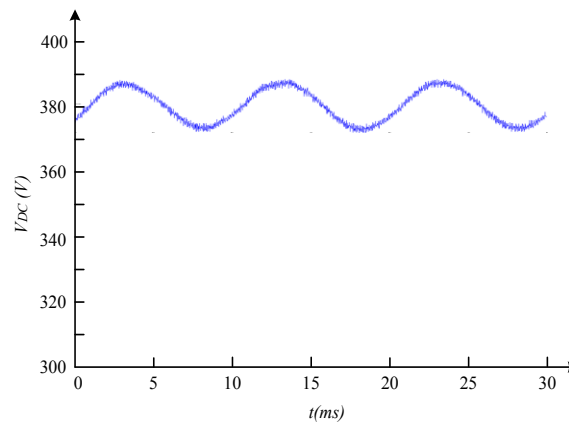


Figure 2.21 Measured DC-link voltage waveform [27]

The DC voltage control block in the PWM controller can decouple the DC-link voltage from the grid voltage [27]. As is shown in Figure 2.21, the measured DC-link voltage waveform is approximately constant except for the double-frequency

harmonic and noises. The following is a discussion on the mechanism of double-frequency harmonics and its impact on the inverter bridge output voltage.

Figure 2.22 illustrates the relationship between the input power and output power for a single-phase PV inverter. Because of the transient power difference, the PV inverter always needs energy storage capacitor for balancing the instantaneous energy between the input and the output. This capacitor is placed in front of the inverter as shown in Figure 2.22 (b).

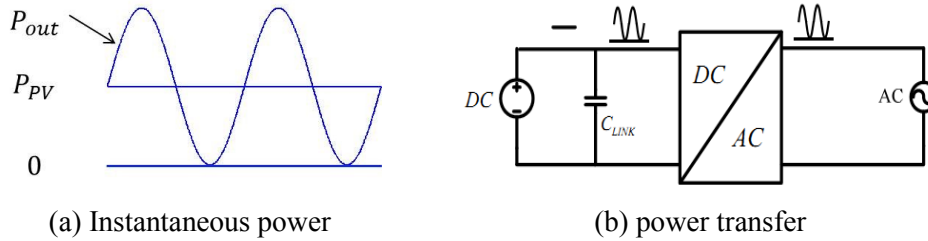


Figure 2.22 Input power and output power for a single-phase PV inverter

For a grid-tied PV inverter, the output current should be in phase with the grid voltage. Thus, the output power can be expressed as [28]:

$$P_{out}(t) = \sqrt{2}V_g \cos(\omega_g t) \cdot \sqrt{2} \frac{P_{PV}}{V_g} \cos(\omega_g t) = P_{PV} - P_{PV} \cos(2\omega_g t) \quad (2.16)$$

where  $P_{out}(t)$  is the instantaneous output power of the inverter;  $P_{PV}$  is the DC power from the input PV panels, and  $V_g$  is the grid voltage magnitude. Then the energy stored in the capacitor can be calculated as below:

$$\int [P_{out}(t) - P_{PV}] \cdot dt = \frac{1}{2} CV_{C_{max}}^2 - \frac{1}{2} CV_{C_{min}}^2 \quad (2.17)$$

Thus, the peak-to-peak value of the voltage ripple can be obtained as below:

$$V_{rip} = \frac{P_{PV}}{\omega_g C_{DC} V_{DC}} \quad (2.18)$$

Theoretically, we can mitigate the  $V_{rip}$  by increasing the size of the DC-link capacitor. However, a large capacitor will increase the cost of the PV inverter. Using the parameters of a practical PV inverter,

$$P_{PV}=3000W, C_{DC}=2350\mu F, V_{DC}\approx 420V$$

The double-frequency voltage ripple is calculated:  $V_{rip} = 0.02V_{dc}$ . The inverter output voltage is expressed as,

$$\begin{aligned} V_{pwm}(t) &= [V_{dc} + 0.01V_{dc} \sin(2\omega t + \varphi_{rip})] \bullet \\ &= V_{dc} [S(t) + 0.01 \sin(2\omega t + \varphi_{rip})S(t)] \\ &= V_{dc} [S(t) + S'(t)] \end{aligned} \quad (2.19)$$

where  $S(t) = |S_1| \cos(\omega t + \varphi_1) + |S_3| \cos(3\omega t + \varphi_3) + |S_5| \cos(5\omega t + \varphi_5) + \dots$ .

Formula (2.19) indicates that the effect of the DC voltage ripple on the voltage  $V_{pwm}(t)$  is equivalent to modifying the switching function  $S(t)$  by adding the term  $S'(t)$ . It should be noted that  $|S_i| \ll 1$  when  $i > 1$ , thus

$$S'(t) \approx 0.01 \sin(2\omega t + \varphi_{rip}) \times |S_1| \cos(\omega t + \varphi_1)$$

By expand  $S'(t)$ , its harmonic spectrum is obtained.

$$\begin{aligned} S'(t) &= 0.01 \sin(2\omega t + \varphi_{rip}) |S_1| \cos(\omega t + \varphi_1) \\ &= 0.005 |S_1| \cos(\omega t + (\varphi_{rip} - \varphi_1 - 90^\circ)) + 0.005 |S_1| \cos(3\omega t + (\varphi_{rip} + \varphi_1 - 90^\circ)) \end{aligned} \quad (2.20)$$

Based on the phase angle difference between  $S(t)$  and  $S'(t)$ , the double-frequency ripple of DC-link voltage can increase or decrease the 3<sup>rd</sup> harmonic of the inverter terminal voltage by up to 0.5% of the fundamental. Besides, the ripple doesn't affect other harmonic orders of the inverter output voltage. For the purpose of PV inverter harmonic modeling, it is reasonable to approximate the DC-link as a constant DC voltage source. This approximation only leads to a

small error in 3<sup>rd</sup> harmonic. In addition, many DC-link control strategies have been proposed to mitigate the 2<sup>nd</sup> ripple of the DC-link voltage [27].

### 2.3.3 Harmonic Model of PV

Theoretical analysis in 2.3.1 and 2.3.2 has reached two main conclusions:

- The switching function contains small amount of low-order harmonic components;
- The DC-link can be modeled as constant DC voltage source and be decoupled from the DC/DC converter.

Based on the above two conclusions, the inverter terminal voltage can be represented as a combination of voltage sources at each odd harmonic order.

$$\begin{aligned}
 m(t) &\xrightarrow{\text{Sampling method}} S(t) \\
 S(t) &= \sum_{h=1,3}^H \sqrt{2} |S_h| \cos(h\omega t + \varphi_h) \\
 V_{pwm}(h) &= V_{dc} \times S(h)
 \end{aligned} \tag{2.21}$$

where  $S(h) = |S_h| e^{j\varphi_h}$  is obtained by the FFT calculation of the switching function  $S(t)$ . Note: the FFT sampling rate should be high enough so that an accurate harmonic spectrum of  $S(t)$  is obtained, and a minimum of 5000 points per cycle is recommended.

An exemplary harmonic spectrum of  $V_{pwm}(t)$  is presented in Figure 2.23.

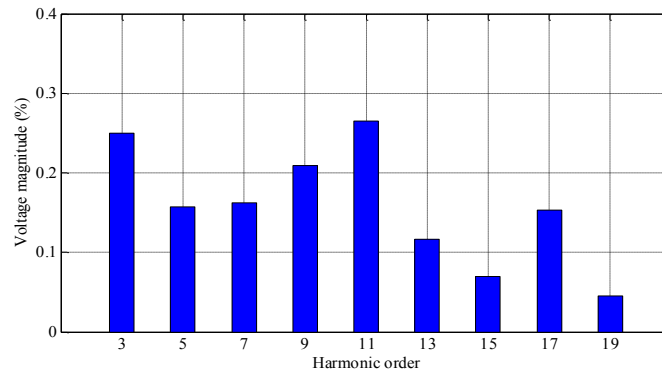
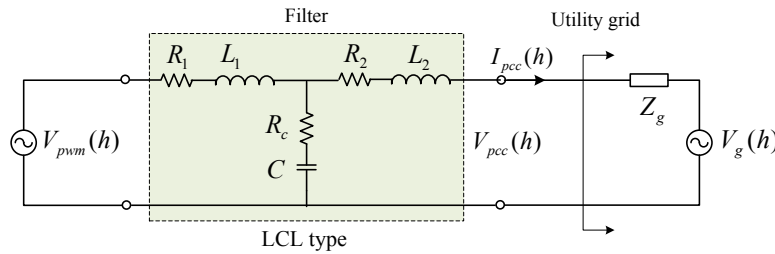


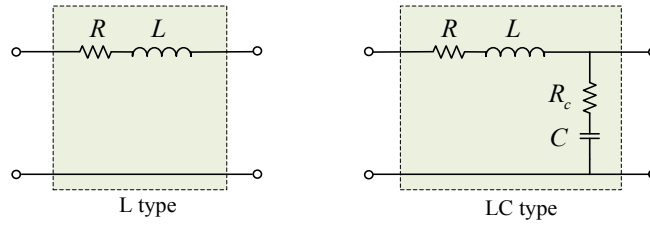
Figure 2.23 Harmonic spectrum of inverter terminal voltage



It has been proved theoretically that at each harmonic order, the inverter bridge output acts as an independent voltage source  $V_{pwm}(h)$ . In addition, a filter is installed between the inverter bridge output terminal and the grid PCC. Therefore, at the harmonic frequency the PV inverter can be modeled as a voltage source and an LCL filter block, as shown in Figure 2.24 (a). In addition, there are two alternative kinds of filter topologies being applied to the PV inverter, as shown in Figure 2.24 (b).



(a) PV inverter model



(b) Filter topologies

Figure 2.24 Harmonic model of PV inverter

According to the Superposition Law, the harmonic current at PCC is the combined effect of two voltage sources: the inverter bridge voltage source  $V_{pwm}(h)$  and the grid voltage source  $V_g(h)$ . Taking LCL filter as an example, the total harmonic current through the PCC is calculated by (2.22).

$$I_{pcc}(h) = \frac{V_{pwm}(h)}{Z_1(h) + Z_c(h) \parallel (Z_2(h) + Z_g(h))} \times \frac{Z_c(h)}{Z_c(h) + (Z_2(h) + Z_g(h))} - \frac{V_g(h)}{Z_1(h) \parallel Z_c(h) + (Z_2(h) + Z_g(h))} \quad (2.22)$$

where:

$$Z_1(h) = R_1 + jh\omega L_1;$$

$$Z_c(h) = R_c + \frac{1}{jh\omega C};$$

$$Z_2(h) = R_2 + jh\omega L_2;$$

$Z_g(h) = R_g + jh\omega L_g$  is the equivalent impedance of the grid;

$V_{pwm}(h)$  is the inverter bridge output harmonic voltage;

$V_g(h)$  is the grid harmonic voltage.

### 2.3.4 Discussion on the Harmonic Model

The harmonic model discussed in Section 2.3 is based on the assumption that the control block only regulates the fundamental voltage/current of the PV inverter. This subsection presents a brief survey of the general control method in the PV inverter manufacture, confirming the assumption.

#### A. Practical Control Strategy in Industry

The basic VSC control strategy is divided into three types: 1) constant voltage control, 2) constant current control, and 3) constant power control. The grid-tied PV inverters usually adopt the constant power control, as shown in Figure 2.25.

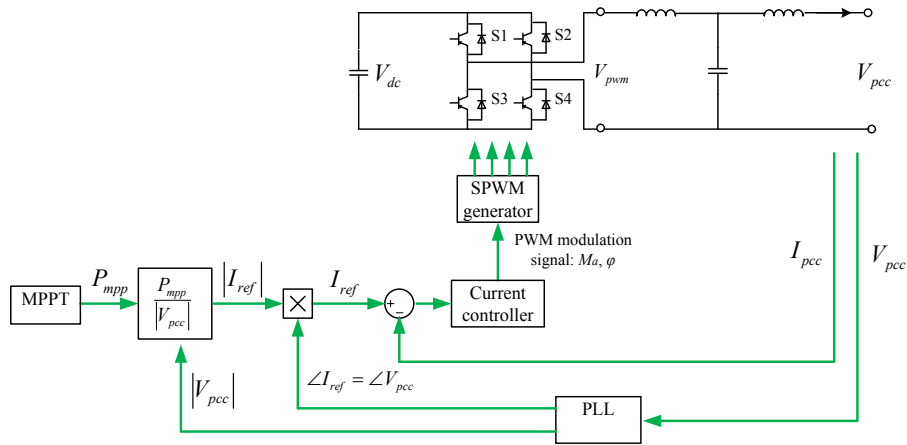


Figure 2.25 PV inverter constant power control

Generally, these control methods only directly regulate the fundamental voltage and current with close-loop control. There is neither harmonic voltage nor harmonic current feedback element in the control scheme [31]. Therefore the

harmonic spectrum of  $V_{pwm}$  is independent of the grid harmonic voltage. Then the inverter bridge can be modeled as an independent harmonic voltage source.

### **B. Harmonic Compensation Control and Its Impact on PV Harmonic Model**

In recent years, researches have been done on the harmonic compensation of VSCs [32]. The basic consideration is to add harmonic feedback element so that the VSC can actively mitigate the harmonic current or the harmonic voltage at the PCC.

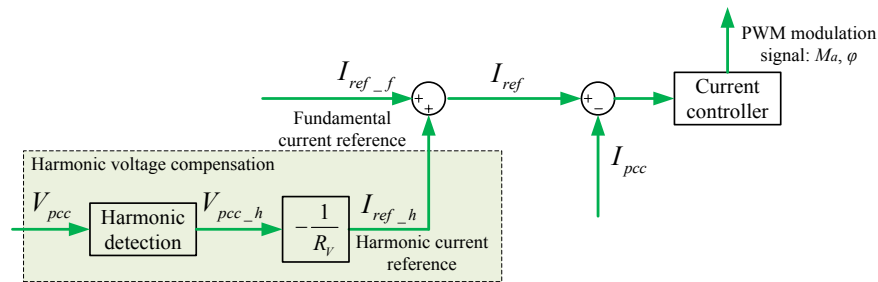


Figure 2.26 Part of the power control block with harmonic compensation

In this method, the current reference  $I_{ref}$  contains both fundamental and harmonic components. The harmonic components are generated by the harmonic feedback control block, as shown in Figure 2.26. A power electronic interfacing converter is utilized to improve the voltage quality of a power distribution system via harmonic voltage compensation. The harmonic voltage at the PCC is extracted to control the PV inverter as a small damping resistor at “selected” harmonic frequencies. The effect of the internal impedance term is to introduce an additional harmonic voltage for the inverter output voltage [32].

However, these harmonic compensation control methods have not been adopted by the PV inverter manufacture [31]. In case the harmonic control methods are applied, the harmonic spectrum of  $V_{pwm}$  will be related to the controller parameters at the “selected” harmonic orders. Thus the inverter bridge is modeled as a controlled voltage source. For other “unselected” harmonic orders, the bridge is still modeled as an independent voltage source.

## 2.4 Verification Study on the PV Inverter Model - Simulation

In order to investigate the validity of the proposed harmonic model, a PV inverter is simulated in MATLAB-Simulink. In the following, the simulation system is introduced and the simulation result is compared with the result obtained from the analytical harmonic model.

### 2.4.1 Simulation System

The simulation model built in Matlab/Simulink software is presented in Figure 2.27. Since this chapter is focused on the steady-state model, the PWM modulation parameters  $M_a$  and  $\varphi$  can be assumed constant. Therefore the control system is not included in the simulation program. The simulation model includes a DC side circuit, PWM inverter bridge, LCL filter circuit and grid side voltage source. In the system, the DC-link is modeled in two ways:

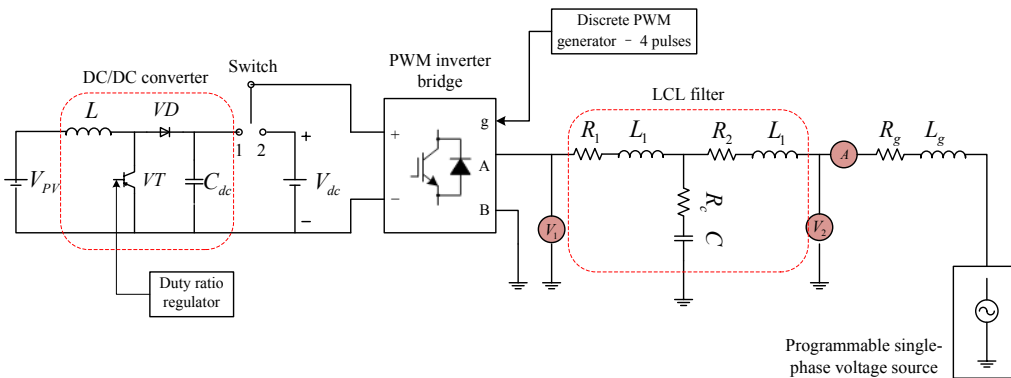


Figure 2.27 Simulated grid-connected PV inverter

- Simulation 1 (turn the switch to “1”): model the DC-link as constant DC voltage source  $V_{dc}$ .
- Simulation 2 (turn the switch to “2”): model the DC-link as a detailed PV inverter circuit. This circuit includes a DC/DC converter and a DC voltage source  $V_{PV}$  that models the PV panel output.

On the AC grid side, a programmable single-phase voltage source models the background harmonic voltage. Table 2.5 lists the parameters of the simulation

system. In addition, the parameters  $V_{dc}$ ,  $V_{PV}$  and the duty ratio of the DC/DC converter are selected to make the PWM inverter operate at the same power level in two simulations.

Table 2.5 Parameter of the PV system

| Components   | Items   | Value                      |
|--------------|---|----------------------------|
| DC-link      | PV panel output voltage $V_{PV}$              | 150V                       |
|              | Boost converter inductor $L$                  | 5 $\mu$ H                  |
|              | DC-link capacitor $C_{dc}$                    | 2350 $\mu$ F               |
|              | DC voltage $V_{dc}$                           | 425V                       |
| PWM Inverter | Modulation frequency $\omega_m$               | 60Hz                       |
|              | Triangle carrier angular frequency $\omega_c$ | 4.8kHz                     |
|              | Modulation index $M_a$                        | 0.85                       |
|              | Modulation index $\varphi$                    | 8.4deg.                    |
| LCL Filter   | Inverter side resistor $R_1$                  | 0.05 $\Omega$              |
|              | Inverter side inductor $L_1$                  | 2.1mH                      |
|              | Grid side resistor $R_2$                      | 0.05 $\Omega$              |
|              | Grid side inductor $L_2$                      | 1.2mH                      |
|              | Damping resistor $R_c$                        | 2 $\Omega$                 |
|              | Shunt capacitor $C$                           | 10.6 $\mu$ F               |
| Grid side    | Grid side voltage source $V_g$                | 257V                       |
|              | Grid side impedance $R_g + jX_g$              | 0.09+j0.055 $\Omega$ @60Hz |

Two simulation scenarios are conducted:

**Scenario 1:** As shown in Figure 2.27, let the grid voltage be sinusoidal and conduct “Simulations 1” and “Simulations 2” in turn. Thus the harmonic spectrum of the PCC current is obtained by the Ampere meter  $A$ .

**Scenario 2:** Add 3rd ~ 19th order harmonic to the grid voltage  $V_g$ , then conduct the two simulations again. Note: the typical grid harmonic voltage spectrum is measured in the lab (shown in Table 2.6).

Table 2.6 Typical grid harmonic voltage spectrum

| Harmonic order | Magnitude (V) | Phase angle (deg.) | Harmonic order | Magnitude (V) | Phase angle (deg.) |
|----------------|---------------|--------------------|----------------|---------------|--------------------|
| 1              | 257           | 0                  | 11             | 2.98          | -91                |
| 3              | 1.42          | -56                | 13             | 1.53          | 71                 |
| 5              | 4.38          | -165               | 15             | 0.23          | 59                 |
| 7              | 2.33          | 72                 | 17             | 0.29          | 42                 |
| 9              | 0.27          | 96                 | 19             | 0.15          | 37                 |

### 2.4.2 Simulation Results and Analysis

In this subsection, three sets of harmonic current spectrums are presented. The first set is obtained from the proposed harmonic model of the PV inverter (Figure 2.24), the second is obtained from “Simulation 1” and the third is obtained from “Simulation 2”. Note that for “Analytical model”, the inverter bridge terminal voltage  $V_{pwm}(h)$  is obtained from equation (2.21) and the harmonic current  $I_{pcc}(h)$  is calculated from equation (2.22). These sets are compared to show the validity and accuracy of the proposed harmonic model.

Figure 2.28 and Figure 2.29 present the harmonic spectrum of the PV inverter output current  $I_{pcc}$  of the two scenarios. The analysis is as follows:

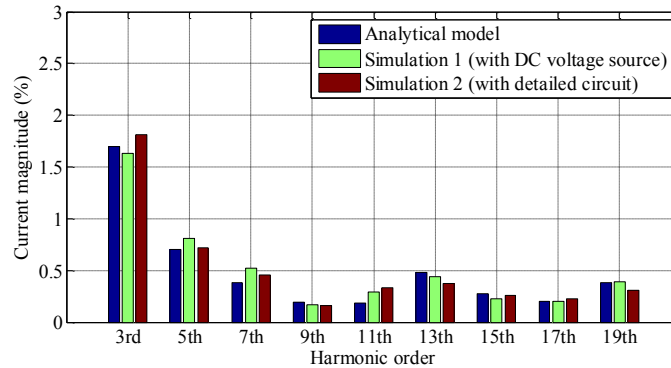


Figure 2.28 Harmonic spectrum of  $I_{pcc}$  (under sinusoidal grid voltage)

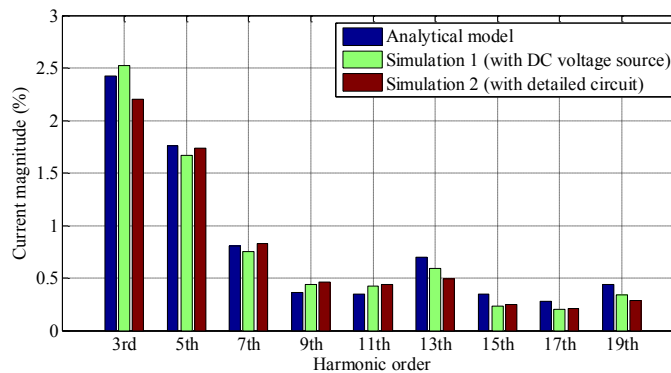


Figure 2.29 Harmonic spectrum of  $I_{pcc}$  (under grid harmonic voltage)

1. The comparison between “Simulation 1” and “Simulation 2”:

When we model the DC link as a DC voltage source and detailed circuit, the simulated harmonic currents through PCC match well for most harmonic orders.

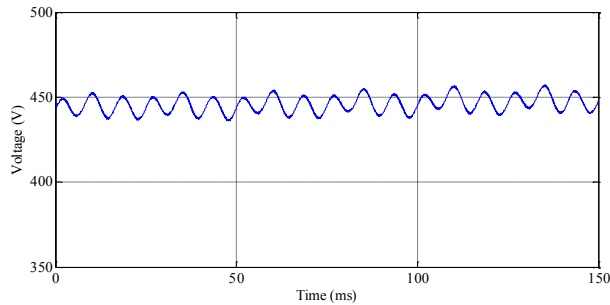


Figure 2.30 Simulated DC-link voltage waveform

The main differences among the two models are 3<sup>rd</sup> harmonic component. In “Simulation 2”, the DC side includes a capacitor. As is analyzed in Section 2.3.2, the DC-link voltage contains double-frequency ripple due to the charging and recharging of the capacitor (shown in Figure 2.30). The ripple modifies the 3<sup>rd</sup> harmonic components of the inverter bridge voltage  $V_{pwm}$  and the inverter output current  $I_{pcc}$ .

2. The comparison between the “Analytical model” and “Simulation 1”:

The harmonic currents obtained from the analytical model approximately match with those obtained from Simulation 1. However, the 11<sup>th</sup> order in Scenario 1 and the 15<sup>th</sup> in Scenario 2 have errors larger than 20%. The main reason is that some small transient exists in the time-domain simulation waveform of  $V_{pwm}(t)$  and the waveform cannot reach the absolute steady-state. As a result, the harmonic spectrum obtained by FFT cannot exactly match the frequency-domain result obtained by the analytical model.

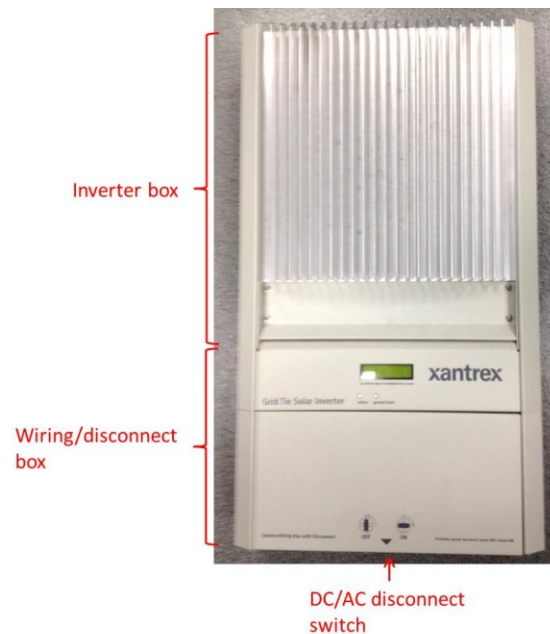
Despite the error in some harmonic orders, overall the harmonic spectrum obtained from the analytical model matches with that obtained from the Simulation 1 and 2. Therefore it is feasible to model the DC-link (inverter bridge input) as a DC voltage source, and further represent the inverter bridge output as an AC voltage source at each harmonic order. Then PV inverter is modeled as a harmonic voltage source and a filter, as shown in Figure 2.24.

## 2.5 Verification Study on the PV Inverter Model – Lab Experiment

In this subsection an experiment will be conducted in order to further verify the proposed harmonic model of the PV inverter. In the experiment we will observe whether the inverter bridge terminal voltage has harmonic interactions with the grid harmonics.

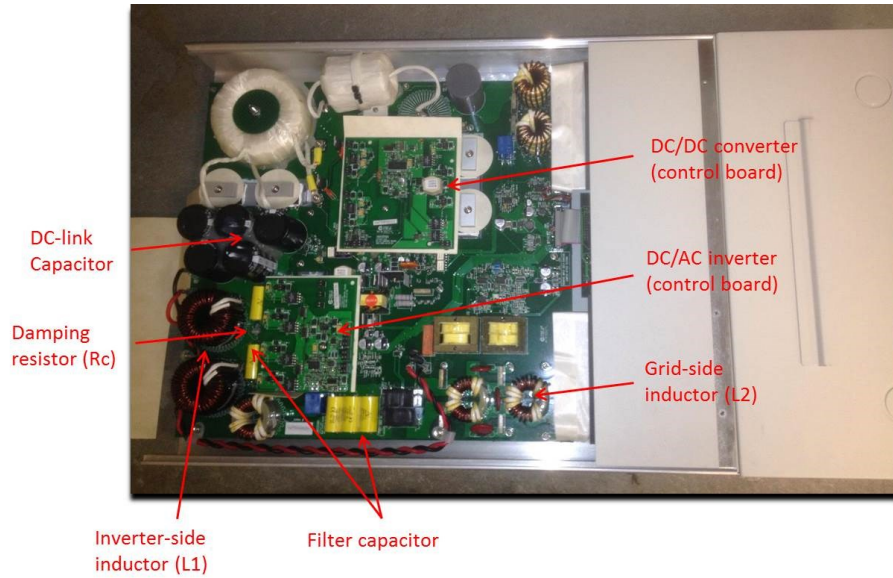
### 2.5.1 Description of the Experimental PV Inverter

In this experiment, the Xantrex Grid-Tied PV Inverter GT3.0-NA-DS-240 is applied. It is designed to convert solar electric power into utility-grid electricity. In order to operate, the inverter must have grid power available and connected. The inverter essentially consists of two separate parts: a PV inverter and a wiring/disconnect box. The front panel and inside circuit of the inverter are shown in Figure 2.31 (a) and Figure 2.31 (b) respectively.



(a) Front panel of Xantrex inverter





(b) Inside circuit board

Figure 2.31 Picture of Xantrex inverter

The basic technical data for the PV inverter is presented in Table 2.7 [20].

Table 2.7 Electrical specification of GT3.0-NA-DS-240

| Item                         | Value                | Remarks |
|------------------------------|----------------------|---------|
| DC input voltage range       | 195 ~ 600V           |         |
| Max. AC power output         | 3000W                |         |
| AC output voltage (nominal)  | 240V                 |         |
| AC output voltage range      | 211 ~ 264V           |         |
| Max. AC current              | 14.2A                |         |
| Current THD (at rated power) | <5%                  |         |
| Power factor                 | >0.9 (nominal power) |         |
| Max. efficiency              | 96.6%                |         |

### 2.5.2 Experiment Principle and Procedure

Unlike the simulation study in which the grid harmonic voltage can be modified, we are not able to observe different levels of grid harmonic voltage within a short period. Therefore an alternative experiment method is proposed.

As is shown in Figure 2.32, insert an inductor  $\Delta X$  in series with the PV inverter so that the grid impedance  $Z_g$  is changed. Thus the harmonic voltage at the PCC is

also changed. In addition, a linear load should be connected in parallel with the inverter to reduce the reverse power flow that is injected into the utility grid.

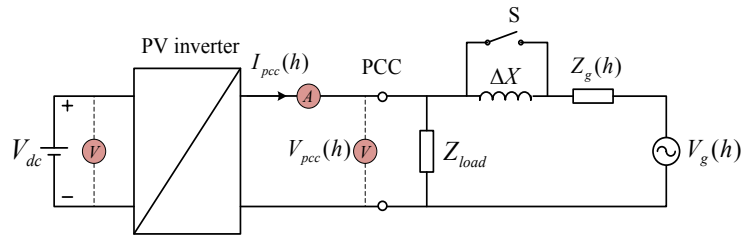


Figure 2.32 Experiment circuit topology

The experiment includes two scenarios:

**Scenario 1:** Close the switcher **S** so that the inductor  $\Delta X$  is short-circuit. Then switch on the PV inverter and keep it operating for about 10 minutes;

**Scenario 2:** Open the switcher **S** so that the inductor is connected to the system. Then follow the same procedure as in Scenario 1.

In each scenario, the measurement data was set continuously sampling (60 cycles/second). Each cycle has 256 snapshots. Three sets of parameters are recorded in the experiment:

- The DC input voltage  $V_{PV}$
- The AC output current  $I_{pcc}$
- The AC integration voltage  $V_{pcc}$

The inverter bridge terminal voltage  $V_{pwm}$  is impossible to measure directly. According to the circuit topology presented in Figure 2.33,  $V_{pwm}$  can be calculated through the measurement data at each time step,

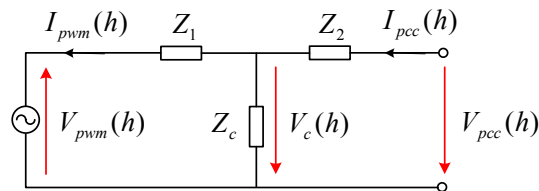


Figure 2.33 PV inverter circuit topology

$$\begin{cases} V_c(h) = V_{pcc}(h) - I_{pcc}(h)Z_2(h) \\ I_{pwm}(h) = I_{pcc}(h) - \frac{V_c(h)}{Z_c(h)} \\ V_{pwm}(h) = V_c(h) - I_{pwm}(h)Z_1(h) \end{cases} \quad (2.23)$$

According to (2.23),  $V_{pwm}$  is expressed as,

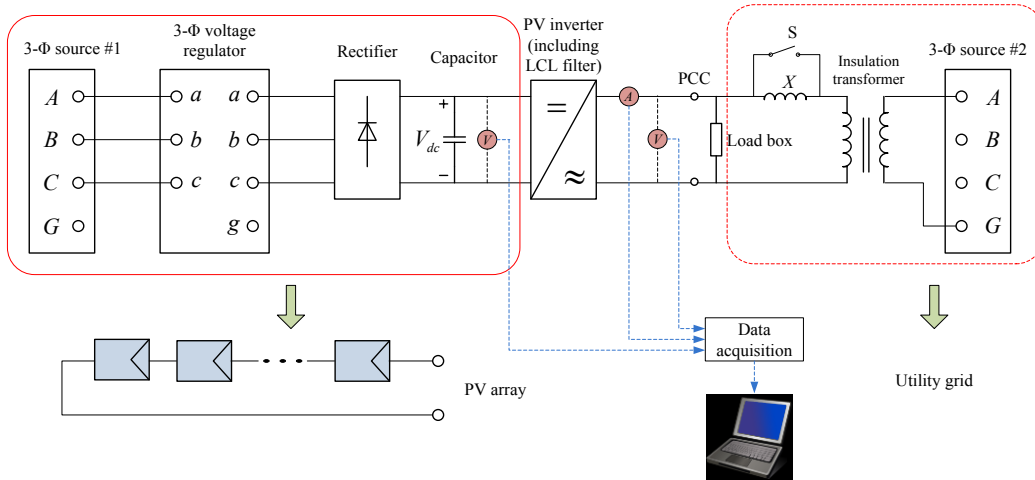
$$V_{pwm}(h) = V_{pcc}(h) - I_{pcc}(h)Z_2(h) - \left( I_{pcc}(h) - \frac{V_{pcc}(h) - I_{pcc}(h)Z_2(h)}{Z_c(h)} \right) Z_1(h) \quad (2.24)$$

Then calculate the average harmonic voltage over a period of time and regard it as the harmonic spectrum of  $V_{pwm}$ .

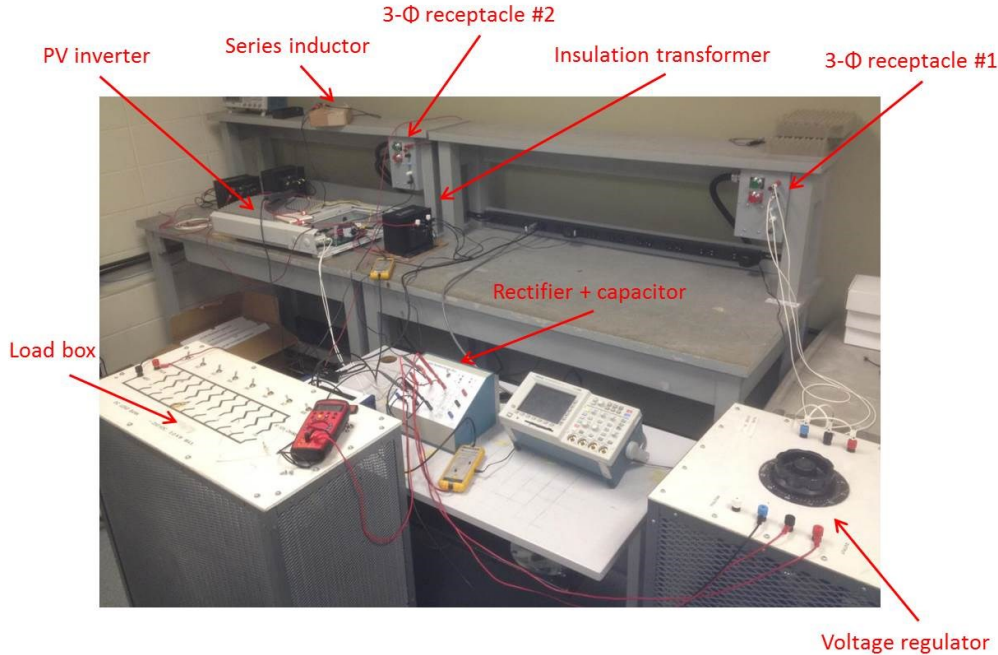
$$\bar{V}_{pwm}(h) = \frac{1}{N} \sum_{n=1}^N V_{pwm}(n, h) \quad (2.25)$$

### 2.5.3 Experiment Implementation

The experiment platform is presented in Figure 2.34. In this experiment, we use three-phase rectifier to generate a sufficient DC voltage supply (>195V) for the PV inverter. The parameter and function of each instrument are shown in Table 2.8.



(a) Practical circuit connection



(b) Instrument set-up

Figure 2.34 The experiment system of PV integration

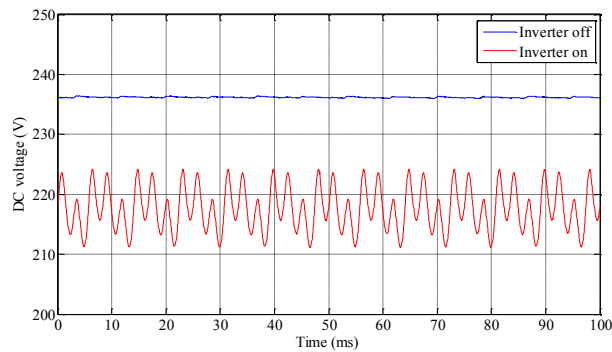
Table 2.8 Parameter and function of the experiment instruments

| Components                                 | Main parameter   | Function/description  |
|--|--|---|
| 3- $\Phi$ source #1<br>3- $\Phi$ source #2 | Phase voltage: 120V<br>Phase voltage: 120V   | Supply the voltage regulator<br>Act as the PCC for PV inverter integration  |
| 3- $\Phi$ voltage regulator                | Phase voltage range: 0~120V  | Generate an appropriate voltage for the rectifier   |
| Rectifier box                              | Maximal AC voltage: 800V ( $V_{peak}$ )<br>Maximal current 25A                             | Generate the DC voltage for the PV inverter   |
| Electrolytic capacitor                     | Maximal voltage: 450V<br>Capacitance: 1440 $\mu$ F   | Mitigate the ripple of DC link voltage  |
| PV inverter                                | Maximal power 3kW<br>DC input voltage range: 195~600V<br>AC output voltage range: 211~264V | The type of PV inverter is Xantrex, GT3.0-NA-DS-240   |
| Inductor                                   | Inductance: 3mH  | The inductor (1.13 $\Omega$ @60Hz) is large enough to affect the system impedance, which is roughly estimated as 0.1 $\Omega$ . |
| Load box                                   | Resistance: 125/N $\Omega$<br>(N = 1~10)   | Consume the AC power generated by PV inverter.  |
| Insulation transformer                     | Truns ratio: 240V/120V   | 1) Boost the receptacle voltage to 240V in order to simulate the 240V phase-to-phase voltage of service panel;                  |

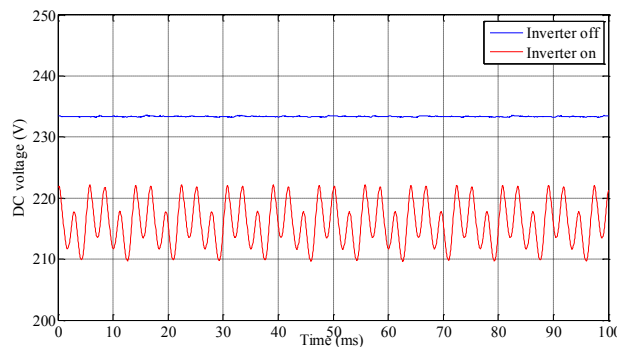
|                  |  |   |
|------------------|--|---|
|                  |  | 2) Insulate the PV inverter, prevent short-circuit. |
| Data acquisition |  | The type is PGSN-DA-08                              |

### 2.5.4 Experiment Result and Analysis

Firstly, we should check the ripple level of the DC-link voltage. Figure 2.35 indicates that when the inverter is switched off, the DC voltage is quite constant. On the contrary, when the inverter is operating with rated power, there is a considerable ripple. However, the ripple ratio  $100 \cdot (V_{max} - V_{min}) / V_{average} = 5\%$  is still acceptable for the PV inverter input.



(a) Scenario 1



(b) Scenario 2

Figure 2.35 Transient DC input voltage of PV inverter

Figure 2.36 shows that the inverter operates at the rated power with obvious power fluctuation. The main reason is that the Volt-Ampere characteristic of rectifier output is a constant voltage source, being different from the Volt-Ampere

characteristic of a practical PV array. Therefore the MPPT controller is always searching for the maximal power point (MPP) and there is a fluctuation in the output power.

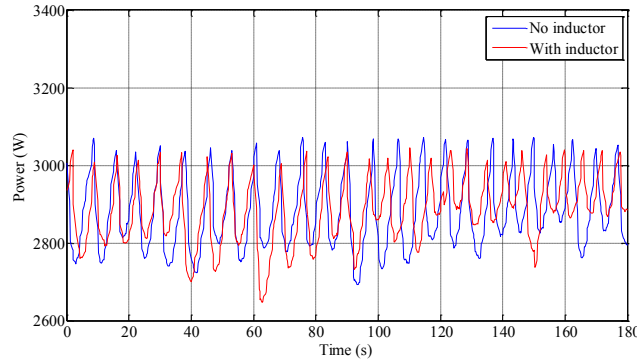


Figure 2.36 Inverter output power under two scenarios

Figure 2.37 indicates that the harmonic spectrum of  $V_{pcc}$  is modified by the series inductor. The fundamental voltages of Scenario 1 and 2 are 258.5V and 256.6V respectively. Figure 2.38 presents the estimated harmonic spectrum of  $V_{pwm}$  in two scenarios. The fundamental voltages of Scenario 1 and 2 are 260.8V and 259.0V respectively. We can observe that the magnitude and phase angle of the harmonic voltages almost match in the two scenarios, which represent the different background harmonic level. This result indicates that the harmonic interaction between  $V_{pwm}$  and  $V_{pcc}$  is quite small. Therefore, at the harmonic frequency, it is reasonable to model the inverter bridge output terminal as an independent voltage source. Consequently the harmonic model of PV inverter is verified.

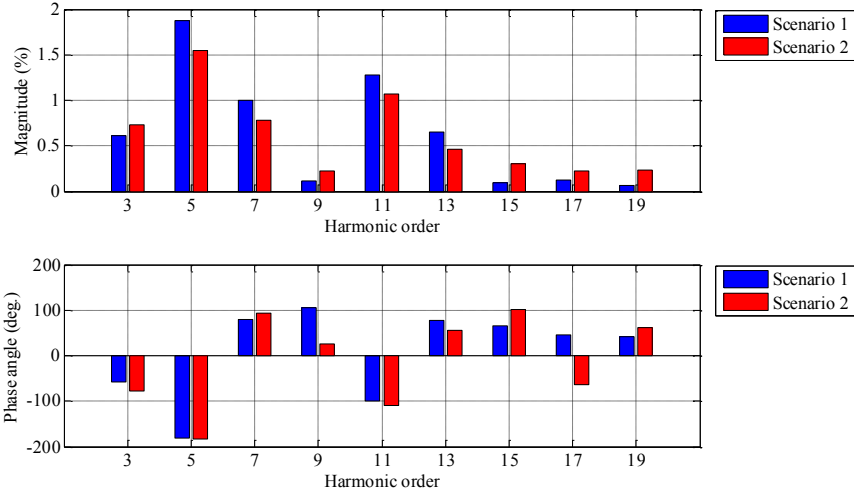


Figure 2.37 Harmonic spectrum of PCC voltage  $V_{pcc}$  (directly measured)

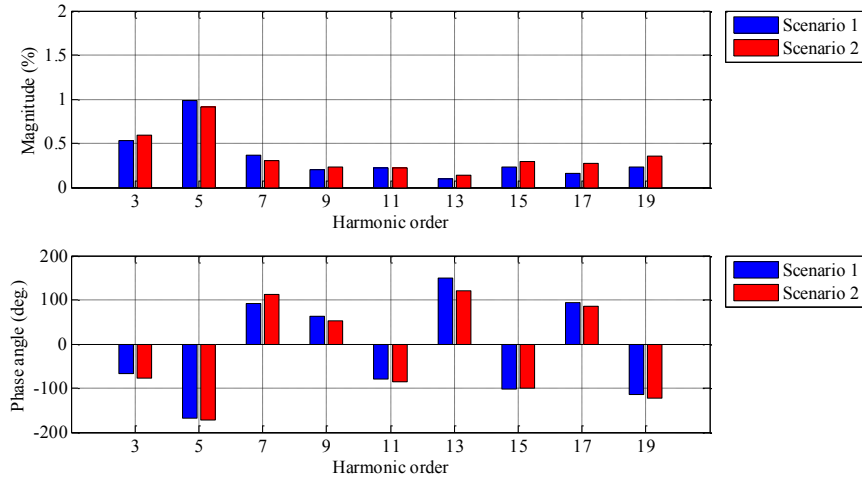


Figure 2.38 Harmonic spectrum of inverter bridge voltage  $V_{pwm}$  (indirectly measured)

## 2.6 Characteristics of the PV Harmonic Model

The harmonic model proposed in Section 2.3.3 described the harmonic source and harmonic impedance characteristics of PV inverters. These two characteristics will be quantified in this section using the practical parameters, as presented in Table 2.9. The filter parameters are measured from a practical PV inverter and the grid impedance is also obtained from field measurement [33].

Table 2.9 Parameter of the PV inverter

| Classification | Items                                   | Value                 |
|----------------|---|-----------------------|
| AC side        | Rated power                             | 3000W                 |
| LCL Filter     | Inverter side resistor $R_1$            | 0.05Ω                 |
|                | Inverter side inductor $L_1$            | 2.1mH                 |
|                | Grid side resistor $R_2$                | 0.05Ω                 |
|                | Grid side inductor $L_2$                | 1.2mH                 |
|                | Damping resistor $R_c$                  | 2Ω                    |
|                | Shunt capacitor $C$                     | 10.4μF                |
| Grid side      | Grid equivalent voltage $V_g$           | 257V                  |
|                | Grid impedance $R_g + jX_g$ (95% index) | 0.09 + j0.055Ω @60Hz  |
|                | Grid impedance $R_g + jX_g$ (5% index)  | 0.008 + j0.015Ω @60Hz |

### 2.6.1 Harmonic Source Characteristics

As a nonlinear element, the PV inverter injects harmonic current to the grid. Assume there is no grid side harmonics, the harmonic current  $I_{pcc}(h)$  is totally caused by the inverter itself, as shown in Figure 2.39.  $I_{pcc}(h)$  is calculated by (2.26).

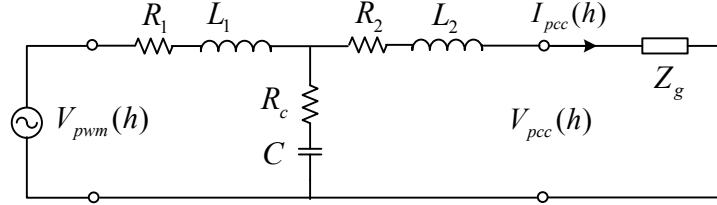


Figure 2.39 Equivalent circuit of PV inverter integration

$$I_{pcc}(h) = \frac{V_{pwm}(h)}{Z_1(h) + Z_c(h) \parallel (Z_2(h) + Z_g(h))} \times \frac{Z_c(h)}{Z_c(h) + (Z_2(h) + Z_g(h))} \quad (2.26)$$

where:

$$Z_1(h) = R_1 + jh\omega L_1; \quad Z_c(h) = R_c + \frac{1}{jh\omega C}; \quad Z_2(h) = R_2 + jh\omega L_2;$$

$$Z_g(h) = R_g + jh\omega L_g;$$

$V_{pwm}(h)$  is the inverter bridge output harmonic voltage.

Since  $Z_g$  is a random variable affected by the grid condition, the field measurement provides the probabilistic distribution of  $Z_g$  [33]. A single index



showing the value that is not exceeded by 95% of the raw data (called the “95% index”) is applied. Two sets of  $Z_g$  (5% index and 95% index) values are used to estimate the  $I_{pcc}(h)$  according to (2.26). Figure 2.40 shows that the harmonic current  $I_{pcc}(h)$  changes very little with the  $Z_g$  fluctuation. The main reason is that  $Z_g$  is much smaller than the total filter impedance.

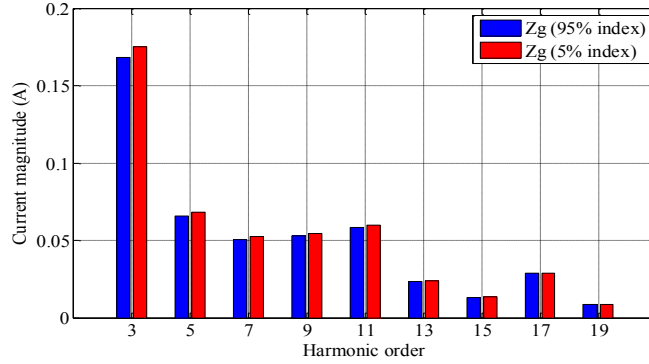


Figure 2.40 Harmonic spectrum of the output current  $I_{pcc}$

In order to compare the harmonic current injection of PVs and other home appliances, an index called the Equivalent-CFL is applied [2]. This index quantifies the harmonic impact of each load by the number of CFLs to which it is equivalent. This index is defined as follows:

$$Ratio_{h\_PV} = \frac{I_{h\_PV}}{I_{h\_CFL}} \quad (2.27)$$

where  $I_{h\_PV}$  is the PV harmonic current magnitude at order  $h$ , and  $I_{h\_CFL}$  is the representative CFL harmonic current magnitude at order  $h$ . In order to obtain a single index and compare the PV with a representative CFL, the ratios of different harmonic orders are aggregated into one value by using a weighted average as follows:

$$Equivalent - CFL_{PV} = \sqrt{\sum_{h=3}^H (w_h \times Ratio_{h\_PV})^2} = \sqrt{\frac{\sum_{h=3}^H I_{h\_PV}^2}{\sum_{h=3}^H I_{h\_CFL}^2}} \quad (2.28)$$

The weighting factor  $w_h$  is the individual harmonic distortion of the CFL current.

Besides PV, other two common home appliances are compared (shown in Table 2.10). Although the power ratio of PV is 200 times of CFL, its harmonic impact is smaller than common nonlinear appliance such as a household.

Table 2.10 Comparing harmonic impact of the PV inverter and home appliances

| Load type                  | CFL  | PV   | Refrigerator | Desktop |
|----------------------------|------|------|--------------|---------|
| <b>Operating power (W)</b> | 15   | 3000 | 150          | 94      |
| <b>Power ratio</b>         | 1    | 200  | 10           | 6.27    |
| <b>Equivalent CFL</b>      | 1.00 | 1.18 | 1.10         | 4.45    |
| <b>Ratio<sub>3</sub></b>   | 1.00 | 1.38 | 0.47         | 5.12    |
| <b>Ratio<sub>5</sub></b>   | 1.00 | 0.77 | 1.91         | 4.57    |
| <b>Ratio<sub>7</sub></b>   | 1.00 | 0.76 | 1.10         | 2.33    |
| <b>Ratio<sub>9</sub></b>   | 1.00 | 1.09 | 0.14         | 1.98    |
| <b>Ratio<sub>11</sub></b>  | 1.00 | 2.00 | 1.13         | 4.00    |
| <b>Ratio<sub>13</sub></b>  | 1.00 | 1.04 | 0.96         | 5.13    |
| <b>Ratio<sub>15</sub></b>  | 1.00 | 0.71 | 0.21         | 2.63    |
| <b>Ratio<sub>17</sub></b>  | 1.00 | 2.06 | 0.86         | 3.57    |
| <b>Ratio<sub>19</sub></b>  | 1.00 | 0.72 | 0.58         | 5.83    |

## 2.6.2 Harmonic Impedance Characteristics

Unlike other linear loads that are modeled as  $R + jhX$ , the PV inverter filter contains a capacitor. The filter total impedance is:

$$Z_{filter}(h) = (R_1 + jh\omega L_1) \parallel \left( R_c + \frac{1}{jh\omega C} \right) + (R_2 + jh\omega L_2) \quad (2.29)$$

The frequency response of the inverter filter impedance is presented in Figure 2.41. The impedance magnitude reaches a peak around the 16<sup>th</sup> order harmonic because of a parallel resonance. Observing from the grid side, the filter is capacitive between the 18<sup>th</sup> and 28<sup>th</sup> harmonics and inductive at other harmonic orders.

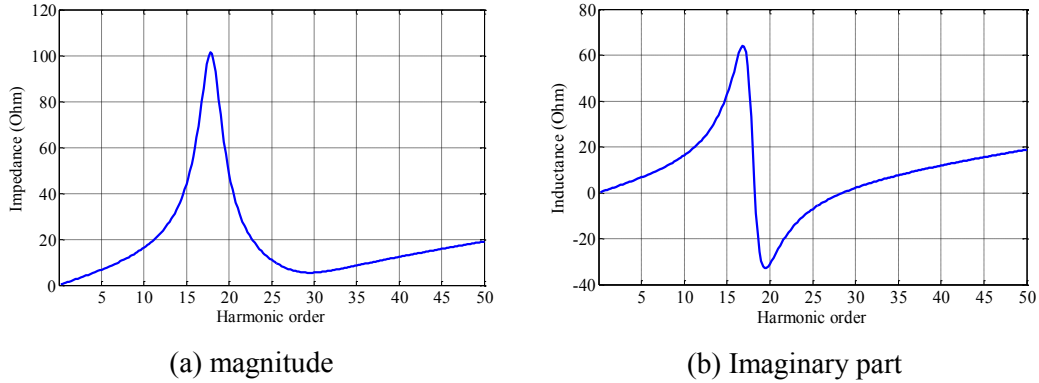


Figure 2.41 Frequency response of the filter impedance

In summary, the harmonic current injection of the PV inverter is almost constant no matter how the grid impedance changes. However, the harmonic current is quite small compared with other nonlinear loads. Therefore we can expect that the PV inverter is close to a passive element at the harmonic frequency.

## 2.7 Summary

In this chapter, both fundamental and low-order harmonic models of the PV inverter are proposed. The models are verified by the field data analysis, time-domain simulation and lab experiment. The following are the main conclusions of this chapter.

1. At the fundamental frequency, the PV inverter is modeled as a negative  $P$ - $Q$  load. In particular,  $Q$  can be neglected for simplification since it is much smaller than  $P$ . The field measurement data analysis suggested that under the constant solar irradiance, the PV output power  $P$  approximately remains constant with grid voltage variation. In order to determine the value of  $P$ , the solar irradiance and temperature of the PV panel are required.
2. At the harmonic frequency, the PV inverter is modeled as the series of a voltage source and a passive filter. It can be used instead of the detailed power electronic circuit for distribution system harmonic analysis. The most important contribution of this study is: it proved that the inverter

bridge output terminal can be represented by a voltage source at each harmonic order. This representation is based on two assumptions: 1) the DC-link of the inverter can be modeled as a constant voltage source so that the inverter bridge is decoupled from the DC/DC converter, and 2) the switching function of the inverter bridge contains low-order harmonic components and its harmonic spectrum is independent of the grid harmonics. The harmonic model is validated by the time-domain simulation and the PV integration experiment.

3. When applying the PV inverter harmonic model, the user should follow the following procedure: 1) calculate the harmonic spectrum of voltage source by doing FFT with the inverter bridge voltage, and 2) decide the filter topology and parameters. Four sets of typical filter parameters are summarized in Appendix A.
4. The harmonic model reflects both the harmonic source characteristic and harmonic impedance characteristic of the PV inverter. As a harmonic source, the PV injects low order harmonic current to the grid. However, the harmonic injection of PV inverter is not significant. Therefore the PV inverter is close to a passive element at harmonic frequency.

## Chapter 3

# Harmonic Impact of PV Inverters on Secondary Distribution Systems

PV inverters (PVs) are integrated to the secondary distribution system through the house service panel side. According to the harmonic model developed in Chapter 2, the PV inverter has two aspects of potential harmonic impact:

- The PV inverter contains harmonic source and can inject harmonic current to the power system. Chapter 2 has proved that the harmonic current injection is quite small. This chapter will further confirm the impact of harmonic source from the power system perspective.
- The PV inverter also contains filter impedance. The filter is capacitive at a certain frequency band and may cause a resonance problem by interacting with the grid impedance [32].

Since the installation number of distributed PV inverters may increase quickly in the future, it is quite essential to assess the severity of above two harmonic issues by using the PV inverter models.

### 3.1 Description of Secondary Distribution System Model

A typical secondary distribution system of North America is shown in Figure 3.1. It contains a primary network equivalent circuit (14.4kV), a single-phase three-winding service transformer (14.4/0.12/0.12kV), several groups of two-phase three-wire secondary conductor and several houses connected in parallel. In this case, the number of houses is assumed 10. And each PV inverter is connected phase-to-phase to avoid the voltage unbalance.

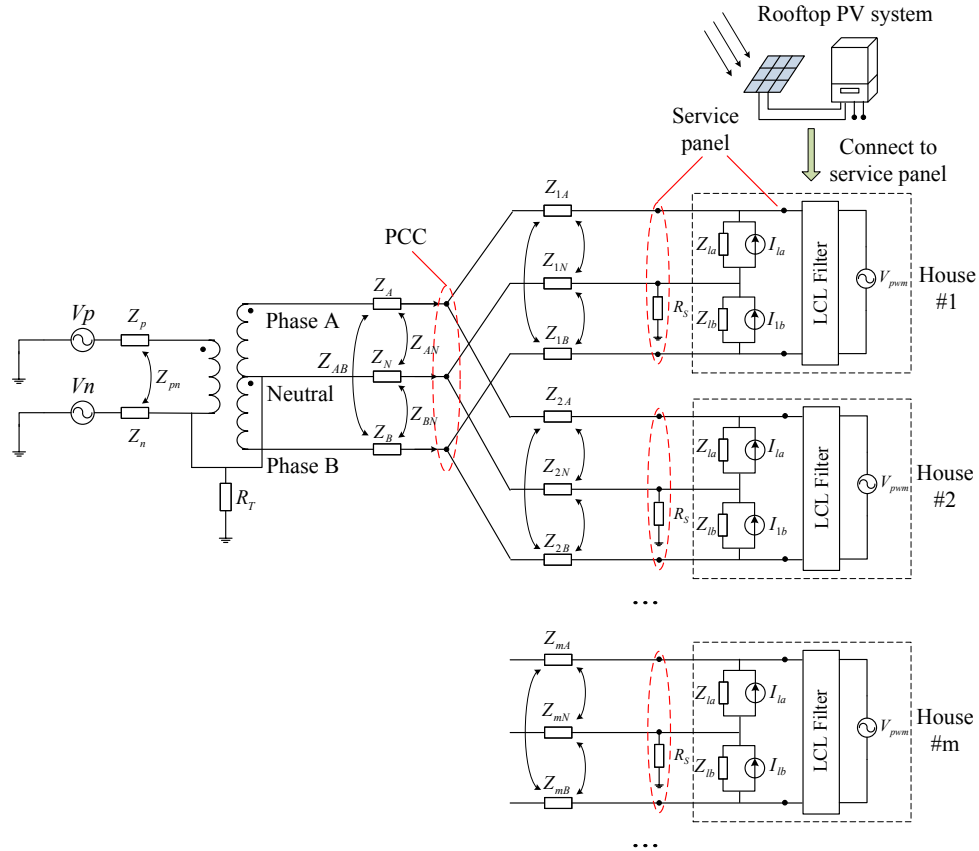


Figure 3.1 Secondary distribution system with PV integration

Below is an explanation of the system.

- 1) *Primary system*: One phase (p) represents the energized conductor and the other phase (n) represents the neutral conductor.  $V_n$  models the neutral voltage rise caused by the upstream system and loads.
- 2) *Transformer*: The three-winding coupled transformer model is applied to the power flow calculation (the detailed modeling is presented in Appendix B.2).
- 3) *Secondary conductor*: The two-phase, three-wire coupled conductor is applied (the detailed modeling is presented in Appendix B.1).
- 4) *Residential houses*: Most of the residential loads are connected phase-to-neutral. Both linear and nonlinear loads are modeled as P+jQ element at the fundamental frequency. At the harmonic frequency, a linear load is modeled as impedance.

$$Z(h) = R + jX(h) = \frac{P}{P^2 + Q^2} V_r^2 + jh \frac{Q}{P^2 + Q^2} V_r^2 \quad (3.1)$$

where  $P$  is the rated real power of the load and  $Q$  is the rated reactive power,  $V_r$  is the rated voltage of the service panel, it equals to 120V or 240V. Also, a nonlinear load (except PV) is modeled as current source. The harmonic current magnitude and phase angle are determined according to the load's harmonic spectrum (the typical harmonic spectrums are presented in Appendix D).

$$I(h) = I(1) \frac{I_{spectr}(h)}{I_{spectr}(1)}, \quad \theta(h) = \theta_{spectr}(h) + h(\theta(1) - \theta_{spectr}(1)) \quad (3.2)$$

Furthermore, in each house, the loads connected to the same phase are lumped into a single impedance and current source, such as  $Z_{la}$  and  $I_{la}$ .

The typical parameters of the secondary distribution network and the PV inverter are shown in Table 3.1 and Table 3.2 respectively.

Table 3.1 Secondary distribution system parameters

| Classification                       | Parameters   | Sample values   |
|--------------------------------------|--|---|
| Primary System (Thevenin equivalent) | Phase voltage $V_p$<br>Neutral voltage $V_n$<br>Source equivalent impedance  | 14.4kV<br>10V<br>$Z_p = 64.04 + j46.58\Omega$<br>$Z_n = 1.537 + j0.448\Omega$<br>$Z_{pn} = 0.439 + j0.834\Omega$  |
| Service Transformer                  | Apparent power rating $S_r$<br>Base power $S_{base}$<br>Voltage rating<br>Short-circuit R<br>Short-circuit X<br>Grounding resistance $R_T$ | 37.5KVA<br>37.5KVA<br>14400/120V<br>0<br>$X_{pa} = 0.04\text{p.u.}, X_{pb} = 0.04\text{p.u.},$<br>$X_{ab} = 0.05\text{p.u.}$<br>12 $\Omega$   |
| Secondary System                     | Secondary conductor impedance (self and mutual impedance)<br>Length of transformer – PCC<br>Length of PCC – House #X                       | $Z_A = Z_B = 0.249 + j0.878\Omega/\text{km}$<br>$Z_N = 0.427 + j0.961\Omega/\text{km}$<br>$Z_{AN} = Z_{BN} = 0.0592 + j0.429\Omega/\text{km}$<br>$Z_{AB} = 0.0592 + j0.491\Omega/\text{km}$<br>$l_0 = 0.10\text{km}$<br>$l_1 = 0.09\text{km}, l_2 = 0.07\text{km}, \dots$ |
| House #X                             | Grounding resistance $R_S$<br>Phase impedance<br>Neutral impedance   | 1 $\Omega$<br>$Z_{ph} = 0.21 + j0.094 \Omega/\text{km}$<br>$Z_{nn} = 0.55 + j0.365 \Omega/\text{km}$  |

Table 3.2 PV inverter parameters

| Parameters                   | Value         |
|------------------------------|---------------|
| Rated power                  | 1.5kW         |
| Inverter side inductor $L_1$ | 2.1mH         |
| Inverter side resistor $R_1$ | 0.05 $\Omega$ |
| Grid side inductor $L_2$     | 1.2mH         |
| Grid side resistor $R_2$     | 0.05 $\Omega$ |
| Shunt capacitor $C$          | 10.4 $\mu$ F  |
| Damping resistor $R_c$       | 2 $\Omega$    |

### 3.2 Harmonic Impact of PVs on the System – Simulation Study

The objective of this section is to evaluate the harmonic impact of PVs on the secondary system. In particular, it is essential to compare the performance of the voltage source and filter impedance of the harmonic model.

#### 3.2.1 Simulation Study Method

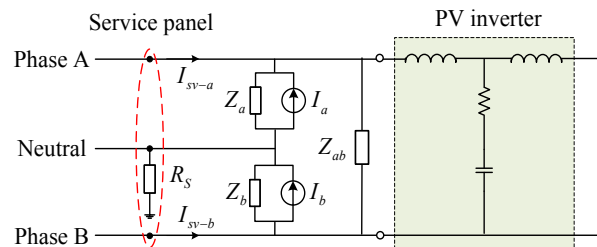
The simulation system and its parameters are introduced in Section 3.1. In addition, the modeling of houses with PV integration is introduced as follows:

**House electric model with PV:** In order to compare the harmonic impact of the voltage source and the filter impedance, three cases are simulated.

*Case 1:* No PV inverter is connected to the house;

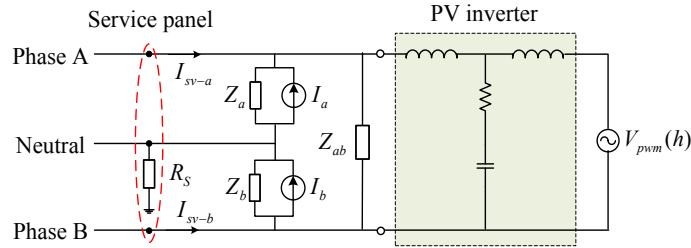
*Case 2:* Each house is installed with a PV inverter. The PV is modeled as a passive filter (filter model), as shown in Figure 3.2 (a);

*Case 3:* Each house is installed with a PV inverter. The PV is modeled as a harmonic voltage source in series with a filter (full model), as shown in Figure 3.2 (b).



(a) Representing PV with filter model





(b) Representing PV with full model

Figure 3.2 Residential house model with PV inverter

In each simulation scenario, the harmonic voltage  $V_{an}$ ,  $V_{bn}$  and harmonic current  $I_{sv-a}$ ,  $I_{sv-b}$  at the service panel side is observed (shown in Figure 3.2).

**House behavior model:** The harmonic impact of PV inverters is related to the grid operating condition. It includes the grid impedance and the grid background harmonic observed from the service panel. The grid impedance is affected by linear loads and the grid background harmonic by nonlinear loads. In this study, three time periods through the day are simulated to represent the random behavior of loads: morning, noon and evening. As is presented in Table 3.3, the common home appliances are manually assigned to each house according to the general lifestyle. For example, the toaster and cooker are likely to be switched on in the morning while TV and computer are switched on at noon or in the evening. During each period, the switch-on schedule of home appliances is defined in the program.

Table 3.3 Description of daily time period for simulation

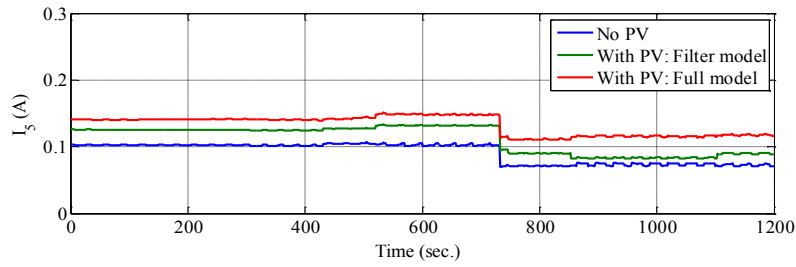
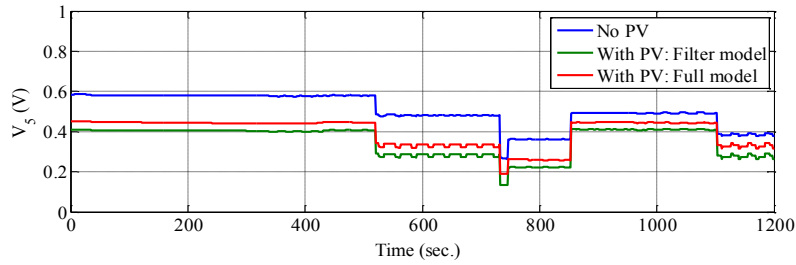
| Time period             | Main household activity                     | Home appliance involved                                  |
|-------------------------|---|--|
| Morning:<br>7:30~7:50   | Preparing breakfast                         | Toaster, cooker, microwave, incandescent light, CFL etc. |
| Noon:<br>12:00~12:20    | Preparing lunch/ entertainment              | Cooker, stove, microwave, TV, PC etc.                    |
| Evening:<br>17:30~17:50 | Preparing dinner, laundry and entertainment | Microwave, stove, incandescent light, CFL, TV, PC etc.   |

In each time period, the simulation of three scenarios is done over an extended period of 20 minutes with 1-second resolution. In each snapshot, the switch-on state of each appliance is determined according to the switch-on schedule. Then, a

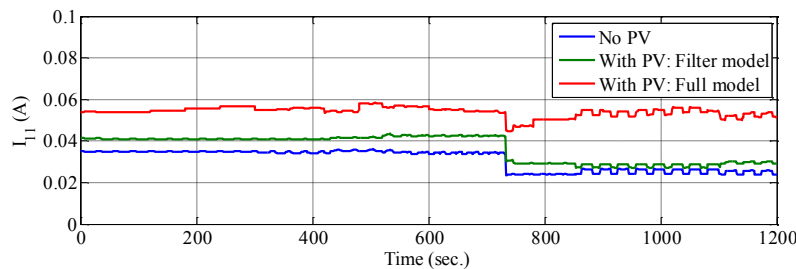
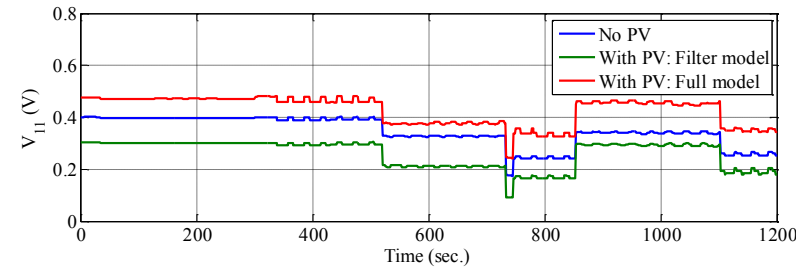
multiphase harmonic power flow calculation is done by using the simulation platform that will be introduced in Chapter 4. Note: the load switch-on schedules of above three scenarios are exactly the same.

### 3.2.2 Simulation Results and Analysis

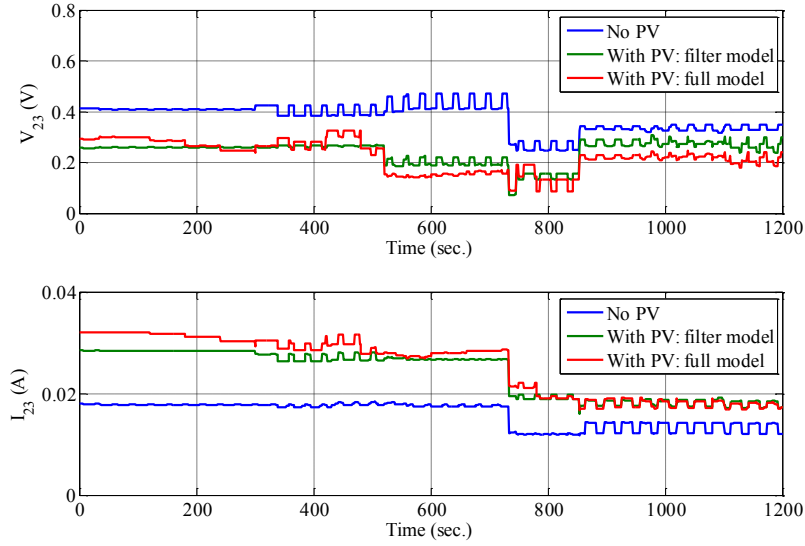
Figure 3.3 presents the examples of 10-house average harmonic voltage and harmonic current trend.



(a) 5<sup>th</sup> harmonic



(b) 11<sup>th</sup> harmonic



(c) 23<sup>th</sup> harmonic

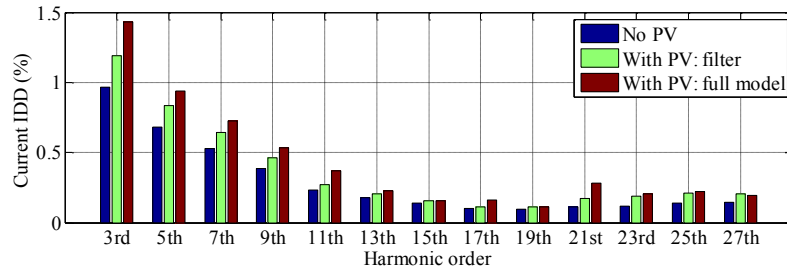
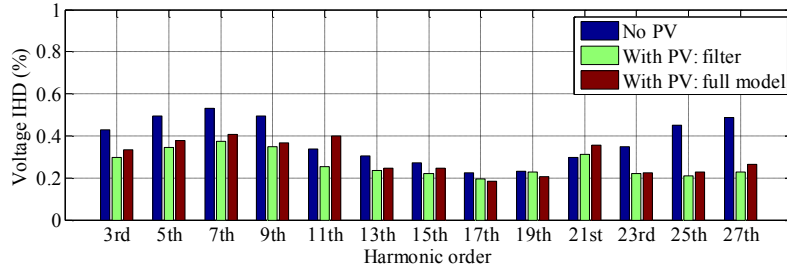
Figure 3.3 Phase B harmonic voltage and current trend at the service panel (7:30~7:50)

As the figures reveal, during a period of 20 minutes, the harmonic voltages trend in three scenarios have deterministic difference with each other. The harmonic currents in three scenarios also have the similar pattern. Therefore one snapshot can be selected for calculating the typical harmonic spectrum of the voltage and current. In this simulation, individual demand distortion (*IDD*) of Phase B is calculated by (3.3).

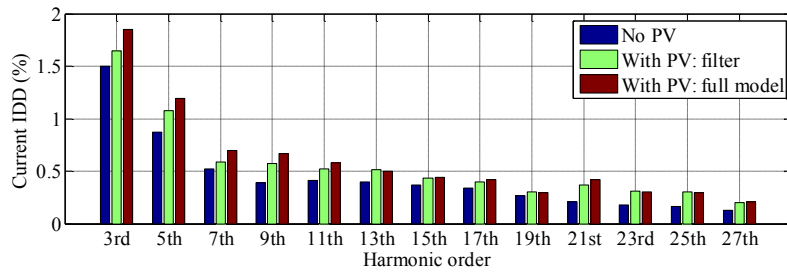
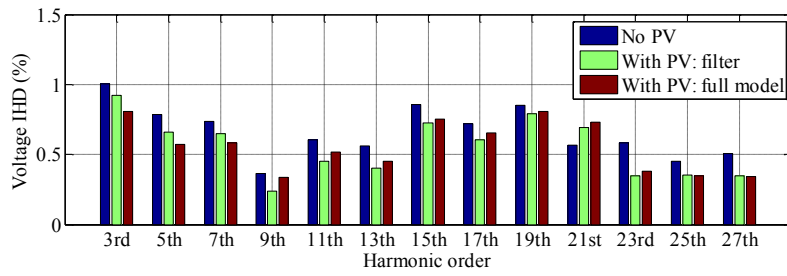
$$IDD = \frac{I_{sv-b}(h)}{I_L} \times 100\% \quad (3.3)$$

where  $I_L$  is the maximal demand current. It is assumed to be 20A in this section.

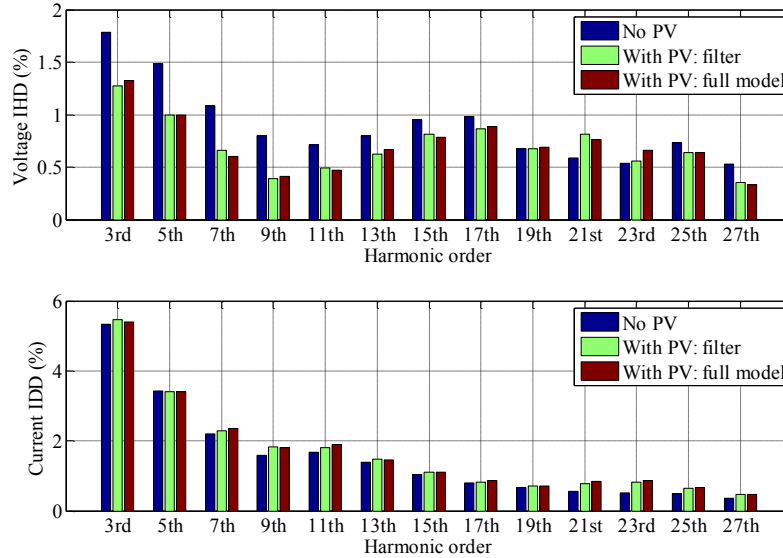
The typical harmonic voltage and current spectrums of three periods are presented in Figure 3.4.



(a) Morning period; 7:30~7:50



(b) Noon period; 12:00~12:20



(c) Evening period: 17:30~17:50

Figure 3.4 Harmonic voltage and current spectrum at the service panel

Based on the simulation result, the harmonic impact of PV inverters can be summarized as follows:

- Harmonic source and filter impedance:** Comparing the results of “filter model” and “full model”, we can observe that the harmonic voltage and harmonic current at the service panel side are quite close to each other. During the morning period when the background harmonic (shown as “No PV” bar) is low, the difference between “filter model” and “full model” is relatively obvious. However, during the evening period when the background harmonic is higher, the difference becomes negligible. Therefore, the voltage source  $V_{pwm}(h)$  doesn’t obviously affect the service panel harmonic voltage and current when the background harmonic is relatively high. In other words, the harmonic impact is mainly caused by the filter impedance. Thus it is reasonable to approximate the PV inverter as the filter model for power system harmonic analysis.
- Effect of filter impedance:** Comparing “no PV” and “filter model”, we can observe that the installation of PV leads to lower harmonic voltage and slightly higher harmonic current. For the 21<sup>st</sup> harmonic, the PV leads

to a larger harmonic voltage. The main reason is that the filter is capacitive around the 21<sup>st</sup> harmonic order and causes a parallel resonance by interacting with the grid impedance. However, the harmonic voltage amplification is not significant.

### 3.3 Harmonic Impact of PVs on the System – Analytical Study

Section 3.2 suggested that the PV inverter filter can cause harmonic resonance in the secondary system. In this section, an analytical study is made to demonstrate the mechanism of the harmonic resonance problem and to estimate its sensitivity to the filter and power system parameters.

#### 3.3.1 Simplification of the Secondary System

In order to study the resonance problem, we need to simplify the secondary system and to express the driving point impedance (the self-impedance observed from a node of the system) as a function of the LCL filter and grid impedance parameters. To achieve this, the following three approximations are made:

- 1) The primary side voltage is sinusoidal. In other words, the harmonic distortion in the secondary system is only caused by the nonlinear loads.
- 2) The service conductor impedance ( $Z_{iA}$ ,  $Z_{iN}$  and  $Z_{iB}$  in Figure 3.1) is neglected because it is much smaller than the load impedance. For instance, a typical service conductor impedance  $Z_{service}$  and Phase A linear load impedance  $Z_{la}$  are as follows [33]:

$$Z_{service} = Z_{mA} + Z_{mN} = 0.017 + j0.0067\Omega$$

$$Z_{la} = \frac{V^2}{P - jQ} = \frac{120^2}{2000 - j100} = 7.2 + j0.36\Omega$$

Hence both real part and imaginary part of  $Z_{service}$  is negligible compared with  $Z_{la}$ . Consequently, the PCC and service panel point are merged and all residential loads and PVs are directly connected to PCC.

- 3) The harmonic voltage source  $V_{pwm}(h)$  of the PV inverter model can be neglected because its harmonic impact is quite small, which has been proved in Section 3.2. As a result, the whole PV inverter is considered to be a passive filter, as shown in Figure 3.5.

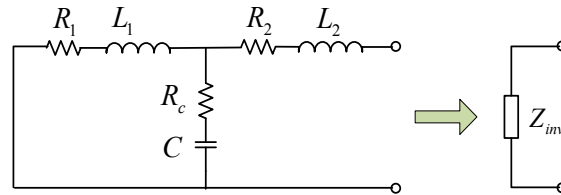


Figure 3.5 Harmonic model of PV inverter (neglecting the harmonic source)

Firstly, assume the secondary system only contains one house. At the harmonic frequency, the system can be simplified step by step (shown in Figure 3.6).

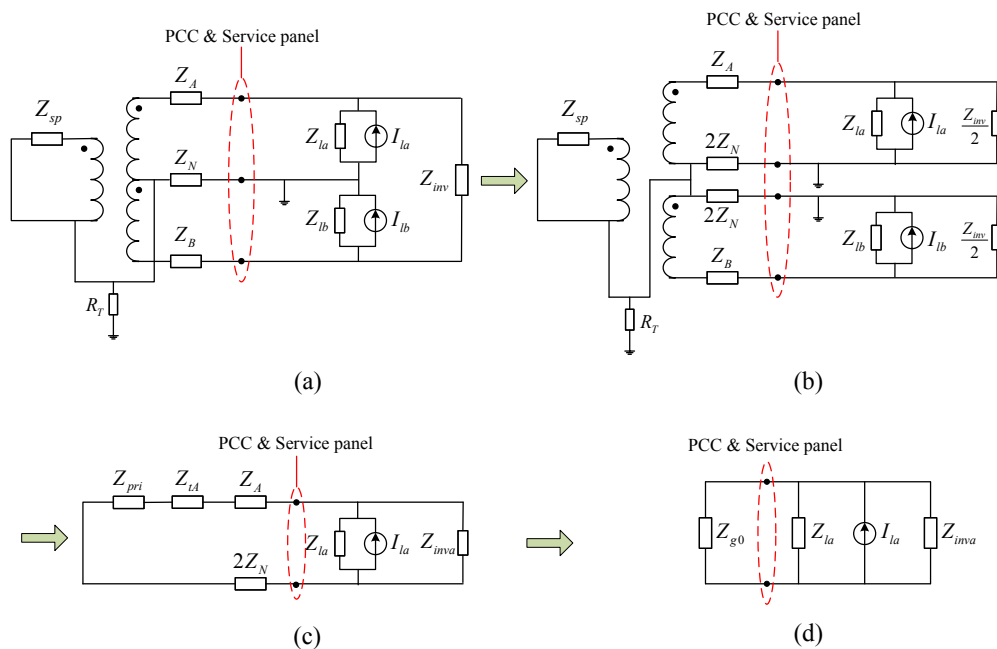


Figure 3.6 Simplification method of the secondary system (at harmonic frequency)

**From (a) to (b):** The inverter impedance is split into two series-connected parts. And the neutral line is split into two parallel-connected parts. In this way the two phase circuit is decoupled.

**From (b) to (c):** Take Phase A as an example,  $Z_{pri}$  is the primary side impedance reflected to secondary side and  $Z_{tA}$  is the transformer impedance.  $Z_{inva}$  is assumed to be  $\frac{Z_{inv}}{2}$ .

**From (c) to (d):** The circuit outside the house is represented by the grid original impedance  $Z_{g0}$ . And the house load can be represented as three components: linear load impedance  $Z_{la}$ , nonlinear load current  $I_{la}$  and inverter filter impedance  $Z_{inva}$ . The parameters are determined as follows:

The grid original impedance is given by,

$$Z_{g0} = Z_{pri} + Z_{tA} + Z_A + 2Z_N \quad (3.4)$$

The inverter impedance is calculated by,

$$Z_{inva} = \frac{Z_{inv}}{2} = \frac{1}{2} \left( \frac{Z_1 Z_c}{Z_1 + Z_c} + Z_2 \right) \quad (3.5)$$

where  $Z_1 = R_1 + j\omega L_1$ ,  $Z_c = R_c + \frac{1}{j\omega C}$  and  $Z_2 = R_2 + j\omega L_2$ .

Secondly, when the secondary system contains multiple houses, each house connected to PCC is considered as a three-component circuit. Figure 3.7 shows how to further simplify the circuit.

**From (a) to (b):** The multiple houses can be merged into one house. The aggregated load impedance, load current and PV filter impedance are given by (3.6). Note: the  $n$  PV inverters are assumed identical.

$$Z_{la} = \frac{1}{\sum_{k=1}^K \frac{1}{Z_{la-k}}}, \quad I_{la} = \sum_{k=1}^K I_{la-k}, \quad Z_{inva} = \frac{Z_{inva-1}}{n} \quad (3.6)$$

**From (b) to (c):** All the loads except PV inverter can be moved to the grid side and merged with the grid original impedance. Then the grid side can be equivalent



to a Norton circuit, and the grid equivalent impedance  $Z_{g-eq}$  and grid current source  $I_g$  are given by (3.7).

$$\begin{cases} Z_{g-eq} = Z_{g0} \parallel Z_{la} = \frac{Z_{g0}Z_{la}}{Z_{g0} + Z_{la}} \\ I_g = I_{la} \end{cases} \quad (3.7)$$

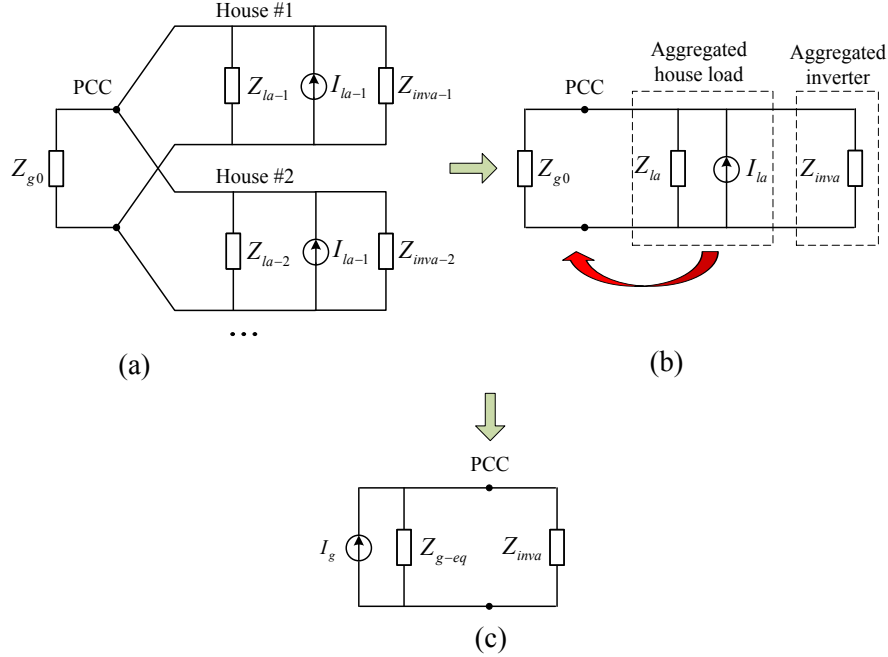


Figure 3.7 Simplification method of multi-house circuit (at harmonic frequency)

For each harmonic order, the driving point impedance at PCC is,

$$\begin{aligned} Z_{pcc} &= Z_{g-eq} \parallel Z_{inva} \\ &= Z_{g-eq} \parallel \frac{1}{n} \left( \left( \frac{Z_1 Z_c}{Z_1 + Z_c} + Z_2 \right) / 2 \right) \\ &= \frac{Z_{g-eq} [(Z_1 + Z_2) Z_c + Z_1 Z_2]}{(Z_1 + Z_2 + 2nZ_{g-eq}) Z_c + Z_1 (Z_2 + 2nZ_{g-eq})} \end{aligned} \quad (3.8)$$

Besides, if there are no PVs in the secondary system, the driving point impedance at PCC is,

$$Z_{pcc-noPV} = Z_{g-eq} \quad (3.9)$$

Therefore the harmonic voltage at PCC is given by (3.10). The equation shows that the driving point impedance  $Z_{pcc}$  plays an important role in the system response to harmonic sources. If  $Z_{pcc}$  becomes very large at a specified frequency, a large harmonic voltage will result.

$$V_{pcc} = I_g Z_{pcc} \quad (3.10)$$

### 3.3.2 Harmonic Resonance Analysis

This subsection aims to analyze the harmonic resonance issue. The first step is to find the resonance frequency  $\omega_r$ . It is roughly estimated that  $\omega_r$  is at least 10 times of fundamental frequency. Within this range, the real part of  $Z_1$ ,  $Z_2$  and  $Z_{g-eq}$  are negligible,

$$Z_1 \approx j\omega L_1, \quad Z_2 \approx j\omega L_2, \quad Z_{g-eq} \approx j\omega L_{g-eq}$$

Thus formula (3.8) is expressed as:

$$\begin{aligned} Z_{pcc}(\omega) &\approx \frac{j\omega L_{g-eq} \left[ j\omega(L_1 + L_2) \left( R_c + \frac{1}{j\omega C} \right) + j\omega L_1 j\omega L_2 \right]}{j\omega(L_1 + L_2 + L'_{g-eq}) \left( R_c + \frac{1}{j\omega C} \right) + j\omega L_1 j\omega(L_2 + L'_{g-eq})} \\ &= j\omega L_{g-eq} \frac{(L_1 + L_2 - \omega^2 L_1 L_2 C) + j\omega(L_1 + L_2) R_c C}{\left[ (L_1 + L_2 + L'_{g-eq}) - \omega^2 L_1 (L_2 + L'_{g-eq}) C \right] + j\omega(L_1 + L_2 + L'_{g-eq}) R_c C} \quad (3.11) \\ &\triangleq \frac{A_1 + jB_1}{A_2 + jB_2} \end{aligned}$$

where  $L'_{g-eq} = 2nL_{g-eq}$ .

If  $R_c < 1\Omega$ , then we can find  $A_1 \gg$  and  $A_2 \gg$  based on the typical filter parameters. Therefore the maximum  $Z_{pcc}(\omega)$  is reached when,

$$A_2 = (L_1 + L_2 + L'_{g-eq}) - \omega^2 L_1 (L_2 + L'_{g-eq}) C = 0 \quad (3.12)$$

Solve for the resonance frequency  $\omega_r$ ,

$$\omega_r = \sqrt{\frac{L_1 + L_2 + L'_{g-eq}}{CL_1(L_2 + L'_{g-eq})}} \quad (3.13)$$

Then the resonance impedance is obtained,

$$Z_{pcc}(\omega_r) \approx j\omega_r L'_{g-eq} \frac{A_1 + jB_1}{jB_2} \approx j\omega_r L'_{g-eq} \left[ 1 + \frac{L_1 + L_2 - \omega_r^2 L_1 L_2 C}{j\omega_r (L_1 + L_2 + L'_{g-eq}) R_c C} \right] \quad (3.14)$$

The **resonance amplification** AMP is defined as (3.15). It means the ratio between the resonance impedance and the system equivalent impedance without PV filters. The larger the AMP becomes, the more serious harmonic voltage amplification occurs.

$$AMP = \left| \frac{Z_{pcc}(\omega_r)}{Z_{pcc-noPV}(\omega_r)} \right| = \left| \frac{Z_{pcc}(\omega_r)}{Z_{g-eq}(\omega_r)} \right| \approx \left| 1 + \frac{L_1 + L_2 - \omega_r^2 L_1 L_2 C}{j\omega_r (L_1 + L_2 + L'_{g-eq}) R_c C} \right| \quad (3.15)$$

Substitute (3.13) to (3.15), gives,

$$AMP = \left| 1 - j \frac{L_1^{3/2} L'_{g-eq}}{R_c \sqrt{C(L_2 + L'_{g-eq})} (L_1 + L_2 + L'_{g-eq})^{3/2}} \right| \quad (3.16)$$

where  $L'_{g-eq} = 2nL_{g-eq}$ .

According to (3.16), we can see that the resonance amplification is affected by two factors:

- AMP decreases with  $R_c$  increasing. Specially, AMP is roughly inversely proportional to  $R_c$  when  $R_c$  is very small.
- AMP is also affected by the PV inverter number  $n$ . However, the variation pattern cannot be directly observed from (3.16).

### 3.3.3 Sensitivity Study on the Harmonic Resonance

In this subsection, a sensitivity study is conducted to demonstrate the impact of above two factors on the severity of the harmonic resonance. The system driving point impedance and the PCC harmonic voltage are calculated by (3.17).

$$Z_{pcc} = \frac{Z_{g-eq} [(Z_1 + Z_2) Z_c + Z_1 Z_2]}{(Z_1 + Z_2 + 2nZ_{g-eq}) Z_c + Z_1 (Z_2 + 2nZ_{g-eq})} \quad (3.17)$$

$$V_{pcc} = I_g Z_{pcc}$$

Typical parameters are applied to this sensitivity study. Below is a specification of the secondary distribution system [33].

1) *Primary system*: The primary side impedance reflected to the secondary side is extremely small due to the large turn ratio of the transformer. Thus  $Z_{pri}$  is assumed to be 0.

2) *Transformer*:  $Z_{tA} = Z_{tB} = 0.010 + j0.020\Omega$

3) *Secondary conductor (Transformer-PCC)*:  $Z_A + 2Z_N = 0.027 + j0.011\Omega$

4) *Residential houses*: 10 houses are connected to PCC and each contains linear loads and nonlinear loads. Table 3.4 shows the load specifications of each house:

Table 3.4 Residential load specifications

| Load type      | Model          | Parameters   |
|----------------|----------------|--|
| Linear load    | Impedance      | - Total power: 2500W<br>- Average power factor: 0.995  |
| Nonlinear load | Current source | - 7 common nonlinear loads are used: CFL, PC, laptop, TV, fridge, furnace and washing machine.<br>- Randomly select several loads from the above 7 loads and calculate their total harmonic current injection $I_{la}$ of each harmonic order. |

5) *PV inverter*: the parameters are presented in Table 3.2.

#### A. Frequency Response of the Driving Point Impedance

The driving point impedance  $Z_{pcc}$  is mainly affected by two main factors: the filter damping resistance and the PV inverter number.

1) *The impact of the filter damping resistance:* In this case, the PV number  $n$  is fixed to 10. The frequency response of  $Z_{pcc}$  is presented in Figure 3.8. As the figure reveals, around the resonance frequency ( $20^{\text{th}} \sim 26^{\text{th}}$  harmonic order),  $Z_{pcc}$  is amplified by the PV inverter; in other frequency band,  $Z_{pcc}$  is reduced by the PV inverter. Furthermore, AMP obviously decreases with the increasing of  $R_c$ . When  $R_c$  equals to  $2\Omega$  (the value of a practical PV inverter), AMP is as low as 1.18.

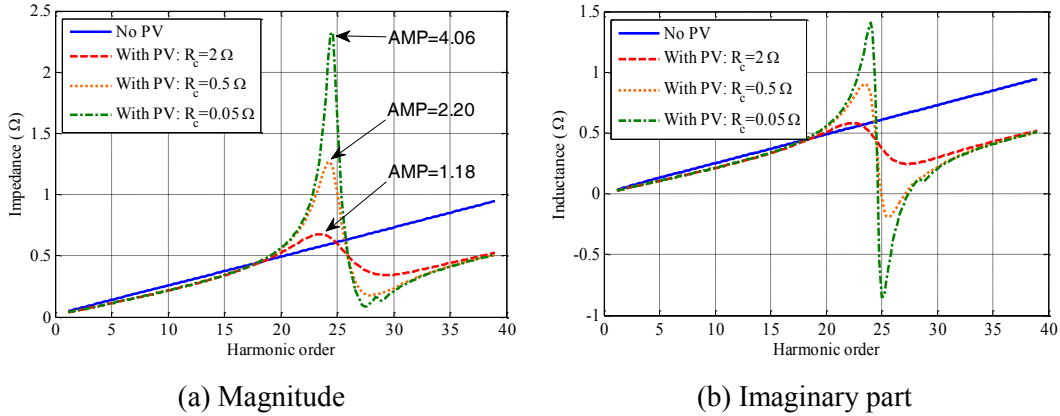


Figure 3.8 Frequency response of  $Z_{pcc}$  with different  $R_c$

2) *The impact of the PV inverter number:* In this case, the damping resistance  $R_c$  is fixed to  $2\Omega$ . The frequency response of  $Z_{pcc}$  is presented in Figure 3.9. With the PV inverter number increasing, the resonance frequency becomes slightly lower and AMP becomes slightly higher. However, the variation of AMP is not significant because the damping resistor  $R_c$  is large enough to mitigate the amplification.

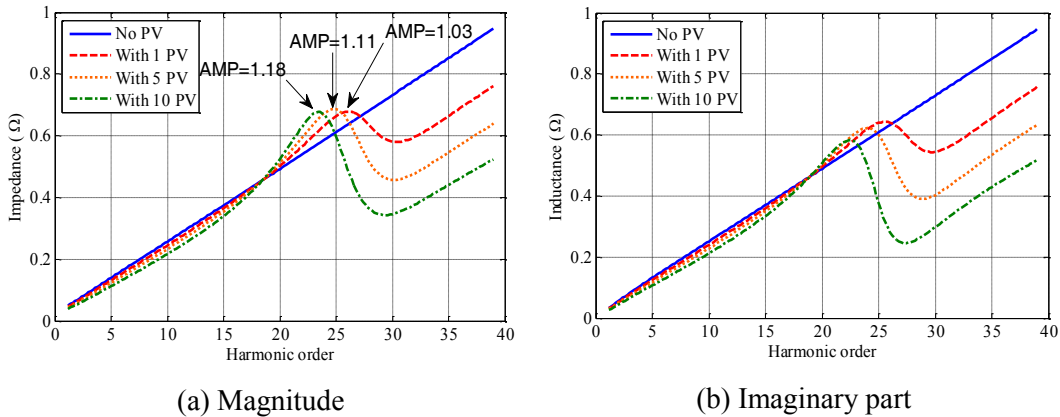


Figure 3.9 Frequency response of  $Z_{pcc}$  with different PV inverter number

In summary, the resonance amplification is quite sensitive to the filter damping resistance but not very sensitive to the PV inverter number. Furthermore, based on the practical secondary system parameters and inverter filter parameters (especially  $R_c$ ), the driving point impedance at PCC will not be seriously amplified at the resonance frequency, even if all houses are installed with PV inverters.

### **B. Harmonic Distortion at PCC**

According to the frequency response of the driving point impedance, the PCC harmonic voltage spectrum can be estimated. It should be noticed that the resonance may not happen at integer harmonic order. Hence the AMP is a conservative index for estimating the maximal harmonic voltage amplification. The individual harmonic voltage distortion  $IHD_V$  can be calculated by (3.18), where the fundamental voltage  $V_{pcc}(1)$  is assumed 120V for simplification.

$$IHD_V(\%) = \frac{V_{pcc}(h)}{V_{pcc}(1)} \times 100\% \approx \frac{V_{pcc}(h)}{120} \times 100\% \quad (3.18)$$

The harmonic voltage at PCC is presented in Figure 3.10. Consequently, for low order harmonics ( $<21^{\text{st}}$ ),  $IHD_V$  is reduced by the PV inverter. For harmonic orders close to the resonance point ( $21^{\text{st}} \sim 25^{\text{th}}$ ),  $IHD_V$  is amplified except for the  $25^{\text{th}}$  order harmonic in the “ $R_c=2.0\Omega$ ” bar. For larger harmonic orders ( $>25^{\text{th}}$ ),  $IHD_V$  is significantly reduced. The estimated harmonic voltage spectrum in Figure 3.10 has the similar trend to the simulated harmonic voltage spectrum.

In particular, when  $R_c=0.05\Omega$ , the  $23^{\text{rd}}$  harmonic voltage is amplified by 100% more and it is likely to exceed the limits if more nonlinear loads are in operation; when  $R_c=2\Omega$ , the  $23^{\text{rd}}$  harmonic voltage is only amplified by 15% less. For a practical PV inverter, the resistor has been designed large enough to mitigate the resonance problem. Therefore the resonance cannot cause significant harmonic voltage amplification.

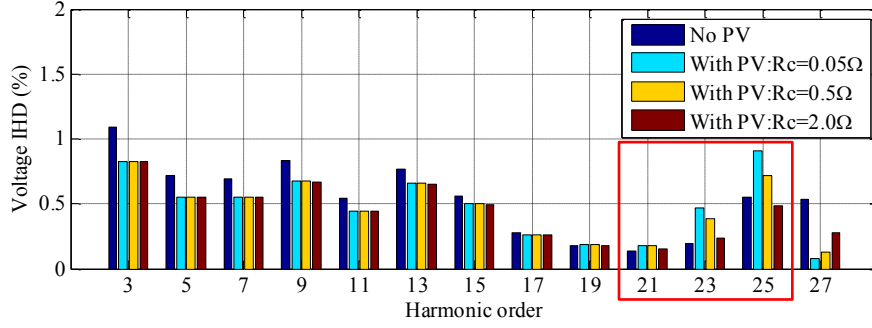


Figure 3.10 Harmonic voltage spectrums under different damping resistance

### C. Power Loss Assessment of the Damping Resistor

The study of Part A and Part B has concluded that a large damping resistor  $R_c$  can greatly mitigate the harmonic resonance amplification. However, the power loss might be a concern when applying a large  $R_c$ . Hence an approximate quantitative study is needed to clarify whether the power loss caused by  $R_c$  is acceptable. As is shown in Figure 3.11, since  $V_{pwm}(h) \ll$  at low harmonic order, the power loss caused by low order harmonics is negligible. Then the power loss is caused by the fundamental and switching-frequency harmonic current through  $R_c$ .

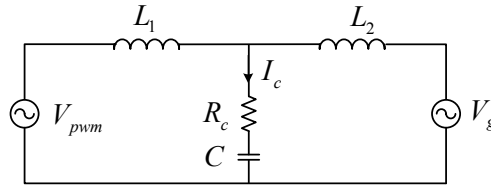


Figure 3.11 PV inverter harmonic model

At the fundamental frequency,  $\frac{1}{\omega C} \gg$ , and the voltage drop on  $L_1$  is negligible. The power loss is,

$$P_{loss}(1) = I_c^2(1)R_c = (\omega_f C V_c(1))^2 R_c \approx (\omega_f C V_{pwm}(1))^2 R_c \quad (3.19)$$

where  $\omega_f$  is the fundamental angle frequency and  $V_c(h)$  is the voltage drop at the capacitor.

Around the switching frequency,  $\omega L_1 \gg \frac{1}{\omega C}$  and the voltage drop on  $C$  is negligible. The power loss at  $h$ -th harmonic is,

$$P_{loss}(h) = |I_c(h)|^2 R_c \approx \left( \frac{V_{pwm}(h)}{h\omega_f L_1} \right)^2 R_c \quad (3.20)$$

Therefore the total power loss of  $R_c$  is estimated by (3.21).

$$P_{loss-Rc} = \omega_f^2 C^2 V_{pwm}^2(1) R_c + \sum_{h=h_{sw} \pm 1, 3} \frac{V_{pwm}^2(h)}{h^2 \omega_f^2 L_1^2} R_c \quad (3.21)$$

Besides, if we assume the PV inverter is operating at 80% rated power and the efficiency is 96%, the total power loss of the PV inverter can be estimated,

$$P_{loss-inv} = 80\% \times 3000 \times (1 - \eta) = 96W$$

The resonance amplification and the corresponding power loss are presented in Figure 3.12. The power loss is almost proportional to  $R_c$  and it reaches 13W when  $R_c=2\Omega$ . However, 13W is still a small part of the inverter total power loss. Therefore the power loss of the damping resistor is not serious in the PV inverter. In addition,  $2\Omega$  is a proper value for balancing the damping effect and the resistor power loss.

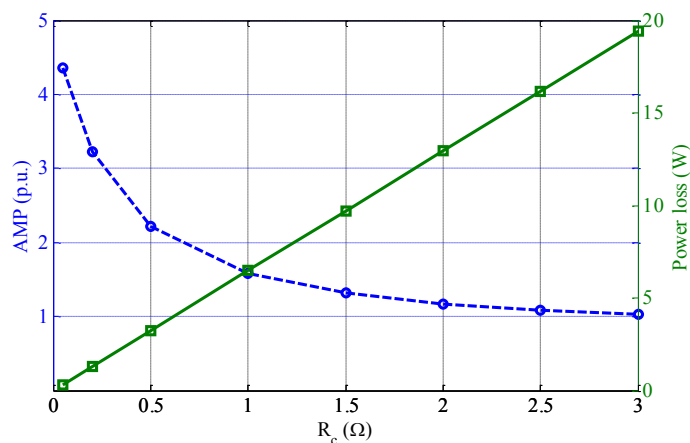


Figure 3.12 The power loss and resonance amplification with different  $R_c$



### 3.4 Summary

This chapter investigated the harmonic impact of PV inverter on the residential distribution system through simulation and analytical study. In particular, it is our interest to investigate how the large penetration of PV inverters affects the harmonic voltage/current distortion at the house service panel side. The main conclusions of this chapter are summarized as follows:

1. **The effect of harmonic source:** It has been demonstrated that when the harmonic voltage source is or isn't included in the PV harmonic model, the difference between their harmonic voltage/current is not significant, especially when the grid background harmonic is high. Therefore the harmonic source can be neglected when doing the system harmonic power flow analysis.
2. **The effect of harmonic impedance:** The harmonic impact of a PV inverter is mainly caused by the filter impedance. For the harmonic orders close to the resonance frequency, the filter impedance can slightly amplify the harmonic voltage. For other harmonic orders, however, the filter help reduce the harmonic voltage. Therefore, the large integration of PV inverters doesn't negatively affect the power quality of secondary distribution system from the perspective of harmonics. Furthermore, the harmonic impact of PVs on the primary system is even lower and needn't be studied in detail.
3. A secondary system simplification method is proposed for evaluating the mechanism of the harmonic resonance. The LCL filter of the PV inverter displays capacitive at a specified frequency band. Consequently it can interact with the system impedance and result in a parallel resonance problem. The resonance amplification decreases significantly with the increasing of the damping resistor. For a practical PV inverter, the damping resistance is large enough for mitigating the resonance

amplification. Meanwhile, the power loss of the damping resistor is not a big concern.

## Chapter 4

### A Monte Carlo Simulation Platform for Studying Low Voltage Residential Networks

Chapter 2 and Chapter 3 have proposed the model of PV inverter and studied its harmonic impact on low-voltage (LV) residential networks. Generally, the harmonic impact of a PV inverter is related to the grid operating conditions, which is directly determined by the amount and characteristic of residential loads in operation. Therefore a stochastic simulation program is highly required to simulate the practical operating condition of residential networks.

Furthermore, low-voltage residential electric networks have become a frontier of research and development due to a number of demand side innovations. Examples are the rooftop PV panels, electric vehicles (EV and associated vehicle-to-grid operation), demand response programs, and home energy use monitoring etc. [34]-[35]. Such developments also result in a great need for a tool that can model and simulate residential networks properly and effectively. Therefore, with the PV inverter model developed in this thesis and the aggregated residential load model developed in another study [3], it is ready to develop such a tool. The tool is expected to support a number of residential network research activities, as illustrated below:

1. *Integration of local generators (such as PVs)*: A number of research topics have been proposed in this direction, such as optimal operation of the residential network, switching between grid-connected and islanded modes, and minimization of load-generation unbalance. A proper simulation platform is an essential tool for evaluating the performance of various proposed or published techniques.

2. *Power quality concerns*: The adoption of new load and generation technologies in homes and LV networks has raised concerns on their potential power quality impacts. An example concern is the neutral-to-earth voltage (NEV) rise due to the connection of large loads such as EV chargers between phase and neutral [40], which could lead to stray voltage incidents. Another concern is the harmonic interactions among the devices. Detailed low voltage network models are needed to analyze such problems.
3. *Non-intrusive Load Monitoring (NILM) research*: This research attempts to determine the energy use of individual home appliances based on the power measured at the service panel side only [36]-[37]. Due to its significant energy-saving and data analytic potentials, NILM has become a very hot research topic pursued by various disciplines [37]-[39]. A notable challenge faced by this research is how to verify the proposed NILM algorithms. A detailed simulation platform that can model the electrical behaviors of various home appliances is one of the attractive solutions to this challenge.
4. *Demand response studies*: Demand response programs control the operation of certain appliances in homes or influence their operation through means such as time-of-use pricing. To predict the effectiveness of a demand response program, one has to understand, model and simulate the household energy consumption characteristics [41]-[42]. Since the home appliances operate in a probabilistic manner, a large number of Monte Carlo style simulations are needed to determine the outcome of a demand response programs statistically.

In response to the above needs, this chapter proposes a generic low voltage residential network simulation platform that can be used to evaluate many of the demand side smart grid ideas and techniques. The platform takes into account the common characteristics of the four research areas identified above. It covers an extended simulation period of 24 hours and has an output resolution of one snapshot per second. The proposed concept, to some extent, is similar to that of

power system dispatch simulators [43]-[44], but the modeling issues and target applications are completely different.

Power system dispatch simulators are mainly used to identify trends on the network, such as load-generation balance, steady-state violations, etc.; which require only the fundamental frequency model of network components at steady-state. On the other hand, the proposed simulator will be used to analyze the random behavior of a residential network, and to produce data for other researches such as appliance identification (NILM). To perform these studies, not only steady-state, but also harmonic and motor starting simulations are required; the behavior of network devices must be modelled in a probabilistic manner; and every conductor of the multiphase secondary networks must be modelled to study load imbalance, poor neutral conditions, harmonic cancellations, etc.

#### **4.1 The Proposed Simulation Platform**

Similar to high voltage power system studies, the residential network studies require two broad types of modeling and simulation tools. One is to simulate the dynamic responses of a network triggered by a single event such as a short-circuit fault. Several commercial tools such as PSCAD and Matlab/Simulink are available to meet these needs. The second type is to simulate the quasi-steady-state behavior of the network over an extended period such as 24 hours. It should provide a realistic consumption behavior of customers, including the individual operation and signature of each residential device. To our knowledge, such a tool has not been developed and its research is needed. The objective of the proposed platform is to satisfy the needs of the quasi-steady-state network studies. Since the simulation covers extended period, a number of unique issues must be addressed, such as when an appliance will be switched-on, how long it will remain in operation, what is the typical solar irradiance level at different snapshots, etc. These issues will be further explained later.

#### **4.1.1 General Requirements on the Simulation Platform**

Through analyzing the common characteristics of the four research areas, the following general requirements have been identified for the quasi-steady-state simulation platform:

**1) Extended simulation period.** The operation of residential loads is highly time-dependent. For example, laundry activities are more likely to take place in the morning, while TVs are mostly switched-on in the evening. Many researches require modeling the network activities over at least a 24 hour period, as the performance of various demand side techniques must be verified over an extended period. A NILM algorithm, for example, is expected to be able to identify the actions of major home appliances at any time of a day.

**2) Modeling of random behaviors of residential loads and generators.** Since the loads and generators in the LV network operate in a random manner over the simulation period, the proposed tool must be able to handle probabilistic events. At any instant, the tool shall determine the operating status of a load or generator based on their operation profiles that are characterized with probabilistic distribution functions.

**3) High resolution output.** The platform should also be able to output the network responses at a resolution of one snapshot per second. This requirement is essential to model the unique electrical signatures of some home appliances (which may last few seconds as will be shown later). Such information is usually taken into account by NILM research. Besides, for the PV integration study, the modeling of solar irradiance variability also requires a high resolution.

**4) Multiphase network model.** The residential network is a multi-conductor circuit with both phase-to-neutral and phase-to-phase connected loads. In addition, it has various grounding points whose grounding resistances can have an impact on the network responses. Therefore, the simulator must include every conductor of the system so that situations such as load unbalance, poor neutrals and harmonic cancellations and so on can be studied.

**5) Harmonics and motor starting.** Harmonics and motor starting dynamics produced by many residential loads carry unique electrical signatures. These signatures are used for appliance identification by many NILM algorithms. It is, therefore, very important for the simulation platform to model such signatures. Additionally, harmonics and motor starting dynamics are disturbances that must be assessed from power quality perspective.

The above requirements can be addressed by using two models for the LV network. One is the **electrical model** which represents the electrical characteristics of the network and loads. Another is the **behavior model** which covers the random operations of loads caused by the behavior of home inhabitants.

#### ***4.1.2 Electric Model***

This model represents the electrical characteristics of the simulated LV system, such as the network topology and impedances. A typical multiphase LV network of North America, selected for the proposed platform, is shown in Figure 4.1 [57]. It contains a primary network equivalent (14.4 kV), a service transformer (14.4/0.12/0.12kV), and several houses connected in parallel. Although the platform has been designed to cover any number of houses, 10 is typically used on the studies. Each house is represented by a further detailed circuit comprising individual devices connected in different rooms (shown in Figure 4.2).

Note that the equivalent circuit for the primary network is a two-phase coupled Thévenin circuit. One phase (p) represents the energized conductor and the other phase (n) represents the neutral conductor.  $V_n$  models the neutral voltage rise caused by the upstream system and loads. This model is very general so one can use it to study the impact of primary system on the LV network.

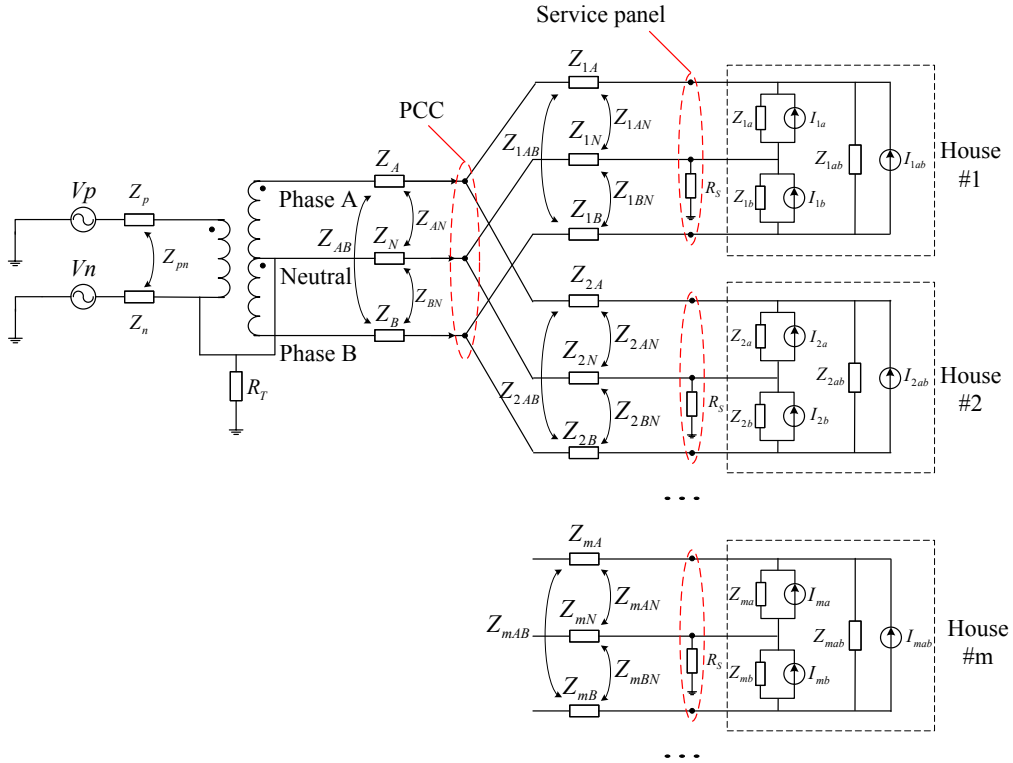


Figure 4.1 Generic multiphase low-voltage residential distribution network

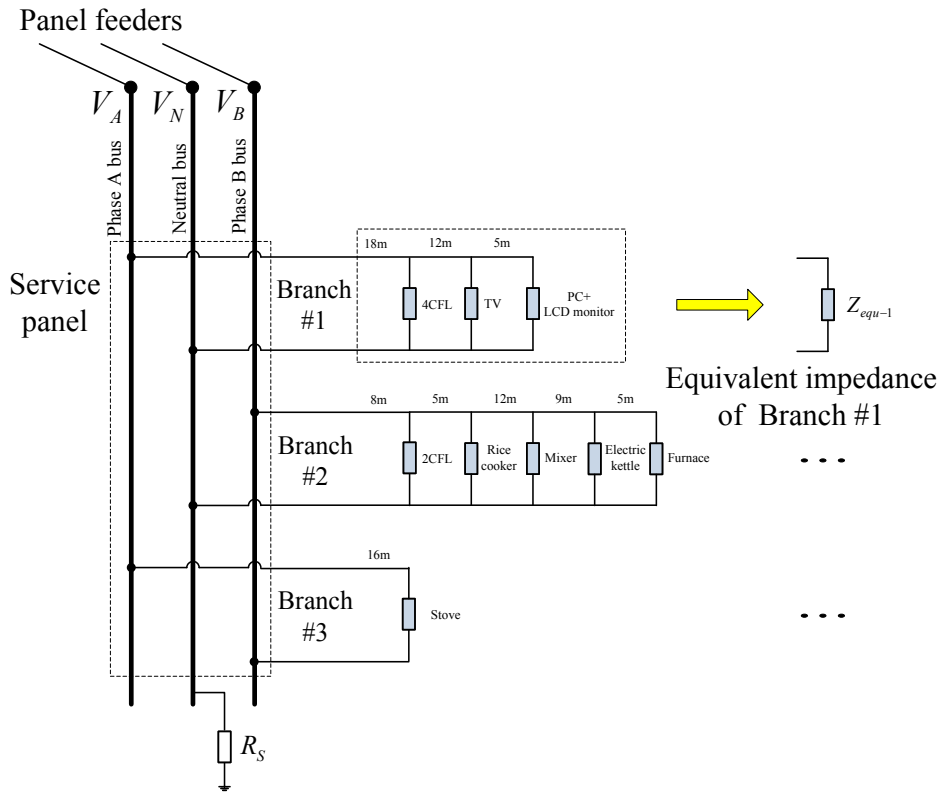


Figure 4.2 Single-house detailed circuit



### 4.1.3 Behavior Model

Behavior model here refers to the chronological operating characteristics of various loads or generators. For example, the behavior model of a microwave oven can be characterized by its on-instant, power setting and off-instant. The behavior model of the simulator is responsible to determine the probabilistic load demand during the simulation. In other words, it establishes which devices are connected to the network at a particular instant based on the time-of-use probability characteristics of the device. An example output of the behavior model over a 24 hour period is shown in Figure 4.3. This figure shows the operating status of several common appliances (high value means in operation and low value means off-line).

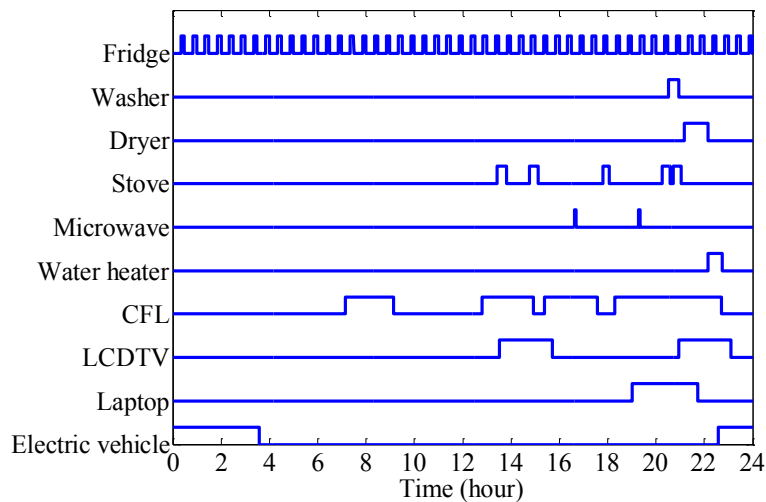


Figure 4.3 Sample household load behavior profile.

### 4.1.4 Sequential Monte Carlo Simulation

The probabilistic operating characteristics of LV loads and generators make it impossible to predict the response of a residential network using a deterministic approach. A sequential Monte Carlo (SMC) simulation technique is adopted to address the problem. SMC is a computer simulation method based on probabilistic theory and statistic technique. When applied to this paper, the SMC simulation method will determine whether the expected operation status of an appliance at a given snapshot is ON or OFF. Such status depends on the previous

appliance states (if appliance was ON or OFF on previous snapshots). Therefore the basic idea is to create a plausible residential behavior profile such as the one presented in Figure 4.3, considering the time-of-use probability of the various devices connected to the network. Once such a behavior profile is created, it is combined with the network electrical model to create an instance of the network for that profile. This instance is a deterministic network. Multiphase power flow, harmonic power flow and motor starting studies are then performed for the instance in a second-by-second sequence. This will yield the network responses over the simulation period for that instance.

In reality, there are many instances of load profiles. So the simulation is repeated many times for various randomly generated instances. Statistical analysis is then conducted on the results to obtain statistically valid performance indices.

## **4.2 Load Behavior Modeling Technique**

This section will present methods to determine the random operating states of residential loads and generators for a 24 hour simulation period.

### ***4.2.1 Home Appliance Time-of-use Probabilistic Behavior***

To model a residential demand scenario, the simulator must determine a time distribution of the ON/OFF states for all home appliances. These are considered random events, since they directly depend on the residence occupants' behavior. Such behavior follows certain statistical distributions, usually referred to as the time-of-use probability curves [46]-[47]. These curves consist of 7 items: cooking, laundry, lighting, breakfast, PC, TV and house clean. Each curve presents the likelihood of a residence starting an activity at each instant of a day and correlates to one or several home appliances. They are obtained through load survey research. The Example curves of laundry and cooking activities are shown in Figure 4.4.

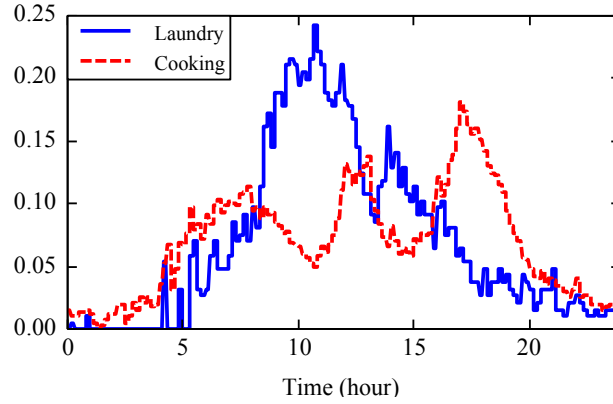


Figure 4.4 Example of time-of-use probability profile for household activities

These activities are associated with specific appliances. For example, microwave and stove are related to cooking and they share the same time-of-use probability profile – cooking. Thus, using the activity time-of-use profile, switch-on behaviors can be determined for all home appliances. This procedure is repeated for every appliance during the entire simulation period. The result is a time-of-use profile, such as that shown in Figure 4.3.

On a single snapshot, if a specific home appliance is NOT connected to the network, the LV simulation platform applies the methodology proposed in [3] to determine whether it will be switched-on or not. Such methodology calculates the appliance switching-on probability according to (4.1).

$$P(n) = P_r(n) \times m \times k \times c \quad (4.1)$$

where:

$P(n)$  – Switching-on probability for the appliance on the current snapshot;

$P_r(n)$  – Base probability read from the time-of-use profile on the current snapshot;

$m$  – Average number of switch-on events per day for the appliance under study;

$k$  – Household size factor. It is determined by the ratio between the number of house occupants and the average number of people per household (2.5 is assumed as default, but may be modified by the user);

$c$  – Calibration scalar determined by (4.2), where  $n$  refers to each time snapshot and the Occupation Function ( $OF(n)$ ) is 1 when house is actively occupied and 0 otherwise.

$$c = \begin{cases} 0, & OF(n) = 0 \\ \frac{1}{\sum_{n=1}^N P_r(n) \times OF(n)}, & OF(n) = 1 \end{cases} \quad (4.2)$$

A random number ( $r$ ) between 0 and 1 is then generated. If  $r$  is smaller than the switch-on probability  $P(n)$ , the appliance is switched-on and remains ON for its associated working cycle duration. The cycle duration of an appliance is determined by (4.3). Otherwise, it remains OFF.

$$T_{dur} = Unif(T_{min}, T_{max}) \quad (4.3)$$

where  $T_{min}$  and  $T_{max}$  are also provided by the time-of-use survey data [47].

An example of the resultant load behavior model is provided on Figure 4.3 for 10 loads. In this example, the house is actively occupied only in the early morning and after 12:00am. However, one may notice that the fridge (RFR) has a periodic switch-on profile, independently of house occupancy pattern. The remaining appliances are switched-on only when house is actively occupied.

#### 4.2.2 Electric Vehicle Charging Behavior

The EV charging behavior is modeled by two random variables: (a) charging start time and (b) charging duration. To some extent, EV behavior model is similar to appliance time-of-use probability curves; however the modeling issues are distinct as described below.

EV charging start time is usually at night, when EV owners are at home, and during off-peak demand to take advantage of time-dependent tariffs. It is modeled by a Normal probability density function (pdf) as in (4.4), where  $x$  is the plug-in time;  $\mu$  and  $\sigma$  are the average and standard deviation of  $x$ , respectively [48]. All variables are given in hours.

$$f(x) = \frac{1}{\sigma\sqrt{2\pi}} e^{\left(-\frac{1}{2}\left(\frac{x-\mu}{\sigma}\right)^2\right)}, \quad \mu = 1, \sigma = 3 \quad (4.4)$$

The charging duration time is determined according to the battery state of charge (SOC) when it is plugged-in. SOC is calculated by (4.5), where  $R$  is the maximum miles an EV can run from electric battery only;  $m$  is the number of miles travelled during 1 day, which is modeled by a lognormal pdf [49].

$$SOC = \begin{cases} \frac{R-m}{R} \times 100\% & 0 \leq m \leq R \\ 0 & m > R \end{cases} \quad (4.5)$$

Once the battery SOC is determined, its charging time duration can be directly calculated according to the total battery capacity and the charger power level.

After determining charging start time and charging duration time variables, the EV behavior may be integrated to the LV simulation platform. Figure 4.5 presents three charging examples.

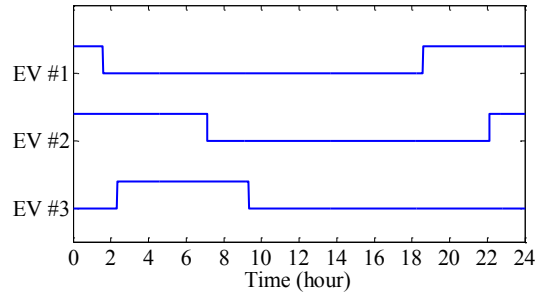


Figure 4.5 Charging profile for three EVs using different charging strategies

### 4.2.3 Solar Irradiance Level Behavior

The power generated by a PV array is directly dependent on the incident solar irradiance level, which, in turn, depends on clouds intermittent behavior [50].

The Beta pdf is generally employed to model the solar irradiance variability for a single snapshot [51]. Although such approach has been used in a number of published works, it considers each snapshot is independent from each other. However, if a cloud starts covering the sun at 14:00, it is unlikely to disappear at

14:01. In view of this drawback, a new approach is herein proposed, based on historical measurements. The method will be introduced using actual historical data from Edmonton, Canada, although its parameters may be readjusted according to weather information available at the location under study.

The sky condition over 1 day is divided into four categories, according to the cloud coverage level (*CCL*): “Clear” “Partly clear” “Mostly cloudy” and “Overcast”. *CCL* is quantified according to the solar irradiance level reaching the surface of earth (*Irr*); and its maximum value on a determined place (*Irr<sub>max</sub>*), both given in *W/m<sup>2</sup>*, as in (4.6). For the city of Edmonton, Canada, *CCL* probabilities are presented in Table 4.1 [52], and a maximum irradiance level curve is extracted from historical measured data [53]. With such information, once a day-type is chosen, the daily solar irradiance curve may be forecasted according to the following algorithm.

$$CCL = 1 - \frac{Irr}{Irr_{max}} \quad (4.6)$$

Table 4.1 Cloud Coverage Level Probability for Different Day-types

| Day-type             | Cloud-type | Cloud coverage level | Probability of occurrence (%) |
|----------------------|------------|----------------------|-------------------------------|
| <b>Clear</b>         | 1          | 0.00-0.05            | 67.4                          |
|                      | 2          | 0.05-0.15            | 18.6                          |
|                      | 3          | 0.15-0.25            | 14.0                          |
| <b>Mostly clear</b>  | 4          | 0.25-0.35            | 38.5                          |
|                      | 5          | 0.35-0.45            | 38.5                          |
|                      | 6          | 0.45-0.55            | 23.0                          |
| <b>Mostly cloudy</b> | 7          | 0.55-0.65            | 35.3                          |
|                      | 8          | 0.65-0.75            | 41.2                          |
|                      | 9          | 0.75-0.85            | 23.5                          |
| <b>Overcast</b>      | 10         | 0.85-0.95            | 45.0                          |
|                      | 11         | 0.95-1.00            | 55.0                          |

Initially, a cloud-type (CT) is randomly chosen according to the probability of occurrence presented in Table 4.1, for the correspondent day-type. According to the selected CT, *CCL* is randomly determined using (4.7), where *Unif* represents a

uniform pdf, and  $CCL_{min}$  and  $CCL_{max}$  are, respectively, the minimum and maximum cloud coverage level for the correspondent CT presented in Table 4.1.

$$CCL = Unif (CCL_{min}, CCL_{max}) \quad (4.7)$$

Since cloud forecast may be up to 80% inaccurate [54], cloud duration period may be randomly determined between 0 and 86400 seconds (24 hours). Therefore, cloud end time is given by (4.8), where  $t$  is the current simulation time snapshot (in seconds).

$$endtime = t + Unif (0, 86400) \quad (4.8)$$

For each snapshot, a random correction factor is applied to  $CCL$  in order to model cloud coverage level variability within different snapshots. The corrected  $CCL$  value  $CCL_{corrected}$  is modeled by a normal distribution ( $Norm(\mu, \sigma)$ ) with average  $\mu$  equal to  $CCL$  and standard deviation  $\sigma$  of 0.05 as in (4.9). Negative values of  $CCL_{corrected}$  are adjusted to zero.

$$CCL_{corrected}(t) = Norm(\mu = CCL, \sigma = 0.05) \quad (4.9)$$

$CCL_{corrected}(t)$  is, then, applied to determine the current solar irradiance level using (4.10), where  $Irr_{max}(t)$  is the maximum irradiance for the corresponding instant  $t$ , and is given in  $W/m^2$ .

$$Irr(t) = Irr_{max}(t) \times [1 - CCL_{corrected}(t)] \quad (4.10)$$

Equations (4.9)-(4.10) are repeated for the subsequent snapshots, until CT end time is reached. Once cloud duration has been completed, a new cloud-type is randomly chosen and the algorithm must be repeated using (4.7)-(4.10).

By the end of the 24-hour simulation, the solar irradiance level curve is determined. Figure 4.6 presents a sample curve derived from the proposed algorithm, for a clear day. The irradiance level is, indeed, close to the maximum ever recorded until 9:00, when a group of clouds cover part of incident irradiance.

This behavior persists up to 14:00, when clouds disappear and the incident irradiance level becomes closer to its maximum limit again.

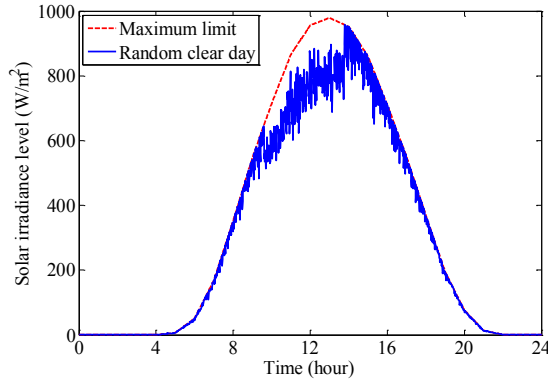


Figure 4.6 Solar irradiance level prediction for a clear day

Once the 24-hour solar irradiance curve has been determined, PV power output for a single snapshot is given by (4.11), according to the fundamental model proposed in Section 2.2..

$$\begin{aligned}
 P_{\max}(T) &= P_{\max\_STC} [1 - 0.0045(T - 25)] \\
 P(T) &= 0.96 \times \min\left(\frac{Irr}{1000 \text{ W/m}^2} \times P_{\max}(T), P_{\max}(T)\right)
 \end{aligned} \tag{4.11}$$

where,

$Irr$  is the solar irradiance level in  $W/m^2$ ;

$T$  is the PV cell temperature ( $^{\circ}C$ ) which can be replaced by the atmosphere temperature  $T'$  if it is difficult to measure  $T$ ;

$P_{\max\_STC}$  is the maximal power under the Standard Test Condition ( $R = 1000 \text{ W/m}^2$ ,  $T = 25^{\circ}C$ );

$P_{\max}$  is the PV array peak power output at temperature  $T$ .

#### 4.2.4 Deterministic device behavior

The capability to model deterministic events is also implemented in the proposed simulation platform. This feature is useful, for instance, for appliance identification. The user may wish to assign the exact time snapshot a certain



appliance is switched-on in order to verify the effectiveness of its NILM algorithm. In addition, it may also be used to study energy storage control algorithms such as the ones discussed in [55], since its working cycle is deterministically related to house demand.

### **4.3 Residential Network Modeling Technique**

There are 86,400 seconds over a 24 hour period. Each second represents one snapshot of the network. For any particular snapshot, the network configuration and the status of loads are known. This is a deterministic network scenario. Various power system solution techniques are developed to solve the scenario.

#### ***4.3.1 Fundamental Power Flow Calculation***

The power flow calculation includes house internal nodal voltages calculation in order to increase the simulator faithfulness to a real low-voltage residential network. Both linear and nonlinear devices are modeled as constant power loads. Thus, an iterative method is applied to solving the nonlinear power flow equations. In each iteration, a two-stage solution algorithm is adopted in order to reduce the network size and simplify the solution process. Rated nodal voltages are used as an initial guess.

The first stage updates voltages of the secondary network (outside the house). In this stage, home loads are transformed into equivalent impedances using their current terminal voltage and correspondent power demand. With the obtained impedances, house equivalent admittance seen from service panel and network admittance matrix ( $Y_N$ ) can be readily calculated.

The second stage updates voltages inside the house. A new estimative for internal nodal voltages is determined, solving the circuit of Figure 4.2 with load equivalent impedances and updating house service panel voltages ( $\hat{V}'_{an}, \hat{V}'_{bn}, \hat{V}'_{ab}$ ).

The techniques for solving the two stages are introduced in details as follows:

### A. Stage 1 – the Secondary Network Model

The nodal voltage method is a good choice for solving multiphase load flow problems. The first step is to generate the nodal admittance ( $Y$ ) matrix of the secondary distribution network.

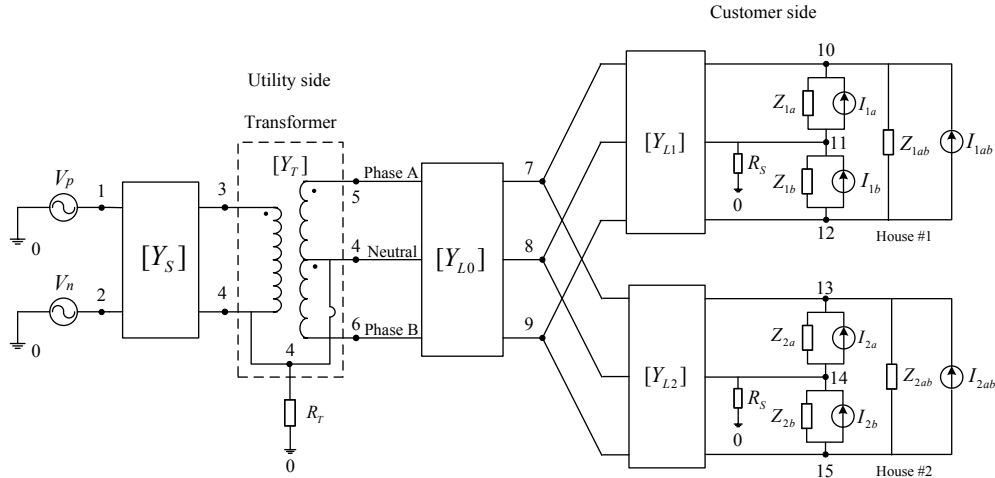


Figure 4.7 Multiphase secondary distribution network

Figure 4.7 shows a secondary network that contains two houses. The network can be divided into two parts: utility side and customer side. The nodal admittance matrix is expressed as the combination of several sub-matrices.

Utility side:

- Primary side equivalent admittance (2\*2 matrix):  $Y_S$
- Single-phase three-winding transformer admittance (3\*3 matrix):  $Y_T$
- Service conductor (transformer-PCC) admittance (3\*3 matrix):  $Y_{L0}$

Customer side:

- Service conductor (PCC-house) admittance (3\*3 matrix):  $Y_{Li}$  ( $i = 1, 2, \dots$ )
- Single house circuit admittance (3\*3 matrix):  $Y_{Hi}$  ( $i = 1, 2, \dots$ )

The detailed method of generating the  $Y$  matrix of the coupled line and the transformer is introduced in Appendix B. Thus the structure of the network branch admittance matrix is,



where  $Y_{i,i}$  is the self-admittance of node  $i$ ,  $Y_{ij}$  is the mutual-admittance between node  $i$  and node  $j$  ( $i, j = 1, 2, \dots, 15$ ). Since  $V_1$  and  $V_2$  are known and  $Y_{i,1} = 0$ ,  $Y_{i,2} = 0$  when  $i > 4$ , equation (4.14) can be transformed to:

$$\begin{cases} Y_{33}V_3 + Y_{34}V_4 \cdots & I_3 = -(Y_{31}V_1 + Y_{32}V_2) \\ Y_{43}V_3 + Y_{44}V_4 \cdots & I_4 = -(Y_{41}V_1 + Y_{42}V_2) \\ Y_{53}V_3 + Y_{54}V_4 \cdots & I_5 = 0 \\ & \vdots \\ Y_{15,3}V_3 + Y_{15,4}V_4 \cdots & I_{15} = 0 \end{cases} \quad (4.15)$$

Rewrite (4.15) in matrix form,

$$\mathbf{I}_N = \mathbf{Y}_N \mathbf{V}_N \quad (4.16)$$

Solved (4.16) for the network nodal voltage,

$$\mathbf{V}_N = \mathbf{Y}_N^{-1} \mathbf{I}_N \quad (4.17)$$

where,

$$\mathbf{Y}_N = \begin{bmatrix} Y_{33} & Y_{34} & \cdots & & \\ Y_{43} & Y_{44} & \cdots & & \\ \vdots & \vdots & \ddots & & \\ Y_{15,3} & Y_{15,4} & \cdots & & \end{bmatrix}, \quad \mathbf{V}_N = \begin{bmatrix} V_3 \\ V_4 \\ \vdots \\ V_{15} \end{bmatrix} \quad \text{and} \quad \mathbf{I}_N = \begin{bmatrix} -(Y_{31}V_1 + Y_{32}V_2) \\ -(Y_{41}V_1 + Y_{42}V_2) \\ \vdots \\ 0 \end{bmatrix} \triangleq \begin{bmatrix} I_{N1} \\ \vdots \\ 0 \end{bmatrix}$$

### **B. Stage 2 – Internal House Model**

Each room is represented by a branch connected to the service panel. The equivalent circuit is shown in Figure 4.8 (take Phase A-N as an example). The method of power flow calculation is as follows.

For the  $i$ -th iteration, transform each load into impedance using the internal room voltage:

$$Z_k^{(i)} = \frac{|V_{l,k}^{(i)}|^2}{P - jQ} \quad (4.18)$$

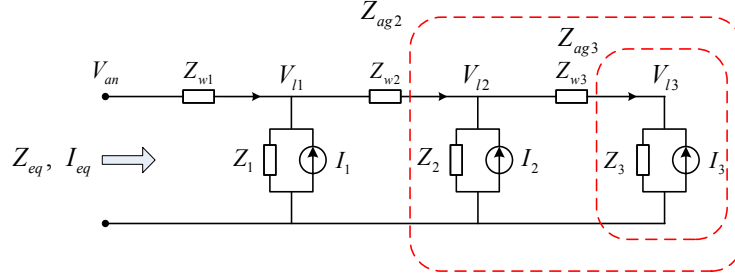


Figure 4.8 Single room equivalent circuit

Lump the load impedance of the same room in turn (house wire impedance is considered).

$$\begin{aligned}
 Z_{ag,K} &= Z_K \\
 Z_{ag,k-1} &= \begin{cases} (Z_{ag,k} + Z_{wk}) \parallel & \text{load k is on} \\ Z_{ag,k} + Z_{wk}, & \text{if load k is off} \end{cases} \\
 &\text{where } k = K, K-1, \dots
 \end{aligned} \tag{4.19}$$

The room equivalent impedance  $Z_{eq}$  is:

$$Z_{eq} = Z_{ag1} + Z_{w1} \tag{4.20}$$

Each phase of a house may include multiple rooms. By using (4.18)~(4.20), we can calculate all the room equivalent impedances of Phase A, House #1. Then the Phase A impedance is:

$$Z_{la} = Z_{eq-1} \parallel Z_{eq-2} \parallel \dots \tag{4.21}$$

Solve nodal voltage equation (4.16) and obtain the service panel voltage of each house. Then go back to the house circuit and calculate the internal room voltage.

$$V_{l,k}^{(i+1)} = V_{l,k-1}^{(i+1)} \times \frac{Z_{ag,k}}{Z_{ag,k} + Z_{wk}} \tag{4.22}$$

Update the equivalent impedance of each load for the next iteration by using (4.18).

### C. Iterative Load Flow Method

Based on the discussion above, the iterative method for solving the nonlinear power flow equations is summarized as follows:

**Step 1.** Initialize house internal voltages with rated value and the iteration counter with zero ( $i = 0$ ).

$$V_a^{(0)} = V_b^{(0)} = 120, \quad V_{ab}^{(0)} = 240$$

**Step 2.** Based on the house internal nodal voltages ( $V_{l1}^{(i)}, V_{l2}^{(i)}, \dots$ ), transform all house loads and PV inverters into impedances by using (4.18). Then calculate the equivalent impedance of each phase by (4.19)~(4.21):

$$Z_{la}, \quad Z_{lb}, \quad Z_{lab}$$

**Step 3.** Formulate the network  $Y_N$  matrix by using (4.12) and (4.13). Solve nodal voltage equation, and we can obtain the updated network nodal voltages. New house service panel voltages are  $V_{an}^{(i+1)}, V_{bn}^{(i+1)}, V_{ab}^{(i+1)}$ .

$$Y_N V_N = I_N \quad (4.23)$$

**Step 4.** Based on new service panel voltage and appliance apparent power, calculate household internal phase voltages by using (4.22):

$$V_{l1}^{(i+1)}, V_{l2}^{(i+1)}, \dots$$

**Step 5.** Check convergence criteria based on maximum voltage update:

$$\Delta V_{pu} (\%) = 100 \times \frac{\max \left\{ \left| V_k^{(i+1)} - V_k^{(i)} \right| \right\}}{V_{k-rated}} \quad k = 1, 2, \dots \quad (4.24)$$

where  $V_{k-rated}$  is the rated voltage at node  $k$  and  $N$  is the number of nodes in the system. If  $\Delta V_{pu} (\%) < 0.1\%$ , stop iteration. Otherwise return to **Step 2**.

This solution algorithm has been thoroughly tested on highly unbalanced networks. It has presented a robust convergence behavior (3 to 5 iterations) for all tested cases.

### 4.3.2 Harmonic power flow Calculation

Harmonic power flow results are needed to assess power quality impact. The solution algorithm adopted is also divided into the two stages as previously described. However, on harmonic frequencies, linear loads are modeled as impedances and nonlinear loads as current sources [56]. Thus the system solution becomes linear and no iteration is required. The network model and house internal circuit model refer to Figure 4.7 and Figure 4.8.

At h-th harmonic order, we aim to solve the nodal voltage equation:

$$\mathbf{Y}_{N,h} \mathbf{V}_{N,h} = \mathbf{I}_{N,h} \quad (4.25)$$

where

$$\mathbf{Y}_{N,h} = \begin{bmatrix} Y_{11} & Y_{12} & \cdots & & \\ Y_{21} & Y_{22} & \cdots & & \\ \vdots & \vdots & \ddots & \vdots & \\ Y_{13,1} & Y_{13,2} & \cdots & & \end{bmatrix}, \mathbf{V}_{N,h} = \begin{bmatrix} V_1 \\ V_4 \\ \vdots \\ V_{13} \end{bmatrix} \text{ and}$$

$$\mathbf{I}_{N,h} = [0, \cdots \quad \cdots \quad I_{2b}]^T.$$

Next is the procedure of the secondary system harmonic load flow that is done separately for each harmonic order.

**Step 1.** Calculate the equivalent impedance of each linear load and the harmonic current of each nonlinear load.

**Case 1:** The linear load is modeled as impedance:

$$Z(h) = R + jX(h) = \frac{P}{P^2 + Q^2} V_r^2 + jh \frac{Q}{P^2 + Q^2} V_r^2 \quad (4.26)$$

where  $P$  and  $Q$  are the real power and reactive power of the load respectively, and  $V_r$  is 120 or 240V.

**Case 2:** The nonlinear load is modeled as current source, based on the load harmonic spectrum:

$$I(1) = \frac{P - jQ}{V_x} \quad (4.27)$$

$$I(h) = I(1) \frac{I_{spectr}(h)}{I_{spectr}(1)}, \quad \theta(h) = \theta_{spectr}(h) + h(\theta(1) - \theta_{spectr}(1)) \quad (4.28)$$

where  $V_x$  is the phase voltage obtained from fundamental power flow calculation.

**Case 3:** The PV inverter model can be transformed to a Norton circuit in series with an impedance. Thus it is convenient to add the model to the nodal voltage equation.

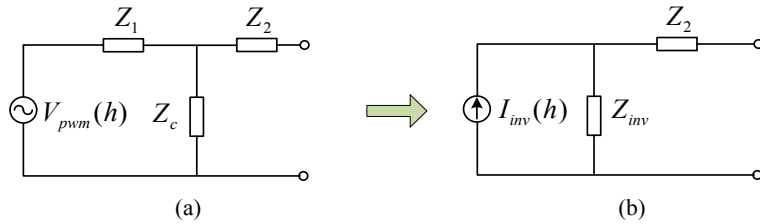


Figure 4.9 PV inverter model for harmonic power flow calculation

$$I_{inv}(h) = \frac{V_{pwm}(h)}{Z_1} \quad (4.29)$$

$$Z_{inv}(h) = Z_1 \parallel Z_c$$

**Step 2.** Calculate the house equivalent impedance and current injection in each phase (the method is similar to that introduced in Section 4.3.2). Then formulate the network nodal admittance matrix.

**Step 3.** Formulate and solve the nodal voltage equation (4.25).



### 4.3.3 Electromechanical Transients Simulation of Motor Starting

Transients in this simulation platform refer to the electromechanical transients associated with motor starting. Traditional motors are still widely used in residential networks nowadays. Examples are fridge, dryer and furnace. The starting of such motors produces unique current spikes. These spikes have been found very useful for NILM algorithms as they represent these motor loads. It is, therefore, important for the proposed platform to include motor starting transients.

A simplified induction motor dynamic behavior can be described as follows [63],

$$J \frac{d\omega}{dt} = T_E - T_L \quad (4.30)$$

where  $J$  is motor inertia coefficient ( $\text{kg.m}^2$ );  $\omega$  is rotor speed ( $\text{rad/s}$ );  $T_E$  is the electromagnetic torque produced by the motor ( $\text{N.m}$ );  $T_L$  is the load torque applied to motor shaft ( $\text{N.m}$ ). In particular,  $T_E$  is a function of  $\omega$ . In order to calculate the dynamic  $T_E$ , a single-phase motor circuit model should be applied.

#### A. Equivalent Circuit of Single-Phase Induction Motor

A single-phase induction motor with one stator winding inherently does not produce any starting torque when the rotor is still. In order to make the motor start, some arrangement is required to produce a starting torque. The simplest method is to connect an auxiliary winding in addition to the main winding in the stator. Then the motor is equivalent to an unbalanced two-phase motor (see Figure 4.10). When the motor reaches a rotating speed of 75% of synchronous speed, the auxiliary winding is automatically disconnected [63].

The capacitor-start/capacitor-run (CSCR) type is widely applied to hard-to-start load such as compressors, refrigerators and air-conditioners. Therefore CSCR is selected as the typical model for simulating the electromechanical transient process in this chapter. The simplified equivalent circuit of CSCR motor is shown in Figure 4.10.

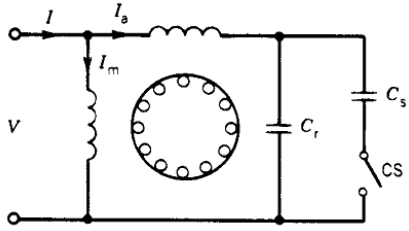


Figure 4.10 Capacitor-start, capacitor run induction motor

According to the double revolving field theory, the equivalent circuit of main/auxiliary winding can be split into two halves, as shown in Figure 4.11. The two halves represent the effects of forward and backward magnitude fields [63]. In the circuit, the deduction of  $Z_f$  and  $Z_b$  are presented in Appendix C.

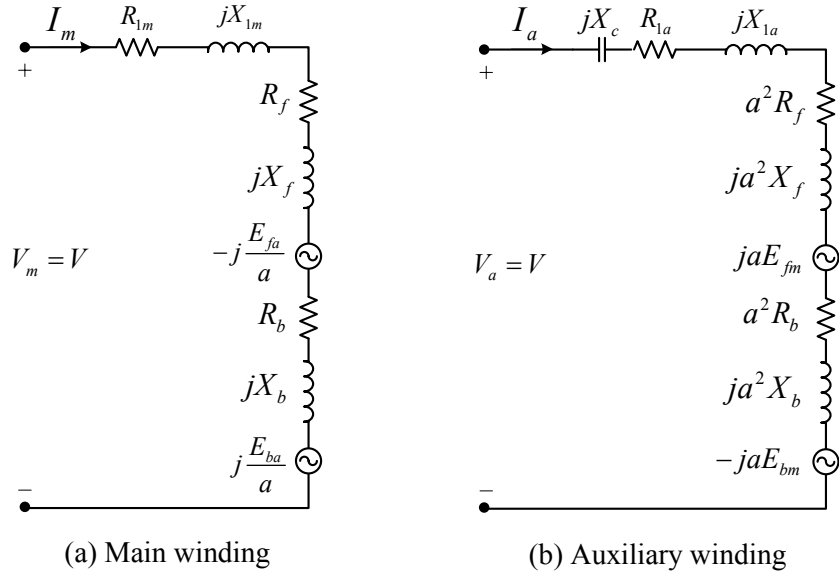


Figure 4.11 Equivalent circuit of single-phase motor we being standstill

The impedance of main winding and auxiliary winding are given by (4.31), where the compensate capacitor  $X_c$  is properly selected to maximize the starting torque per Ampere.

$$\begin{cases} Z_m = R_{lm} + jX_{lm} + Z_f + Z_b \\ Z_a = R_{la} + j(X_{la} - X_c) + a^2(Z_f + Z_b) \end{cases} \quad (4.31)$$

where  $a$  is the turns ratio between the auxiliary winding and the main winding.

$a = \frac{N_a}{N_s}$ , it is generally close to 1. With the impedance and the terminal voltage  $V$

known, the winding input currents can be solved from equations (4.32).

$$\begin{cases} Z_m I_m - ja(Z_f - Z_b) I_a = V \\ ja(Z_f - Z_b) I_m + Z_a I_a = V \end{cases} \quad (4.32)$$

Then the dynamic torque is,

$$T_E = \frac{2a |I_a| |I_m| (R_f + R_b)}{\omega_{syn}} \sin \langle I_a, I_m \rangle \quad (4.33)$$

Initially, default (or user input) values are assigned to motor parameters, such as impedances, inertia coefficient  $J$ , rated slip  $s_r$  and rated efficiency  $\eta_r$ . Then, one may calculate rated load torque according to (4.34), where  $\omega_{sync}$  is the rotor synchronous speed in rad/s; and  $P_{in}$  is the power consumed by the motor in watts.

$$T_{L-rated} = \frac{P_{out}}{\omega_{mec-rated}} = \frac{\eta_r \times P_{in}}{\omega_{sync} \times (1 - s_r)} \quad (4.34)$$

Load torque relationship with rotor speed depends on load type. For fans (present in the furnace) torque depends on rotor speed squared, while for compressors (present in the fridge) load torque is constant for any rotor speed [64].

Since the angular speed of motor varies smoothly in a dynamic process, the differential equation (4.30) can be transformed into a difference equation with a time step of 1 cycle (1/60 second).

$$\omega(t + \Delta t) = \frac{\Delta t}{J} (T_E(t) - T_L) + \omega(t) \quad (4.35)$$

Since the time resolution for NILM study is 1 second, the first recorded motor starting instant is randomly determined within a 1 second window of the simulation period, as in (4.36), where  $t_0$  is the first recorded time, given in seconds.

$$t_0 = Unif(0,1) \quad (4.36)$$

Once the motor starting instant has arrived, its speed  $\omega(t + \Delta t)$  and correspondent slip  $s(t + \Delta t)$  must be updated using (4.35), where  $\Delta t$  is the integration step and  $T_E(t)$  is determined according to (4.31)~(4.33) with slip  $s(t)$  (initial speed is zero and, consequently, initial slip is 1).

$$t + \Delta t = t_0 + n \times 1 \text{sec}, \quad n \text{ is integer} \quad (4.37)$$

When (4.37) is satisfied, the motor dynamic power demand is calculated as (4.38). Thus the appliance is modeled as  $P(t) + jQ(t)$  at this snapshot and one network power flow solution is performed using the algorithms described in Section 4.3.1, 4.3.2. This algorithm must be repeated for the next integration step  $t + \Delta t$  until steady-state operation is achieved.

$$\begin{cases} I(t) = I_a(t) + I_m(t) \\ P_{start}(t) = V_s(t)I(t) \cos \langle V_s, I \rangle \\ Q_{start}(t) = V_s(t)I(t) \sin \langle V_s, I \rangle \end{cases} \quad (4.38)$$

### **B. Case Study**

During the dynamic simulation process explained above, it should be verified whether appliance terminal voltage can be regarded as constant. If the assumption is true, it greatly simplifies the solution algorithm, since the terminal voltage does not need to be updated at every integration step  $\Delta t$ . The real measurement data (Figure 4.12) have shown that service panel voltage drop during motor start is around 0.01 p.u. and lasts for less than one second, while the simulator resolution is 1 second. Therefore we can use the rated service panel voltage for the dynamic simulation.

$$\begin{cases} I(t) = I_a(t) + I_m(t) \\ P_{start}(t) = 120 \times I(t) \cos \langle I \rangle \\ Q_{start}(t) = 120 \times I(t) \sin \langle I \rangle \end{cases} \quad (4.39)$$

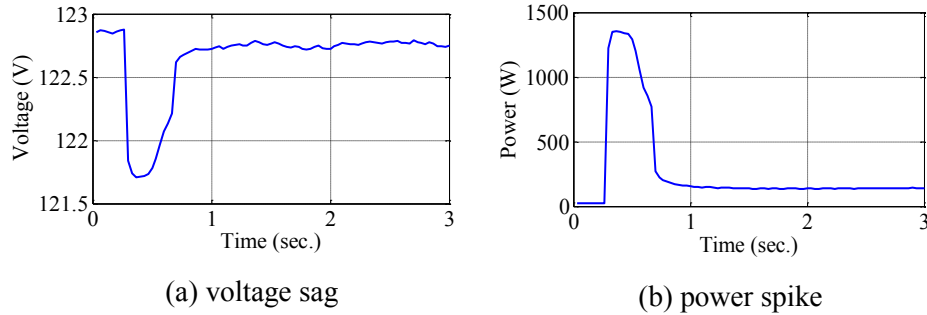


Figure 4.12 Measurement results during fridge starting transient

Based on the typical single-phase induction motor parameters (shown in Appendix C), the motor starting dynamic power is simulated and presented in Figure 4.13.

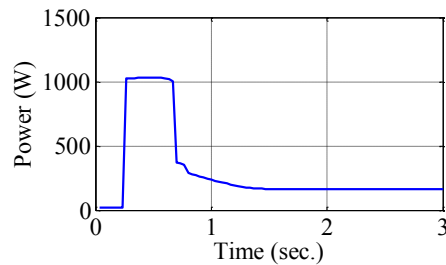


Figure 4.13 Simulation results during a fridge starting transient

#### 4.3.4 Simulation of Home Appliances Dynamic Behavior

Some appliances operate with multistage/multilevel power demand characteristics, which is called trend signature [37]. An example is the washing machine that has wash, rinse, and spinning modes. Modeling such appliances is essential for the simulator and is done as follows. Once an appliance is ON, the simulator also models a set of random variables that compose its signature.

The classification of load trend signature is summarized in Table 4.3 [37]. The simulation platform should be able to simulate these signatures. In this simulation platform, only the signature of rising spike (caused by motor starting) is modeled analytically. Other 5 signatures are modeled according to the measurement data. Due to the parameter variation of these signatures, we have to introduce a series of random parameters to describe the dynamic operating behavior of appliances.

Table 4.3 List of power trend signatures

| Trend signature | Characteristic   | Cause or when to happen  | Example appliances |
|-----------------|--|--|--------------------|
| Rising spike    | Short-term high-level of dynamic power                               | Inrush current when the motor is starting  | Fridge, furnace    |
| Falling spike   | Short-term low-level of dynamic power                                | At the moment of switching channels  | TV                 |
| Pulses          | Repetitive switch-on or switch-off event through the operation cycle | Caused by power electronic devices in two situations   | Stove, washer      |
| Multi-stage     | Several steady-state power level                                     | The appliance is operating in different states   | Furnace, PC        |
| Fluctuation     | Continues low-frequency variation of power                           | Caused by power electronic devices   | Freezer            |
| Noises          | Continues high-frequency variation of power                          | For laptops and TV, the power consumptions constantly vary with the sound, visual display or other tasks | Laptop, TV         |

### A. Rising Spike

The rising spike is caused by the inrush current of the motor starting. Take fridge as an example, the load signature is presented in Figure 4.14.

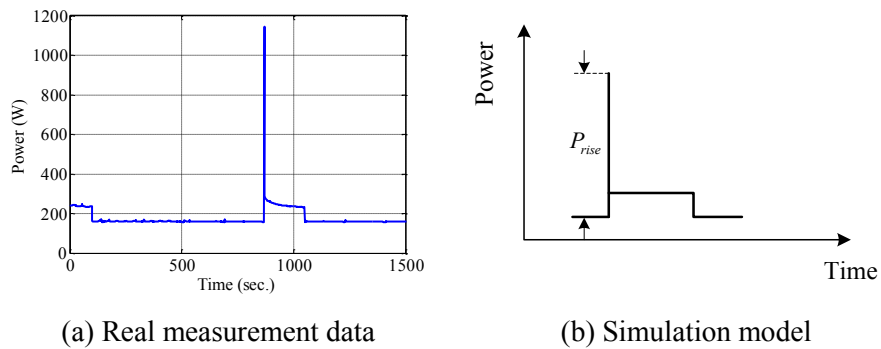


Figure 4.14 Rising spike signature

The duration of dynamic process is,  $T_r = 2s$ . During this two seconds, a subprogram is called for calculating the motor starting dynamic power  $P_{rise}$ . The method is discussed in Section 4.3.3.

$$P_{rise}(n) = P_{start}(t_0 + n) \quad t_0 = Unif(0,1), n = 0, 1 \text{ or } 2$$

### B. Falling Spike

Falling spike is caused by channel changing of TVs. Take LCD TV as an example, the load signature is presented in Figure 4.15, and the duration and power level of falling spike are listed in Table 4.4:

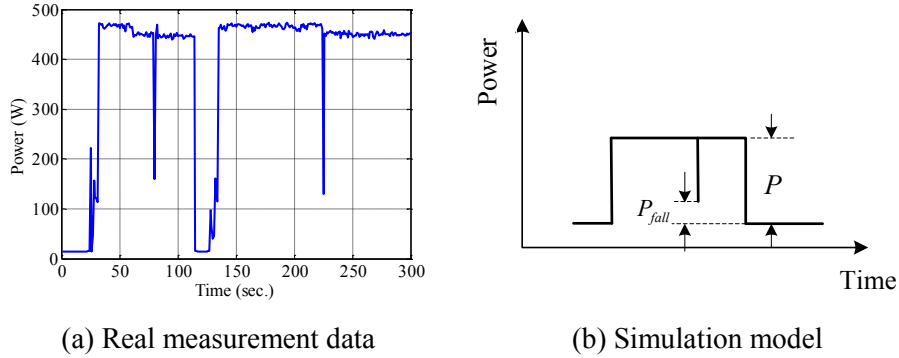


Figure 4.15 Falling spike signature

Table 4.4 Example of LCD TV as a falling spike model

| Variable          | Value            |
|-------------------|------------------|
| $P$ (W)           | user-defined     |
| $T_{fall}$ (sec.) | $Unif(1,3)^*$    |
| $P_{fall}/P$      | $Norm(0.2,0.02)$ |

\* All the random timespan values are rounded because the simulation time step is 1 second.

### C. Pulses

Many heating appliances have pulses when they are operating, such as stove and heater. The duty ratio may differ, for example, from 0.2~0.6, depending on the tap position the user chooses. The duty-ratio of each cycle is modeled as norm distribution. The load signature and random parameters are presented in Figure 4.16 and Table 4.5 respectively.

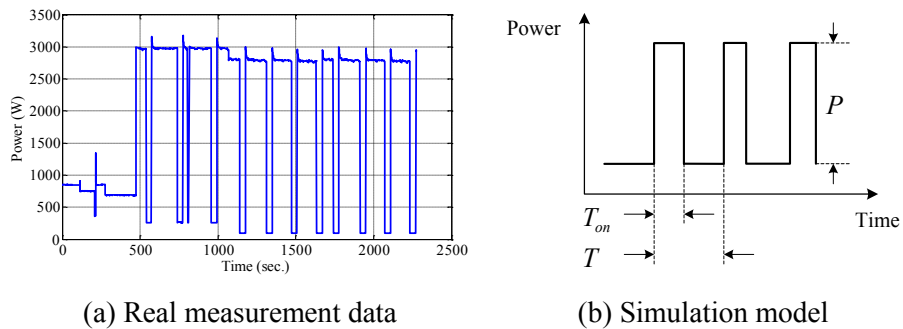


Figure 4.16 Duty cycle of pulses

Table 4.5 Example of stove as a pulses model

| Variable   | Value           |
|------------|-----------------|
| $P$ (W)    | user-defined    |
| $T$ (sec.) | $Norm(30,2)$    |
| $T_{on}/T$ | $Unif(0.2,0.6)$ |

#### D. Multi-level and Multi-stage

The furnace signature (shown in Figure 4.17), for instance, has four power levels and three different stages. The ratio between each power stage and the rated power should be determined randomly. The random parameters are presented in Table 4.6.

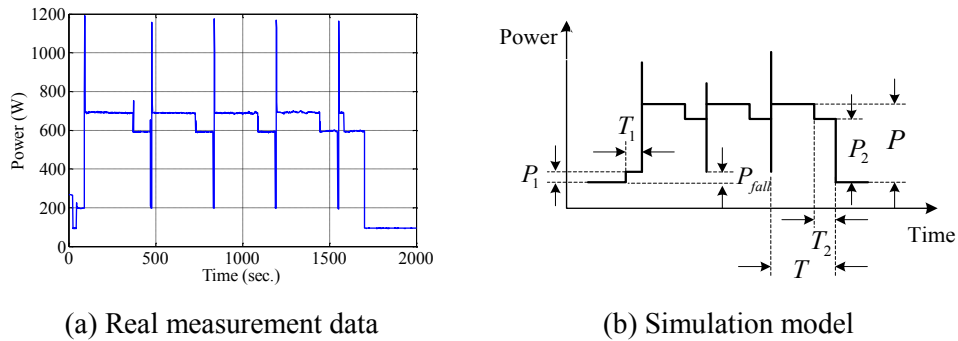


Figure 4.17 Multi-stage appliances

Table 4.6 Example of furnace as a multi-level, multi-stage model

| Variable     | Value            |
|--------------|------------------|
| $P$ (W)      | user-defined     |
| $P_1/P$      | $Norm(0.8,0.01)$ |
| $P_2/P$      | $Norm(0.2,0.01)$ |
| $P_3/P$      | $Norm(0.2,0.01)$ |
| $T$ (sec.)   | $Norm(360,30)$   |
| $T_1/T$      | $Unif(0.3,0.7)$  |
| $T_2$ (sec.) | 60               |

#### E. Fluctuation

Some appliances contain continuous low-frequency variation of power. Take the freezer as an example, the load signature and random parameters are presented in Figure 4.19 and Table 4.7 respectively.



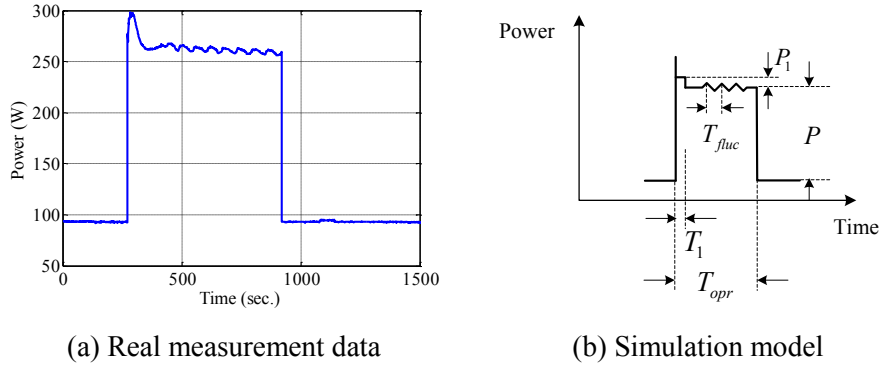


Figure 4.18 Fluctuation signature

Table 4.7 Example of freezer as a fluctuation model

| Variable          | Value                                  |
|-------------------|--|
| $P$ (W)           | user-defined                           |
| $T_{fluc}$ (sec.) | $Norm(60,5)$ model it as triangle wave |
| $T_1/T_{opr}$     | $Unif(0.05,0.1)$                       |

### F. Noise

Some appliances contain continues high-frequency variation of power. Take the laptop as an example, the load signature and random parameters are presented in Figure 4.19.

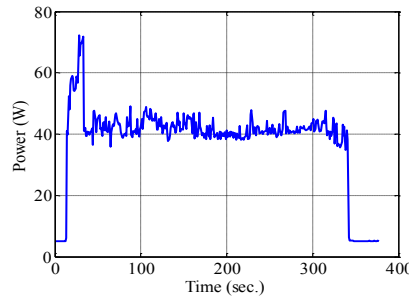


Figure 4.19 Multi-stage appliances

We use “typical noise” to model the power noise of the laptop. The “standard noise” is extracted from the real measurement data and normalized, as is shown in Figure 4.20.

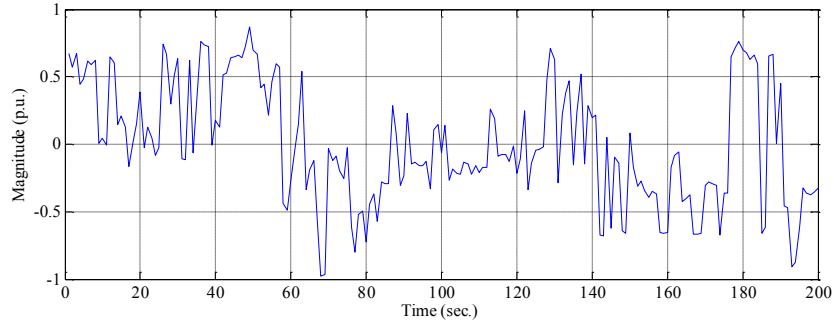


Figure 4.20 Standard noise for simulating the random load behavior

## 4.4 Summary of Simulation Platform

### 4.4.1 Structure of the Simulation Platform

The simulation tool proposed in this paper may be summarized with a high-level flowchart presented in Figure 4.21, which is further described below.

We aim to develop such an easy-to-use simulation platform for studying the electric feature of the residential network. Therefore, the “Read Input Data” routine provides a user-friendly input data structure divided into two files, which are described as follows:

**1) Network electrical information:** this file contains utility related information (primary network equivalent, transformer parameters, distribution lines parameters, grounding impedances, etc.), in addition to nonlinear appliances harmonic spectrum. Default information is provided for all parameters, for the user unfamiliar with such electrical data.

**2) Residential houses information:** this file contains household device connections. The user must specify which devices are installed at which room. A generic type and number of appliances can be specified, which provides the user with great flexibility to create a realistic house scenario. The only electrical information required is the device rated power and power factor. Therefore, this file may be edited by any users, even those who are not familiar with network

electrical concepts. Additionally, specific non-default appliance behavior patterns can also be provided on this input file.

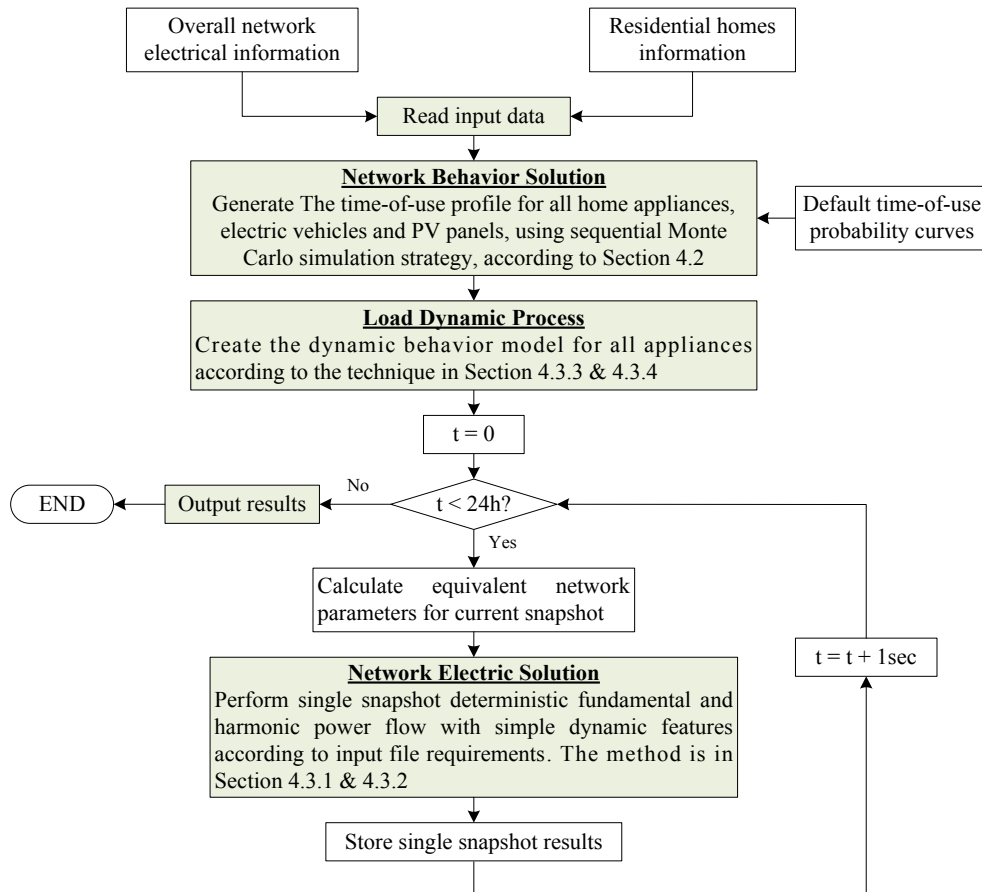


Figure 4.21 Overall LV network simulation platform flowchart

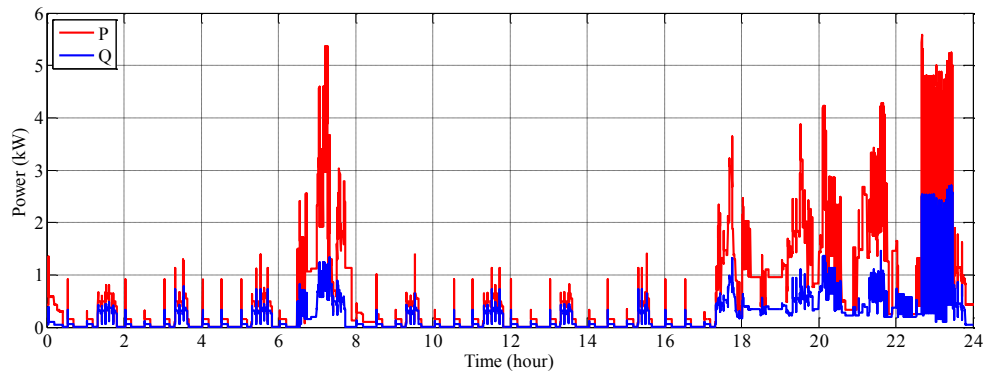
Firstly, the input information feeds the “Network Behavior Solution” core, which determines the switch-on states of all household devices throughout the 24-hour simulation. If no specific behavior information is provided by the user for a device, default time-of-use probability curves are considered. Secondly, the dynamic behavior of home appliances is added to the load profile. Thirdly, for each time snapshot (one second), corresponding load states (per-unit operating power level) are retrieved, equivalent network parameters are calculated, and the “Network Electric Solution” core is executed. After each electric solution snapshot, fundamental and harmonic voltages at the house service panel are stored. Then, based on house equivalent impedances, both power and current demand at each phase are determined. Once the simulation has finished, “Output results”

routine is performed to provide the study outcome in a table format with the output variables behavior over the simulated period. Results may be later read and processed according to user needs. The structure of the input file will be introduced in Appendix D.

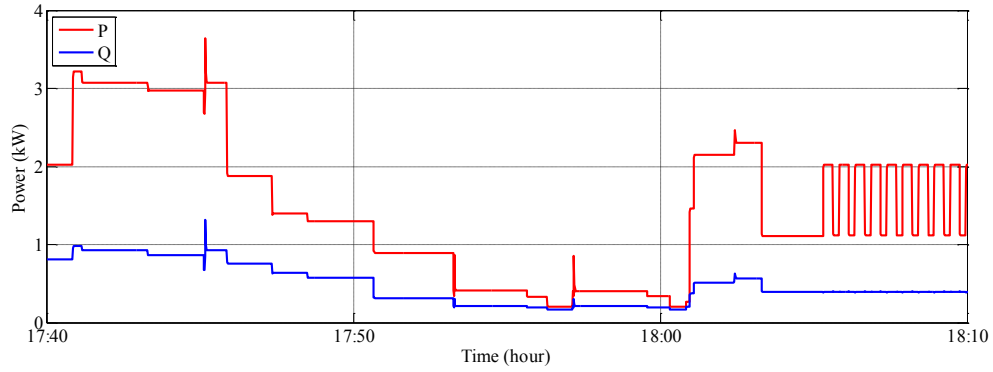
A platform prototype has been developed using the Matlab environment. In terms of computational processing, the highest efforts involved are the calculation and factorization of the network admittance matrix for fundamental and each harmonic frequency. The simulation time of 1 snapshot on a 10-house network with over 100 appliances (about 250 nodes) up to the 9<sup>th</sup> harmonic is approximately 100 ms. This value may be drastically reduced if sparse matrix techniques, code optimization and, overall, a compiled programming language is used.

#### 4.4.2 Examples of the Simulation Result

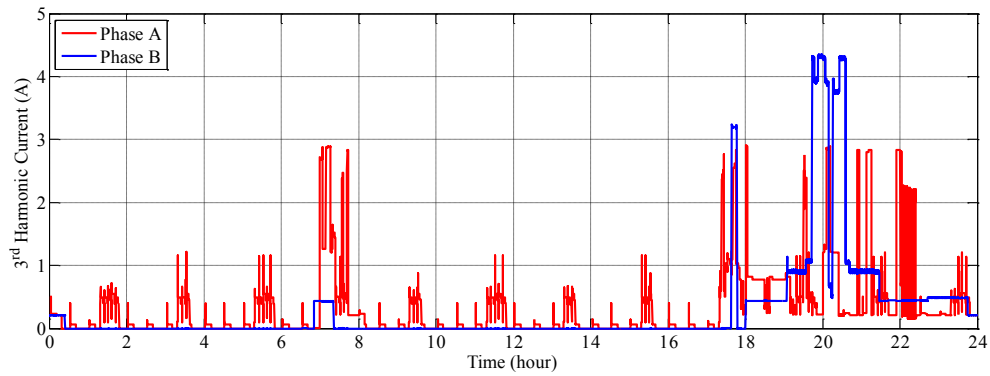
Figure 4.22 shows an example power demand and third harmonic profile of a home produced by the simulator over a 24 hour period. The Figure 4.22 (b) and (d) indicates that the load signature such as spike, pulses and multi-stages are clearly simulated, which provide the NILM study with good test examples.



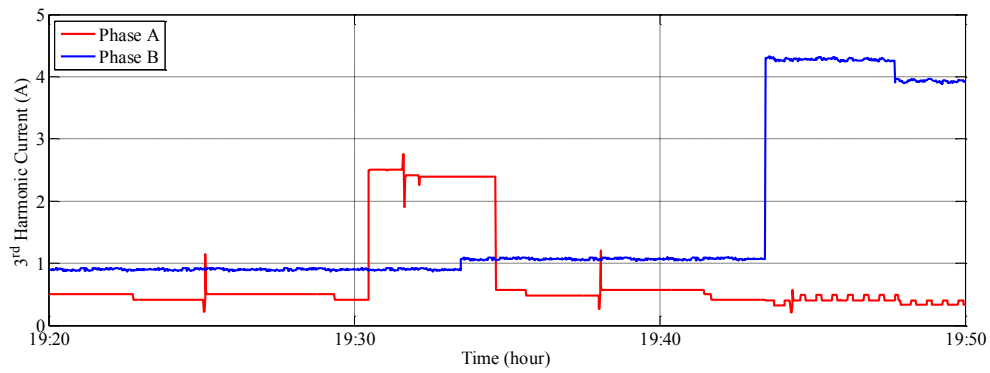
(a) 24-hour profile



(b) 30-min partial amplitude



(c) 24-hour profile



(d) 30-min partial amplitude

Figure 4.22 Sample power demand and third harmonic simulation results

## 4.5 Case Studies

This section presents several case study results. They are used to illustrate the potential applications of the platform. The network electrical parameters and residential house parameters are presented in Table 4.8 and Table 4.9 respectively.

Table 4.8 Input / built-in parameters

| Classification                          | Parameters   | Sample values   |
|---|--|---|
| Primary System<br>(Thevenin equivalent) | Phase voltage $V_p$<br>Neutral voltage $V_n$<br>Source equivalent impedance  | 14.4kV<br>10V<br>$Z_p = 64.04 + j46.58\Omega$<br>$Z_n = 1.537 + j0.448\Omega$<br>$Z_{pn} = 0.439 + j0.834\Omega$  |
| Service Transformer                     | Apparent power rating $S_r$<br>Base power $S_{base}$<br>Voltage rating<br>Short-circuit R<br>Short-circuit X<br><br>Grounding resistance $R_T$ | 37.5 KVA<br>37.5 KVA<br>14400/120V<br>0<br>$X_{pa} = 0.04\text{p.u.}$ , $X_{pb} = 0.04\text{p.u.}$ ,<br>$X_{ab} = 0.05\text{p.u.}$<br>12 $\Omega$   |
| Secondary System                        | Secondary conductor impedance (self and mutual impedance)<br><br>Length of transformer – PCC<br>Length of PCC – House #X                       | $Z_A = Z_B = 0.249 + j0.878\Omega/\text{km}$<br>$Z_N = 0.427 + j0.961\Omega/\text{km}$<br>$Z_{AN} = Z_{BN} = 0.0592 + j0.429\Omega/\text{km}$<br>$Z_{AB} = 0.0592 + j0.491\Omega/\text{km}$<br>$l_0 = 0.10\text{km}$<br>$l_1 = 0.09\text{km}$ , $l_2 = 0.07\text{km}$ , ... |
| House #X                                | Grounding resistance $R_S$<br>Phase impedance<br>Neutral impedance   | 1 $\Omega$<br>$Z_{ph} = 0.21 + j0.094 \Omega/\text{km}$<br>$Z_{nn} = 0.55 + j0.365 \Omega/\text{km}$  |

Table 4.9 Home appliance parameters

| Room | Phase connection | Appliance code | Quantity | P (W) | PF   | Distance to service panel (km) |
|------|------------------|----------------|----------|-------|------|--------------------------------|
| 1    | A                | WSH*           | 1        | 180   | 0.45 | 0.009                          |
| 1    | A                | TOA            | 1        | 1000  | 1    | 0.012                          |
| 1    | A                | MW             | 1        | 1200  | 0.99 | 0.014                          |
| 1    | A                | HEA            | 1        | 220   | 0.99 | 0.014                          |
| 1    | A                | MBL            | 4        | 33    | 0.38 | 0.021                          |
| 1    | A                | RFR            | 1        | 150   | 0.94 | 0.024                          |
| 2    | B                | PC             | 1        | 100   | 1    | 0.015                          |
| 2    | B                | LCD            | 1        | 40    | 0.96 | 0.015                          |
| 3    | B                | CFL            | 6        | 15    | 0.9  | 0.010                          |
| 3    | B                | FRZR           | 1        | 180   | 0.9  | 0.019                          |

|   |    |       |   |      |      |       |
|---|----|-------|---|------|------|-------|
| 3 | B  | LAP   | 1 | 75   | 0.96 | 0.024 |
| 3 | B  | LCDTV | 1 | 300  | 0.99 | 0.033 |
| 4 | A  | FUR   | 1 | 500  | 0.84 | 0.020 |
| 5 | AB | STO   | 1 | 1200 | 0.95 | 0.010 |
| 5 | AB | DRY   | 1 | 4000 | 0.88 | 0.016 |

\* The meaning of each appliance code refers to Appendix D.

Five scenarios of case study are made by using the simulator.

#### 4.5.1 Power Quality Impact of PV Inverter Integration

A utility company may want to investigate technical impacts arisen from the increasing connection of residential rooftop PV systems on low voltage networks. To achieve such goal, a sample case study is performed on a 10-house network scenario. On the considered network, 5 houses are randomly selected to contain PV systems with power ratings of 2~3 kW. The PV systems are phase-to-phase connected to avoid the voltage unbalance. A clear day is considered in this case. Figure 4.23 compares the 1-min average service panel phase voltages before and after PV integration.

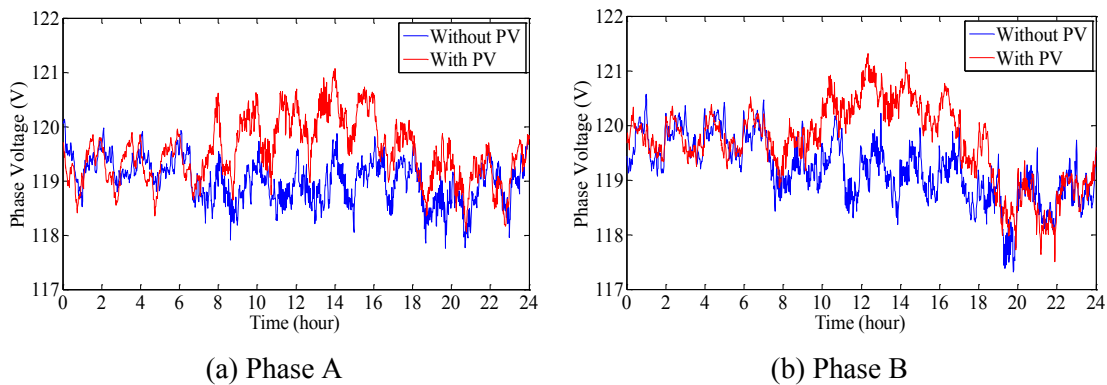


Figure 4.23 PV array integration impact on service panel voltages

Simulation results can identify a voltage rise around noon. The main reason is as follows: during the noon period with high solar irradiance, the PV output power is likely to far exceed the house power demand. Therefore there is a reverse power flow from the customer side to the utility side, and a voltage rise at the service panel occurs. Such results indicate that the overvoltage during the day may

become a concern for the utilities according to PV penetration levels. Specially, if the grid is not stiff enough (grid impedance observed from house entrance point is large), the overvoltage caused by the PV integration would be even more significant.

The simulation platform is also suitable for more detailed studies, such as 1) identifying the impacts of an increasing PV penetration trend over the years, and 2) investigating the cloud transient impact on the voltage regulation of LV networks with high PV penetration.

#### ***4.5.2 Neutral-to-earth Voltage Incidence***

In this example, a brief investigation is made about the impact of neutral condition and PEV load on neutral-to-earth voltage (NEV) at the service entrance point of a house. NEV has been considered as the main source of stray voltage in residential houses [40]. It is an important branch of the distribution system condition monitoring.

To simulate a damaged neutral condition, an impedance of  $0.3\Omega$  is added in series with the neutral conductor connected to one of the 10 houses in the network. According to Figure 4.24 and Table 4.10, a damaged neutral condition will negatively impact the NEV, increasing the risk of stray voltage incidents. The 95%-index presented in Table 4.10 shows the NEV values that are not exceeded during 95% of the simulation duration (24 hours). The result clearly indicates that the broken neutral can make the NEV more sensitive to the load variation. As a result, the NEV is more likely to exceed the limit.



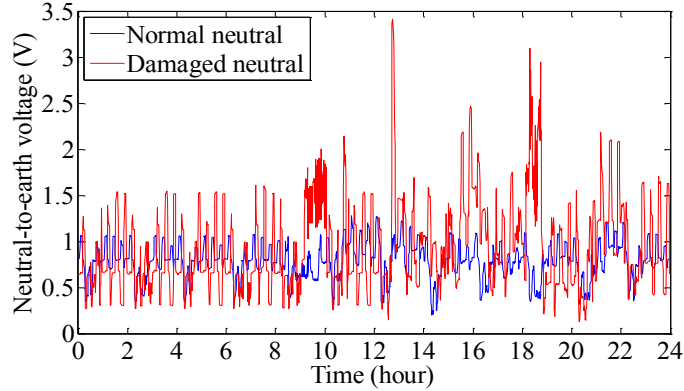


Figure 4.24 Impact of neutral condition on neutral-to-earth voltage level

Table 4.10 95%-index of NEV for Different Neutral Conditions

| Normal neutral | Damaged neutral | Difference |
|----------------|-----------------|------------|
| 1.08 V         | 1.83 V          | 69.4%      |

Another example is the impact of plug-in electric vehicle (PEV) on the neutral-to-earth voltage. When the PEV is connected phase-to-neutral, the high power level of the load may lead to a neutral voltage rise. Figure 4.25 presents the comparison between 1-min-average neutral voltages in two cases. The result indicates that the neutral voltage can obviously increase at night when the PEV charger is in operation.

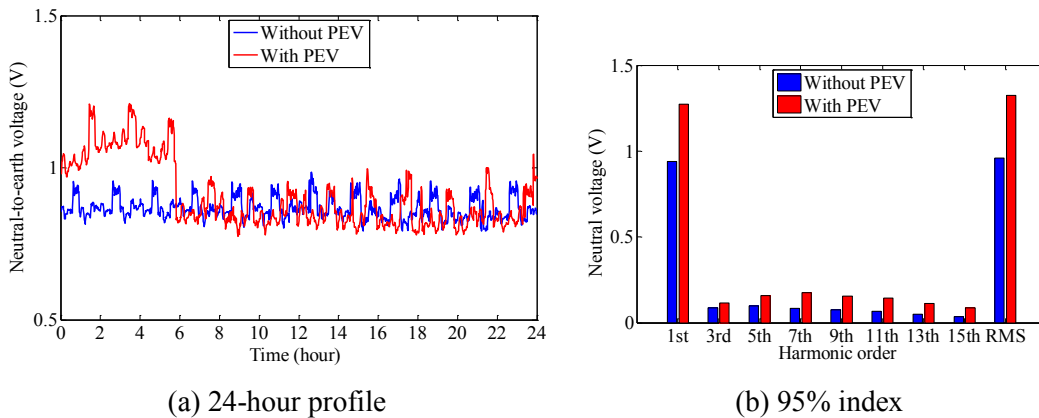


Figure 4.25 Neutral-to-earth voltage at the service panel side (House #9)

### 4.5.3 Residential load Identification

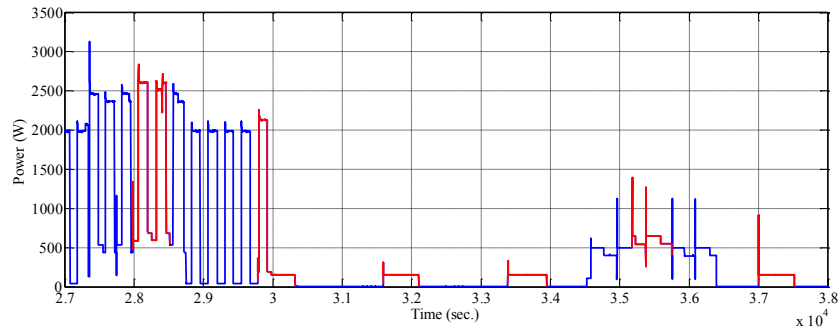
This subsection evaluates the effectiveness of NILM algorithm proposed in [37]. A 5-day simulation is performed using the platform. The power demand profile

for one household over the 5 days is fed into the appliance identification program. The success rate of appliance identification for some of the major appliances is shown in Table 4.11.

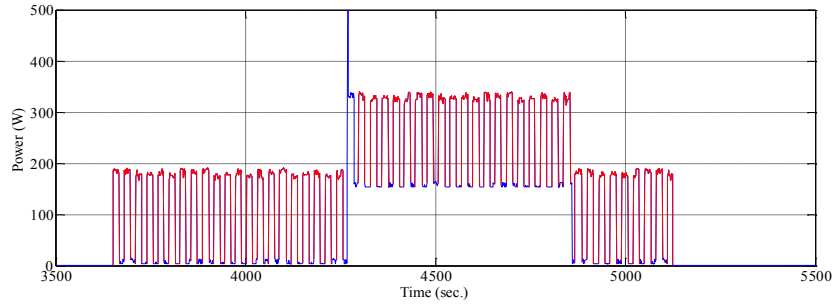
Some examples of the load identification result (the identified load are labeled with the red curve) are presented in Figure 4.26.

Table 4.11 Identification accuracy summary

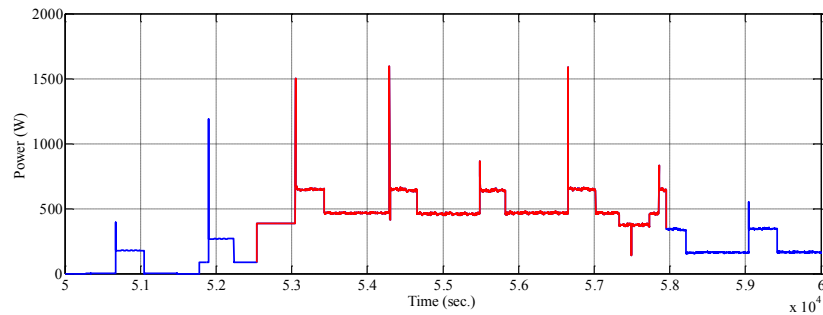
| Appliance name | Actual operation times | Correctly identified times | False identified times | Identification accuracy (%) |
|----------------|------------------------|----------------------------|------------------------|-----------------------------|
| Fridge         | 240                    | 218                        | 0                      | 90.8                        |
| Freezer        | 360                    | 345                        | 0                      | 95.8                        |
| Microwave      | 36                     | 31                         | 0                      | 86.1                        |
| Stove          | 14                     | 14                         | 0                      | 100                         |
| Furnace        | 60                     | 56                         | 0                      | 93.3                        |
| Washer         | 2                      | 2                          | 0                      | 100                         |
| Dryer          | 2                      | 2                          | 0                      | 100                         |
| Laptop         | 3                      | 3                          | 0                      | 100                         |
| PC & LCD       | 4                      | 3                          | 0                      | 75                          |
| LCDTV          | 9                      | 9                          | 0                      | 100                         |
| CFL            | 17                     | 14                         | 0                      | 82.4                        |
| Water heater   | 3                      | 3                          | 0                      | 100                         |
| Toaster        | 4                      | 4                          | 1                      | 75                          |
| MBL            | 11                     | 9                          | 0                      | 82.0                        |



(a) Fridge



(b) Washer



(c) LCD TV

Figure 4.26 Identification of home appliances

#### 4.5.4 Demand Response Analysis

Demand response is shifting or shaving of electricity use during peak demands in response to price signals or other criteria. By smoothing peaks in demand, consumers can both reduce their electricity costs and their environmental footprint [65].

Time-of-use prices reflect the fact that the cost to provide electricity changes throughout the day. When demand is low, less expensive sources of electricity are used. When demand rises, more expensive forms of electricity production are called upon, making prices higher. There are three different time-of-use prices: 6.7¢/kWh for off-peak, 10.4¢/kWh for mid-peak, 12.4¢/kWh for on-peak. These prices are changed every May 1 and November 1 by the *Ontario Energy Board* (OEB) [65] (shown in Table 4.12).

Table 4.12 Time-of-use electricity price in Ontario

| Day type | Time period   | Summer<br>(May 1 <sup>st</sup> ~ Oct. 31 <sup>st</sup> ) |       | Winter<br>(Nov. 1 <sup>st</sup> ~ Apr. 30 <sup>th</sup> ) |       |
|----------|---------------|--|-------|---|-------|
|          |               | Feature  | ¢/kWh | Feature   | ¢/kWh |
| Weekday  | 7:00 ~ 11:00  | Mid-peak   | 10.4  | On-peak   | 12.4  |
|          | 11:00 ~ 17:00 | On-peak  | 12.4  | Mid-peak  | 10.4  |
|          | 17:00 ~ 19:00 | Mid-peak   | 10.4  | On-peak   | 12.4  |
|          | 19:00 ~ 7:00  | Off-peak   | 6.7   | Off-peak  | 6.7   |
| Weekend  | All day       | Off-peak   | 6.7   | Off-peak  | 6.7   |

In this example, the proposed platform is used to evaluate a demand response strategy. It consists on scheduling the laundry activity (washer and dryer working cycles), which is more likely to occur from 8:00 to 15:00 [46], to an off-peak time, in order to take advantage of a time dependent tariff. If a time dependent tariff is considered, such action could reduce the total energy bill, in addition to reduce the household peak demand. The result of the proposed demand response program is presented in Figure 4.27. The strategy effectiveness is confirmed by over 10% electricity bill reduction (shown in Table 4.13).

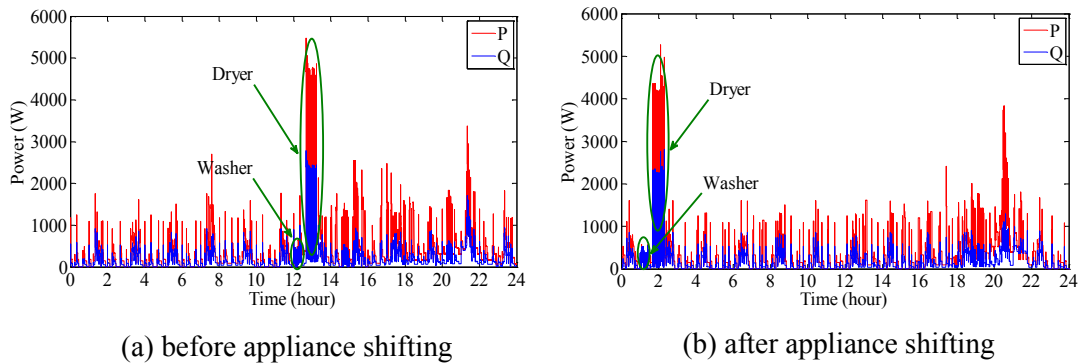


Figure 4.27 Demand response technique evaluation on LV simulator

Table 4.13 Daily Expense Saving with Demand Response Strategy Application

|                           | Energy demand<br>(kWh) | Total expense<br>(CAD ¢) |
|---------------------------|------------------------|--------------------------|
| Before appliance shifting | 8.02                   | 79.2                     |
| After appliance shifting  | 8.03                   | 68.4                     |

## 4.6 Summary

A sequential Monte Carlo simulation platform for residential networks has been proposed in this chapter. This platform can be used to assist the research of power quality impact of PV inverters. It can also be used to verify and demonstrate demand-side based smart-grid techniques. The platform consists of two main components. The first is a multiphase network model with power flow, harmonic and dynamic study capabilities. The second is a load/generation behavior model that established the operating characteristics of various loads/generators based on time-of-use probability curves. These two components are combined together through a sequential Monte Carlo simulation scheme. The usefulness of the platform has been demonstrated through application case studies.

## Chapter 5

### Conclusions and Future Works

#### 5.1 Thesis Conclusions and Contributions

This thesis discussed the power quality impact of small-scale PV inverters on the low voltage residential networks. A systematic method was established for the modeling of PV inverters at both fundamental and harmonic frequency. In addition, the harmonic impact assessment was conducted for the low voltage residential networks.

The major conclusions and contributions of this thesis are summarized as follows:

- An extensive survey was conducted to extract the general features of the authentic PV system. The information such as PV system circuit topology, the typical parameters of the PV module and PV inverters were summarized. These practical technical data ensures that the study is of considerable industry application.
- The steady-state model of the PV inverter was developed. At the fundamental frequency, the PV inverter is modeled as a negative constant power load. The output power is determined by two external environmental factors, solar irradiance and temperature. At the harmonic frequency, it is modeled as a voltage source in series with a passive filter. The PV inverter models were verified through the field data analysis, the Matlab-Simulink simulation and the lab experiment. According to the harmonic model, the PV inverter has both harmonic source characteristic and harmonic impedance characteristic.
- Based on the PV inverter model, a harmonic impact assessment was conducted for secondary distribution system. It was concluded that the

harmonic impact of PV inverters is mainly caused by the filter impedance of the harmonic model. Furthermore, the resonance issue of PV inverter was studied. For harmonic orders that are close to the resonance frequency, the filter impedance can result in a slightly higher harmonic voltage. For other harmonic orders, the filter can decrease the harmonic voltage. The simulation and analytical study shows that the harmonic resonance resulting from large PV penetration is not serious. Therefore from the perspective of harmonics, the PV inverter will not negatively affect the power quality of residential distribution networks.

In addition, another research work related to the power quality issue of residential distribution networks is presented in Chapter 4. This work developed a Monte Carlo simulation platform tool for studying the electric feature of low-voltage system. The platform includes both the electrical model and behavior model of the loads and PV inverters. In particular, it can be used to study the power quality impact of PV inverters on the system under practical operating state. The simulation result indicates that although the harmonic-related issue is not serious, the voltage rise can be a concern with large PV penetration. In addition, the platform can support a number of studies related to the residential distribution system, such as non-intrusive load monitoring (NILM), distribution system condition monitoring and demand response.

## **5.2 Suggestion for Future Works**

This thesis can be improved and extended in the following three aspects:

- To make the harmonic impact study more accurate and comprehensive, a more sophisticated secondary system model could be introduced in Chapter 3, considering the various house connection ways: series-connection, parallel-connection or both. Furthermore, other loads such as the electric vehicle (EV) charger and the fuel cell also contain a PWM converter and low-pass filter. Hence it is interesting to study the collective

harmonic impact of these filter-based converters if more practical technical data is available.

- As discussed in Chapter 1, the PV inverter includes both high-order and low-order harmonics. The characteristics and models of low-order harmonic have been studied in this thesis. However, further researches can be done on the high-order harmonic characteristic of PV inverters and on how these harmonics propagate in the low voltage system.
- Besides the harmonic related issue and voltage rise, the voltage fluctuation is another critical power quality concern of PV inverters. This issue is closely related to the PV output power variability, which is affected by the random solar irradiance. Compared with other DGs, the PV panel has no rotating device and no mechanical inertia. Therefore during a cloudy day the PV output power can fluctuate seriously with the solar variability. The statistical indices of solar variability have been obtained and presented in Appendix E. Further work can be done to develop a comprehensive model for characterising the temporal and geographic distribution pattern of the solar variability. Also, it is critical to evaluate the cloud transient impact on the voltage regulation of the distribution system with high PV penetration.



## References

- [1] German Advisory Council on Global Change WBGU Berlin 2013, Renewable Energy Policy Network for the 21st Century, Global Status Report 2013, available online at: <http://www.ren21.net/>.
- [2] Nassif, A., "Measurement, modeling and mitigation of harmonics" Ph.D. dissertation, University of Alberta, fall 2009.
- [3] Jiang, C., "A Probabilistic Bottom-up Technique for Modeling and Simulation of Residential Distributed Harmonic Sources," M.Sc. dissertation, University of Alberta, spring 2012.
- [4] Xu, W.; Marti, J.R.; Dommel, H.W., "A multiphase harmonic load flow solution technique," *Power Systems, IEEE Transactions on*, vol.6, no.1, pp.174,182, February 1991.
- [5] M.J. Ortega, J.C. Hernández, O.G. García, "Measurement and assessment of power quality characteristics for photovoltaic systems: Harmonics, flicker, unbalance, and slow voltage variations," *Electric Power Systems Research*, Volume 96, Mar. 2013, pages 23-35.
- [6] Canova, A.; Giaccone, L.; Spertino, F.; Tartaglia, M., "Electrical Impact of Photovoltaic Plant in Distributed Network," *Industry Applications, IEEE Transactions on*, vol.45, no.1, pp.341,347, January-February. 2009.
- [7] Papaioannou, I.T.; Alexiadis, M.C.; Demoulias, C.S.; Labridis, D.P.; Dokopoulos, P.S., "Modeling and field measurements of photovoltaic units connected to LV grid. Study of Penetration Scenarios," *Power Delivery, IEEE Transactions on*, vol.26, no.2, pp.979,987, April 2011.
- [8] Aprilia, E.C.; Cuk, V.; Cobben, J.F.G.; Ribeiro, P.F.; Kling, W.L., "Modeling the frequency response of photovoltaic inverters," *Innovative Smart Grid Technologies (ISGT Europe), 2012 3rd IEEE PES International Conference and Exhibition on*, vol., no., pp.1,5, 14-17 Oct. 2012.
- [9] Wang, F.; Duarte, J.L.; Hendrix, M. A M; Ribeiro, P.F., "Modeling and analysis of grid harmonic distortion impact of aggregated DG inverters," *Power Electronics, IEEE Transactions on*, vol.26, no.3, pp.786,797, March 2011.
- [10] Yang Du, Dylan Dah-Chuan Lu, Geoffrey James, and David J. Cornforth. "Modeling and analysis of current harmonic distortion from grid connected PV inverters under different operating conditions," *Solar Energy* 94 (2013): 182-194.
- [11] Hong Soo Goh, "The effect of grid operating conditions on the harmonic performance of grid-connected PV inverters," Ph.D. dissertation, Newcastle University, September 2011.
- [12] T. A. Short, *Electric Power Distribution Handbook*, CRC Press, Washington DC, 2003.
- [13] Kresimir Fekete, Zvonimir Klaic, Ljubomir Majdandzic, "Expansion of the residential photovoltaic systems and its harmonic impact on the distribution grid," *Renewable Energy*, Volume 43, July 2012, Pages 140-148.

- [14] Minas Patsalides, Andreas Stavrou, Venizelos Efthymiou, George E. Georghiou, "Towards the establishment of maximum PV generation limits due to power quality constraints," *International Journal of Electrical Power & Energy Systems*, Volume 42, Issue 1, November 2012, Pages 285-298.
- [15] Bhowmik, A.; Maitra, A.; Halpin, S.M.; Schatz, J.E., "Determination of allowable penetration levels of distributed generation resources based on harmonic limit considerations," *Power Delivery, IEEE Transactions on*, vol.18, no.2, pp.619,624, April 2003.
- [16] Enslin, J. H R; Heskes, Peter J M, "Harmonic interaction between a large number of distributed power inverters and the distribution network," *Power Electronics, IEEE Transactions on*, vol.19, no.6, pp.1586,1593, November 2004.
- [17] (Product manual) Mitsubishi Electric - Photovoltaic Modules, Mitsubishi Inc., available online at:  
[http://www.mitsubishielectric.com/bu/solar/pv\\_modules/monocrystalline/documentation.html](http://www.mitsubishielectric.com/bu/solar/pv_modules/monocrystalline/documentation.html).
- [18] Utility scale PV variability workshop, National Renewable Energy Laboratory (NREL), U.S., July 2009, available online at:  
<http://www.nrel.gov/docs/fy10osti/47514.pdf>.
- [19] (Product manual) PVS300 string inverters, ABB Inc., available online at:  
<http://www.abb.ca/product/us/9AAC172308.aspx?country=CA>.
- [20] (Product manual) Xantrex Grid-tied Solar Inverter, Schneider Electric Inc., available online at: <http://www.solarelectricsupply.com/solar-inverter/xantrex>.
- [21] (Product manual) PV inverter CSI-1500TLD-GW, Canadian Solar, available online at: [http://www.canadiansolar.com/product\\_pro\\_detail.aspx?id=35](http://www.canadiansolar.com/product_pro_detail.aspx?id=35).
- [22] Solar Pro, Apr./May 2009, available online at:  
<http://solarprofessional.com/print-issue/april-may-2009>.
- [23] Characteristics of the Utility Interface for Photovoltaic (PV) Systems, IEC 61727 CDV (Committee Draft for Vote), 2002.
- [24] Papaioannou, I.T.; Bouhouras, A.S.; Marinopoulos, A.G.; Alexiadis, M.C.; "Harmonic impact of small photovoltaic systems connected to the LV distribution network," *Electricity Market, 2008. EEM 2008. 5th International Conference on European*, vol., no., pp.1,6, 28-30 May 2008.
- [25] X. Zhang, R. Cao, "Solar photovoltaic integration generation and its inverter control," China Mechanical Press, Beijing, China.
- [26] Task Force on Harmonics Modeling and Simulation, IEEE PES Harmonic Working Group, "Characteristics and modeling of harmonic sources-power electronic devices," *Power Delivery, IEEE Transactions on*, vol.16, no.4, pp.791,800, Oct 2001.
- [27] Fanbo He; Zhengming Zhao; Liqiang Yuan; Sizhao Lu, "A DC-link voltage control scheme for single-phase grid-connected PV inverters," *Energy Conversion Congress and Exposition (ECCE), 2011 IEEE*, vol., no., pp.3941,3945, 17-22 Sept. 2011.
- [28] Zhao, Z., "High Efficiency Single-stage Grid-tied PV Inverter for Renewable Energy System", Ph.D. dissertation, Virginia Tech, April 2012.

- [29] IEEE Standard for Interconnecting Distributed Resources with Electric Power Systems, *IEEE Std.* 1547, 2003.
- [30] Chang, G.W.; Hsin-Wei Lin; Shin-Kuan Chen, "Modeling characteristics of harmonic currents generated by high-speed railway traction drive converters," *Power Delivery, IEEE Transactions on*, vol.19, no.2, pp.766,773, April 2004.
- [31] S. Chakraborty, B. Kroposki, and W. Kramer, "Advanced Power Electronic Interfaces for Distributed Energy Systems, Part 1: Systems and Topologies, Part 2: Modeling, Development, and Experimental Evaluation of Advanced Control Functions for Single-Phase Utility-Connected Inverter," Technical Report NREL/TP-550-44313, Nov. 2008.
- [32] J. He, "Damping and harmonic control of DG-grid interfacing," Ph.D. dissertation, University of Alberta, fall 2013.
- [33] "Typical impedance of residential power systems," Hydro Quebec Report, No. PQ01-5129.
- [34] A. Ipakchi, and F. Albuyeh, "Grid of the Future," *IEEE Power & Energy Mag.*, vol. 7, no. 2, pp. 52-62, Mar./Apr. 2009.
- [35] H. Farhangi, "The path of the smart grid," *IEEE Power & Energy Mag.*, vol. 8, no. 1, pp. 18-28, Jan.-Feb. 2010.
- [36] G. W. Hart, "Nonintrusive appliance load monitoring," *Proc. IEEE*, vol. 80, no. 12, pp. 1870-1891, Dec. 1992.
- [37] M. Dong, "Decomposition Techniques for Power System Load Analysis", PhD dissertation, University of Alberta, summer 2013.
- [38] J. Liang, S. Ng, G. Kendall, and J. Cheng, "Load signature study—Part I: Basic concept, structure, and methodology," *IEEE Trans. Power Delivery*, vol. 25, no. 2, pp. 551–560, Apr. 2010.
- [39] D. Srinivasan, W. S. Ng, and A. C. Liew, "Neural-network-based signature recognition for harmonic source identification," *IEEE Trans. Power Delivery*, vol. 21, no. 1, pp. 398–405, Jan. 2006.
- [40] J. Burke, C. Untiedt, "Stray voltage: two different perspectives," *IEEE Ind. Applications Mag.*, vol. 15, no. 3, pp. 36-41, May/Jun. 2009.
- [41] M. Pipattanasomporn, M. Kuzlu, and S. Rahman, "An algorithm for Intelligent home energy management and demand response analysis," *IEEE Trans. Smart Grid*, vol. 3, no. 4, pp. 2166-2173, Dec. 2012.
- [42] R. Garcia-Valle, L. C. P. da Silva, Z. Xu, and J. Ostergaard, "Smart demand for improving short-term voltage control on distribution networks," *IET Gen. Trans. Distr.*, vol. 3, no. 8, pp. 724-732, Aug. 2009.
- [43] OpenDSS – Open Distribution System Simulator, available online at: <http://sourceforge.net/projects/electricdss/files/OpenDSS/>.
- [44] GridLAB-D™ Simulation Software, available online at: <http://www.gridlabd.org/>.
- [45] A. Doucet, N. de Freitas, and N. Gordon (Editors), "Sequential Monte Carlo Methods in Practice," Ed. Springer-Verlag, 2001.
- [46] R. Hendron, "Building America Research Benchmark Definition," Golden, CO, Tech. Rep. NREL/TP-550-40968, 2007.
- [47] IPSOS-RSL, and Office for National Statistics, "United Kingdom Time of Use Survey, 2000" (computer file), 3<sup>rd</sup> ed. Colchester, Essex, U.K., U.K. Data

- Archive (distributor), 2003.
- [48] K. Qian, C. Zhou, M. Allan, and Y. Yuan, "Modeling of load demand due to EV battery charging in distribution systems," *IEEE Trans. Power Syst.*, vol. 26, no. 2, pp. 802-810, May 2011.
  - [49] J. A. Orr, A. E. Emanuel, and D. G. Pileggi, "Current harmonics, voltage distortion, and powers associated with battery chargers Part I: comparisons among different types of chargers," *IEEE Trans. PAS*, vol. PAS-101, no. 8, pp. 2703-2710, Aug. 1982.
  - [50] G. S. Campbell, and J. M. Norman, "An Introduction to Environmental Biophysics," 2nd ed., vol. 1, Ed. Springer, 2000, pp. 173-175.
  - [51] S. A. Arefifar, Y. A. I. Mohamed, and T. H. M. El-Fouly, "Supply-adequacy-based optimal construction of microgrids in smart distribution systems," *IEEE Trans. Smart Grid*, vol. 3, no. 3, pp. 1491-1502, Sep. 2012.
  - [52] Edmonton Clear Sky Chart History, available online at: <http://cleardarksky.com/clmt/c/Edmontonct.html>.
  - [53] Current and Historical Alberta Weather Station Data Viewer, Alberta Agriculture and Rural Development, available online at: <http://www.agric.gov.ab.ca/acis/alberta-weather-data-viewer.jsp>.
  - [54] J. Kleissl. (2010). Current state of the art in solar forecasting. California Institute for Energy and Environment, CA, available online at: <http://uc-ciee.org/downloads/appendixA.pdf>.
  - [55] S. Teleke, M. E. Baran, S. Bhattacharya, and A. Q. Huang, "Rule-based control of battery energy storage for dispatching intermittent renewable Sources," *IEEE Trans. Sust. Energy*, vol. 1, no. 3, pp. 117-124, Oct. 2010.
  - [56] "Task force on harmonics modeling and simulation, modeling and simulation of the propagation of harmonics in electric power networks– part I: concepts, models, and simulation techniques," *IEEE Trans. Power Del.*, vol. 11, no. 1, pp. 452–465, Jan. 1996.
  - [57] Harry W. Sorge, "Residential Wiring: An Introductory Approach," 2nd Edition, Thomson Delmar Learning, NY.
  - [58] H. A. Smolleck, R. R. Shoultz, "A straightforward method for incorporating mutually-coupled circuits into the admittance matrix using the concept of artificial branches," *IEEE trans. Power Syst.*, vol. 5, No. 2, May 1990.
  - [59] W. Xu, "MHLF Reference Manual: Documentation in Support of the Multiphase Harmonic Load Flow Program," 1991.
  - [60] Low Voltage General Purpose Motors, available online at: <http://www.abb.ca/product/seitp322/f953a470c6cfb217c1256ddd0042a0ae.aspx?productLanguage=us&country=CA>.
  - [61] Motor Selection, available online at: [http://industrial.panasonic.com/ww/e/25000/fa\\_pro\\_sgeard\\_shing1\\_e/fa\\_pro\\_sgeard\\_shing1\\_e/ctlg\\_geared\\_e\\_9.pdf](http://industrial.panasonic.com/ww/e/25000/fa_pro_sgeard_shing1_e/fa_pro_sgeard_shing1_e/ctlg_geared_e_9.pdf).
  - [62] Albadi, M. H.; El-Saadany, E.F., "Demand response in electricity markets: an overview," *Power Engineering Society General Meeting, 2007. IEEE*, vol., no., pp.1,5, 24-28 June 2007.
  - [63] P. C. Sen, "Principles of Electric Machines and Power Electronics," 2nd ed., vol. 1, Ed. John Wiley & Sons, 1997.

- [64] Wallace, A.K.; Spee, R.; Martin, L.G., "Current harmonics and acoustic noise in AC adjustable-speed drives," *Industry Applications, IEEE Transactions on*, vol. 26, no. 2, pp. 267-273, Mar./Apr. 1990.
- [65] IESO (2013, Jun.). Time-of-use Prices. ON, Canada, available online at: [http://www.ieso.ca/imoweb/siteshared/tou\\_rates.asp?sid=ic](http://www.ieso.ca/imoweb/siteshared/tou_rates.asp?sid=ic).
- [66] Yun Tiam Tan; Kirschen, D.S.; Jenkins, N., "A model of PV generation suitable for stability analysis," *Energy Conversion, IEEE Transactions on*, vol.19, no.4, pp.748,755, Dec. 2004.
- [67] Yun Tiam Tan; Kirschen, D.S., "Impact on the power system of a large penetration of photovoltaic generation," *Power Engineering Society General Meeting, 2007. IEEE*, vol., no., pp.1,8, 24-28 June 2007.
- [68] Jewell, W.; Ramakumar, R., "The effects of moving clouds on electric utilities with dispersed photovoltaic generation," *Energy Conversion, IEEE Transactions on*, vol.EC-2, no.4, pp.570,576, Dec. 1987.
- [69] Ari, G. K.; Baghzouz, Y., "Impact of high PV penetration on voltage regulation in electrical distribution systems," *Clean Electrical Power (ICCEP), 2011 International Conference on*, vol., no., pp.744,748, 14-16 June 2011.
- [70] Golnas, A.; Voss, S., "Power output variability of PV system fleets in three utility service territories in New Jersey and California," *Photovoltaic Specialists Conference (PVSC), 2010 35th IEEE*, vol., no., pp. 535, 539, 20-25 June 2010.
- [71] National Renewable Energy Laboratory (NREL), United State. Available online at: [http://www.nrel.gov/midc/srrl\\_bms/](http://www.nrel.gov/midc/srrl_bms/).
- [72] Thomas E. Hoff, Richard Perez, "Quantifying PV power output variability," *Solar Energy*, Volume 84, Issue 10, October 2010, Pages 1782-1793.
- [73] Thomas E. Hoff, Richard Perez, "Modeling PV fleet output variability," *Solar Energy*, Volume 86, Issue 8, August 2012, Pages 2177-2189.
- [74] Mills, A.; Wiser, R.; "Implications of Wide-Area Geographic Diversity for Short-Term Variability of Solar Power," Lawrence Berkeley National Laboratory Technical Report, 2010.
- [75] Richard Perez, Sergey Kivalov, Jim Schlemmer, Karl Hemker Jr., Thomas E. Hoff, "Short-term irradiance variability: preliminary estimation of station pair correlation as a function of distance," *Solar Energy*, Volume 86, Issue 8, August 2012.
- [76] Marcos, J., Marroyo, L., Lorenzo, E. and García, M., "Smoothing of PV power fluctuations by geographical dispersion," *Progress in Photovoltaics: Research and Applications*, Volume 20, Issue 2, pages 226–237, March 2012.
- [77] Marcos, J., Marroyo, L., Lorenzo, E., Alvira, D. and Izco, E., "Power output fluctuations in large scale PV plants: One year observations with one second resolution and a derived analytic model," *Progress in Photovoltaics: Research and Applications*, Volume 19, Issue 2, pages 218–227, March 2011.

## Appendix A

### PV Inverter Filter Parameters

The harmonic characteristic of a PV inverter largely depends on the topology and parameter of its built-in low-pass filter. Through detailed measurement, the equivalent circuit of a PV inverter is figured out (shown in Figure A. 1). The  $L_1$  is the inverter side inductor and  $L_2$  is grid side inductor.  $R_1$  and  $R_2$  represent the stray resistance of the inductor winding.  $C$  is the shunt capacitor and  $R_c$  is the damping resistance, which is a physical resistor in the electric board.

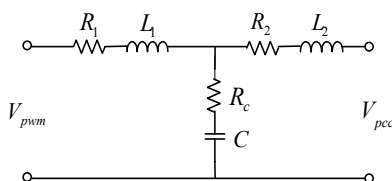


Figure A. 1 Filter topology of Xantrex Grid-tied inverter GT3.0-NA-DS-240

In addition to the measured filter parameters in the lab, four groups of typical filter parameters are summarized from the references (shown in Table A.1).

Table A.1 A summary of typical filter parameters

| Parameters          | Lab inverter measured | Reference [11] | Reference [32] | Reference [9] |
|---------------------|-----------------------|----------------|----------------|---------------|
| $L_1$               | 2.1mH                 | 1.8mH          | 2mH            | 2mH           |
| $R_1$               | 0.05 $\Omega$         | 0.15 $\Omega$  | 0.05 $\Omega$  | 0.1 $\Omega$  |
| $L_2$               | 1.2mH                 | 0.3mH          | 1.3mH          | 0.8mH         |
| $R_2$               | 0.05 $\Omega$         | 0 $\Omega$     | 0.05 $\Omega$  | 0.4 $\Omega$  |
| $R_c$               | 2.2 $\Omega$          | 0.566 $\Omega$ | 0.25 $\Omega$  | 0 $\Omega$    |
| $C$                 | 10.4 $\mu$ F          | 10 $\mu$ F     | 10 $\mu$ F     | 5 $\mu$ F     |
| Rated power         | 3kVA                  | <0.5kVA        | N/A            | N/A           |
| Switching frequency | N/A                   | 20kHz          | 12kHz          | 16kHz         |

## Appendix B

### Modeling of Multiphase Network Components

#### B.1 Modeling of the Multiphase Coupled Line

The modeling of three-phase mutual-coupled distribution line is the basis for the distribution system multiphase load flow study. The three-phase conductor with self and mutual impedance is shown in Figure B.1 [58]. Considering the universal case where the three phase parameters are unsymmetrical, the line voltage drop is represented by (B.1).

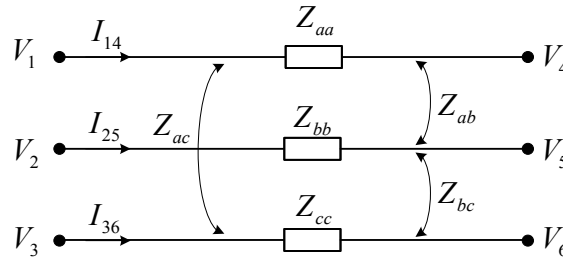


Figure B.1 Three-phase conductor

$$\mathbf{V}_L = \mathbf{Z}_L \mathbf{I}_L \quad (\text{B.1})$$

$$\text{Where } \mathbf{V}_L = \begin{bmatrix} V_{14} \\ V_{25} \\ V_{36} \end{bmatrix} = \begin{bmatrix} V_1 - V_4 \\ V_2 - V_5 \\ V_3 - V_6 \end{bmatrix}, \mathbf{Z}_L = \begin{bmatrix} Z_{aa} & Z_{ab} & Z_{ac} \\ Z_{ab} & Z_{bb} & Z_{bc} \\ Z_{ac} & Z_{bc} & Z_{cc} \end{bmatrix}, \text{ and } \mathbf{I}_L = \begin{bmatrix} I_{14} \\ I_{25} \\ I_{36} \end{bmatrix}.$$

The three-phase conductor can be modeled as a 6-bus, 3-branch network for multiphase load flow calculation. The equivalent circuit is shown in Figure B.2. The imaginary branches among line (a), (b) and (c) represent the effect of mutual impedance. Thus the network can be represented as a 6\*6 nodal voltage equation. Next step is to demonstrate how to transfer the branch current equation (B.1) into nodal voltage equation.

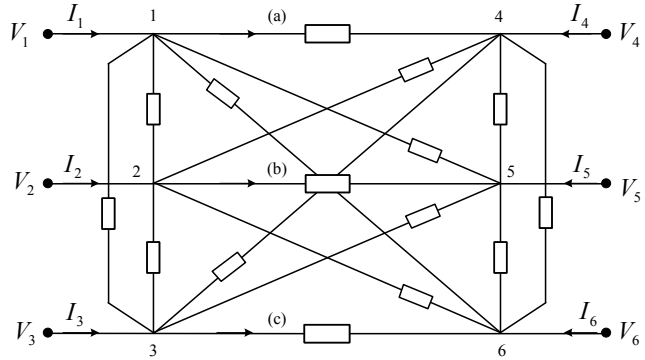


Figure B.2 Equivalent circuit of three-phase conductor

Equation (B.1) can be rewritten as

$$\mathbf{I}_L = \mathbf{Y}_L \mathbf{V}_L \tag{B.2}$$

where  $\mathbf{Y}_L = \mathbf{Z}_L^{-1} = \begin{bmatrix} Y_{aa} & Y_{ab} & Y_{ac} \\ Y_{ab} & Y_{bb} & Y_{bc} \\ Y_{ac} & Y_{bc} & Y_{cc} \end{bmatrix}$ .

In computer algorithm, we use the **correlation matrix**  $\mathbf{A}$  to formulate the nodal admittance matrix. According to the circuit theory,  $\mathbf{A}$  is a 6\*3 matrix in this case. “6” represents the number of buses and “3” represents the number of branches. The element of  $\mathbf{A}$  is defined as:

$$a_{jk} = \begin{cases} 0, & \text{when branch } k \text{ is not connected to bus } j \\ 1, & \text{when branch } k \text{ is connected to bus } j, \text{ with branch current depart} \\ & \text{from } j \\ -1, & \text{when branch } k \text{ is connected to bus } j, \text{ with branch current come} \\ & \text{to } j \end{cases}$$

Based on the above principle, the correlation matrix  $\mathbf{A}$  is generated.



$$A = \begin{bmatrix} 1 & 0 & 0 \\ 0 & 1 & 0 \\ 0 & 0 & 1 \\ -1 & 0 & 0 \\ 0 & -1 & 0 \\ 0 & 0 & -1 \end{bmatrix}$$

Multiply equation (B.2) by  $A$ ,

$$A\mathbf{I}_L = AY_L\mathbf{V}_L \quad (\text{B.3})$$

The relations between nodal voltage and line voltage drop, nodal injected current and line current are,

$$\begin{cases} \mathbf{V}_L = A^T\mathbf{V}_N \\ A\mathbf{I}_L = \mathbf{I}_N \end{cases} \quad (\text{B.4})$$

Substitute (B.4) to (B.3), gives,

$$\mathbf{I}_N = AY_LA^T\mathbf{V}_N \quad (\text{B.5})$$

Let  $\mathbf{Y}_N = AY_LA^T$ , then (B.5) is expressed as,

$$\mathbf{I}_N = \mathbf{Y}_N\mathbf{V}_N \quad (\text{B.6})$$

where  $\mathbf{I}_N = [I_1, I_2, I_3, I_4, I_5, I_6]^T$ ,  $\mathbf{V}_N = [V_1, V_2, V_3, V_4, V_5, V_6]^T$ , and  $\mathbf{Y}_N$  is the 6\*6 admittance matrix.

The calculation procedure is summarized as below:

$$\begin{array}{ccccc} Z_L (3*3) & \xrightarrow{Z_L^{-1}} & Y_L (3*3) & \xrightarrow{AY_LA^T} & Y_N (6*6) \\ \text{matrix} & & \text{matrix} & & \text{matrix} \end{array}$$

The element of 6\*6 matrix is shown (B.7). Each element is also labeled in the Figure B.3.

$$\mathbf{Y}_N = \begin{bmatrix} Y_{aa} & Y_{ab} & Y_{ac} & -Y_{aa} & -Y_{ab} & -Y_{ac} \\ Y_{ab} & Y_{bb} & Y_{bc} & -Y_{ab} & -Y_{bb} & -Y_{bc} \\ Y_{ac} & Y_{bc} & Y_{cc} & -Y_{ac} & -Y_{bc} & -Y_{cc} \\ -Y_{aa} & -Y_{ab} & -Y_{ac} & Y_{aa} & Y_{ab} & Y_{ac} \\ -Y_{ab} & -Y_{bb} & -Y_{bc} & Y_{ab} & Y_{bb} & Y_{bc} \\ -Y_{ac} & -Y_{bc} & -Y_{cc} & Y_{ac} & Y_{bc} & Y_{cc} \end{bmatrix} \quad (\text{B.7})$$

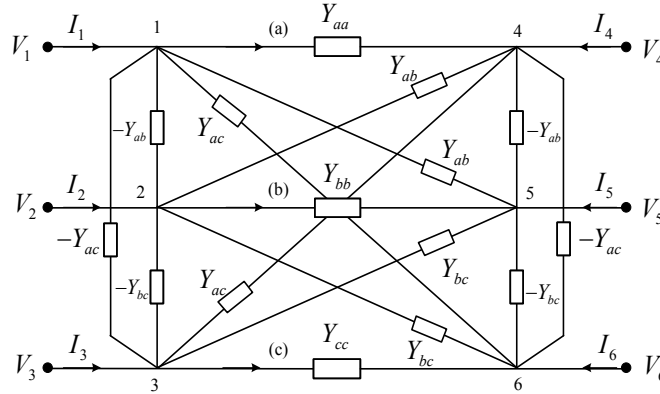


Figure B.3 Equivalent circuit of three-phase conductor (with parameters)

## B.2 Modeling of Single-Phase Three-Winding Transformers

For a single-phase three-winding transformer (shown in Figure B.4), the following procedure can be followed to obtain its nodal admittance matrix [59]:

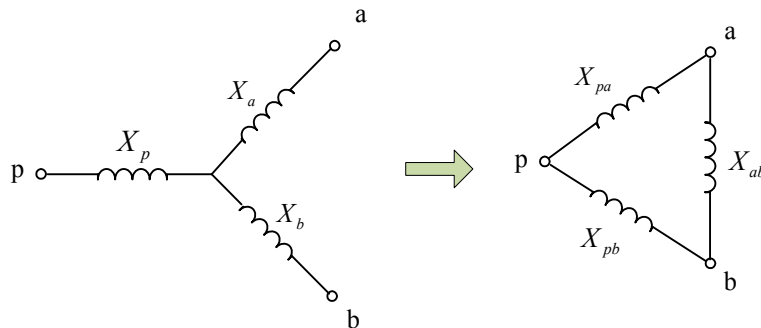


Figure B.4 Single-phase three-winding transformer

1) Convert the short-circuit test data into a common power base  $S_{base}$ , and construct the well-known star circuit of transformers with the converted data:

$$\begin{aligned}
X_p &= \frac{S_{base}}{2} \left( \frac{X_{pa}}{S_{pa}} + \frac{X_{pb}}{S_{pb}} - \frac{X_{ab}}{S_{ab}} \right) \\
X_a &= \frac{S_{base}}{2} \left( \frac{X_{ab}}{S_{ab}} + \frac{X_{pa}}{S_{pa}} - \frac{X_{pb}}{S_{pb}} \right) \\
X_b &= \frac{S_{base}}{2} \left( \frac{X_{pb}}{S_{pb}} + \frac{X_{ab}}{S_{ab}} - \frac{X_{pa}}{S_{pa}} \right)
\end{aligned} \tag{B.8}$$

2) Convert the start circuit to delta circuit:

$$\begin{aligned}
X^2 &= X_{pa}X_{ab} + X_{an}X_{pb} + X_{pa}X_{pb} \\
B_{pa} &= \frac{X_b}{X^2}, \quad B_{ab} = \frac{X_p}{X^2}, \quad B_{pb} = \frac{X_a}{X^2}
\end{aligned} \tag{B.9}$$

3) The per-unit matrix is obtained by forming the nodal admittances matrix of the delta circuit:

$$Y = \begin{bmatrix} B_{pa} + B_{pb} & -B_{pa} & -B_{pb} \\ -B_{pa} & B_{pa} + B_{ab} & -B_{ab} \\ -B_{pb} & -B_{ab} & B_{pb} + B_{ab} \end{bmatrix} \tag{B.10}$$

## Appendix C

### Single-phase Induction Motor Parameters

Typical motor parameters are required for modeling the motor starting transient. A set of typical motor parameters are extracted from the manuals of two commercial single-phase induction motors and presented in Table C.1 [60]-[61].

Table C.1 Typical parameters of the single phase induction motor

| Classification        | Values   |
|-----------------------|--|
| Electric parameter    | Rated power: 100W<br>Main winding:<br>$R_{1m} = 3.6\Omega$ , $X_{1m} = 5\Omega$ ; $R_{2m} = 7.4/2\Omega$ , $X_{2m} = 3.8/2\Omega$ ; $X_{em} = j120/2\Omega$ ,<br>Auxiliary winding:<br>$R_{1a} = 12.8\Omega$ , $X_{1a} = 5.8\Omega$ ; $R_{2a} = 7.4/2\Omega$ , $X_{2a} = 3.8/2\Omega$ ; $X_{em} = j120/2\Omega$ ,<br>Running capacitor: $C_r = 30\mu\text{F}$<br>Turns ratio: $a = 0.75$<br>Synchronous rotating speed $n_s = 1800\text{rpm}$<br>Efficiency $\eta$ : <i>Unif</i> (0.5, 0.7)<br>Slip $s$ : <i>Unif</i> (0.04, 0.05) |
| Mechanical parameters | Rotational inertia J: $0.0003 \text{ kg}\cdot\text{m}^2$   |

These parameters, applicable to the 100-watt motor are regarded as the base value for single-phase motor simulation. For other power levels, we can scale the motor parameters based on the following assumptions: 1) the motor impedance is inversely proportional to the power level, and 2) the rotational inertia is proportional to the power level.

For a single-phase motor with a rated power of  $P_r$ , the per-unit power is

$$P_{pu} = P_r / 100$$

Then the motor parameters are scaled as follows:

Impedance (the stator and rotor impedance):  $R_r = \frac{R_{base}}{P_{pu}}$ ,  $X_r = \frac{X_{base}}{P_{pu}}$

$$\text{Load torque: } T_{load} = \frac{P_r \times \eta}{\omega_s (1-s)}$$

$$\text{Rotational inertia: } J_r = J_{base} \times P_{pu}$$

In addition, the forward and backward impedance of the rotor are shown in Figure C.1.

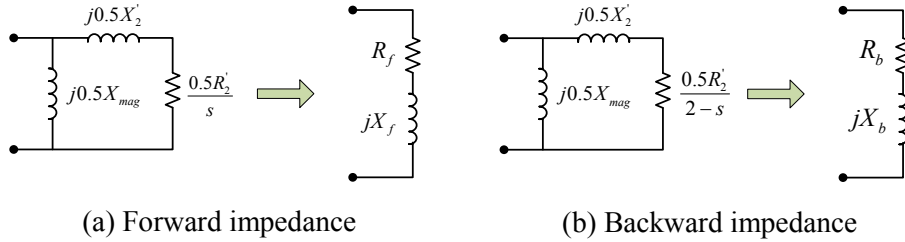


Figure C.1 Forward and backward impedance

$$\begin{aligned}
 Z_f &= R_f + X_f = j0.5X_{mag} \parallel \left( \frac{j0.5X'_2}{s} + j0.5X'_2 \right) \\
 Z_b &= R_b + X_b = j0.5X_{mag} \parallel \left( \frac{j0.5X'_2}{2-s} + j0.5X'_2 \right)
 \end{aligned} \tag{C.1}$$

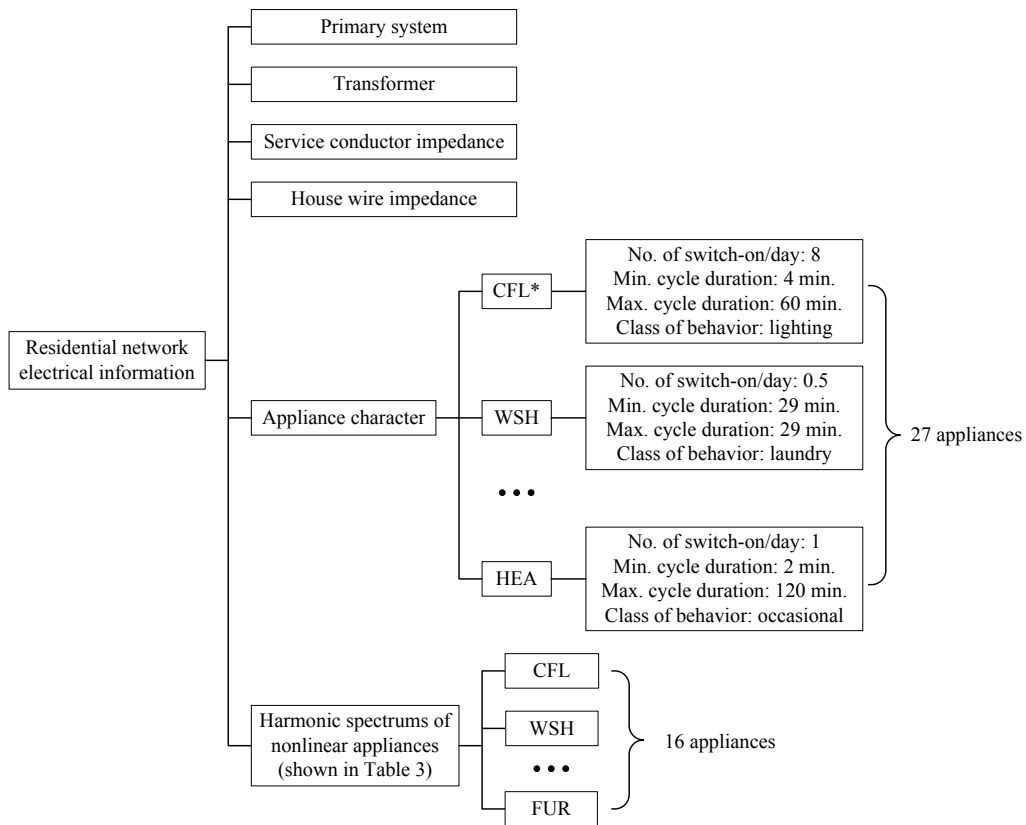
With the stator side impedance, rotor side impedance, load torque and rotational inertia, the motor starting dynamic current and power can be calculated.

## Appendix D

### Input Data Summary of Monte Carlo Simulation

#### Platform

The users should prepare the input file by themselves before using the simulation platform. The input file is divided into three parts: 1) residential network electrical information; 2) appliance time-of-use probability curves; 3) residential home information.



\* The abbreviation code for home appliances refers to Table D.5

Figure D.1 Input data file 1 – system and appliance electric data

**Input file 1: residential network electrical information** (default and change by \*.mat file). This data file includes the secondary distribution network electric

parameters and the nonlinear load harmonic spectrum parameters. The structure of this file is shown in Figure D.1. In particular, the measured harmonic spectrums of 6 major nonlinear loads are shown in Table D.1 and Table D.2 [2].

Table D.1 Harmonic spectrum of home appliance – Part I

| Appliances          | CFL      |             | PC       |             | Laptop   |             |
|---------------------|----------|-------------|----------|-------------|----------|-------------|
| Operating power (W) | 15       |             | 94       |             | 70.7     |             |
| THD (%)             | 120      |             | 99.5     |             | 151      |             |
|                     | Mag. (A) | Ang. (deg.) | Mag. (A) | Ang. (deg.) | Mag. (A) | Ang. (deg.) |
| H1                  | 0.156    | 26.4        | 0.823    | 0.5         | 0.647    | 20.6        |
| H3                  | 0.125    | 81.4        | 0.65     | 1.6         | 0.512    | 65.7        |
| H5                  | 0.091    | 148.0       | 0.407    | 3.6         | 0.346    | 125.5       |
| H7                  | 0.070    | -137.5      | 0.161    | 8.6         | 0.292    | -158.1      |
| H9                  | 0.050    | -66.8       | 0.099    | 58.1        | 0.313    | -92.4       |
| H11                 | 0.030    | 10.2        | 0.12     | 168.7       | 0.298    | -34.2       |
| H13                 | 0.020    | 110.4       | 0.118    | 178         | 0.264    | 27.3        |
| H15                 | 0.018    | -154.2      | 0.05     | -170.2      | 0.245    | 90.4        |
| H17                 | 0.013    | -60.8       | 0.05     | -64.8       | 0.225    | 150.3       |
| H19                 | 0.012    | 41.7        | 0.07     | -17.7       | 0.192    | -149.1      |
| H21                 | 0.014    | 133.1       | 0.041    | -7.9        | 0.164    | -84.8       |
| H23                 | 0.015    | -131.0      | 0.025    | 12.6        | 0.145    | -21.8       |
| H25                 | 0.018    | -50.1       | 0.031    | 144.6       | 0.123    | 38.9        |
| H27                 | 0.018    | 26.1        | 0.031    | 161.6       | 0.097    | 102.4       |

Table D.2 Harmonic spectrum of home appliance – Part II

| Appliances          | Regular Fridge |             | Furnace  |             | Washer   |             |
|---------------------|----------------|-------------|----------|-------------|----------|-------------|
| Operating power (W) | 150            |             | 535      |             | 189      |             |
| THD (%)             | 18             |             | 10.5     |             | 75.4     |             |
|                     | Mag. (A)       | Ang. (deg.) | Mag. (A) | Ang. (deg.) | Mag. (A) | Ang. (deg.) |
| H1                  | 1.275          | -19.7       | 5.16     | -33         | 2.31     | -63.6       |
| H3                  | 0.06           | -131.6      | 0.505    | -159.4      | 1.538    | 164.5       |
| H5                  | 0.17           | 173.5       | 0.199    | 78.6        | 0.528    | 19.2        |
| H7                  | 0.076          | 34.4        | 0.049    | 141.5       | 0.289    | 126.1       |
| H9                  | 0.007          | 5           | 0.027    | -30.8       | 0.38     | -19.7       |
| H11                 | 0.034          | -129        | 0.02     | -131.7      | 0.118    | 174.3       |
| H13                 | 0.022          | 76          | 0.006    | -78.7       | 0.18     | -76.5       |
| H15                 | 0.004          | 145.1       | 0.004    | 125.7       | 0.192    | 147.5       |
| H17                 | 0.012          | -37.9       | 0.006    | -0.1        | 0.042    | -91.1       |
| H19                 | 0.007          | 146         | 0.002    | -179.2      | 0.122    | 88.6        |
| H21                 | 0.002          | -155.3      | 0.001    | 45          | 0.105    | -41.1       |
| H23                 | 0.004          | 34.4        | 0.003    | -120.9      | 0.021    | 25.6        |
| H25                 | 0.002          | -126.1      | 0.001    | 94.1        | 0.082    | -101.9      |
| H27                 | 0.001          | -100.6      | 0.004    | 55          | 0.057    | -63.5       |

**Input file 2: appliance time-of-use probability curves** (default/change by \*.mat file). This data file includes the time-of-use probability curve for household activities that are related to home appliance usage [47]. The activities are classified into 9 categories. The structure of data file is shown in Figure D.2. The Example curves of laundry and cooking activities are shown in Figure D.3.

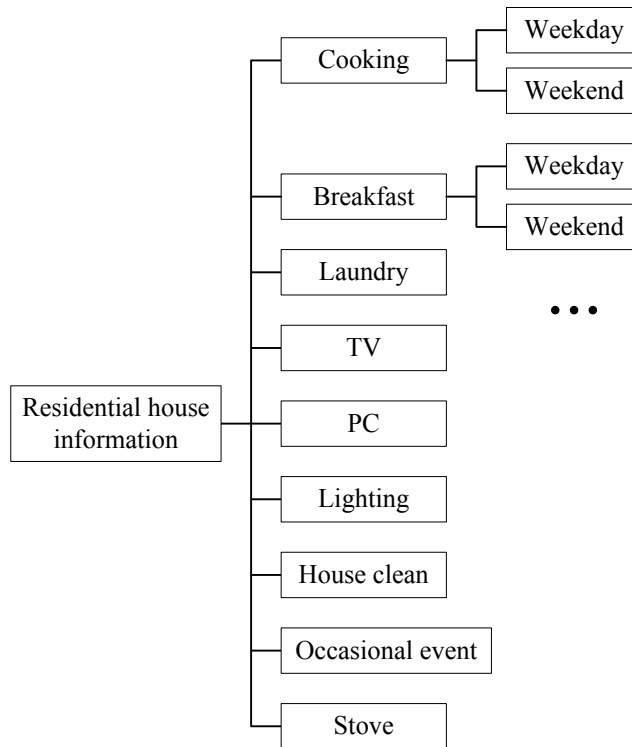


Figure D.2 Input data file 2 – appliance usage probability data

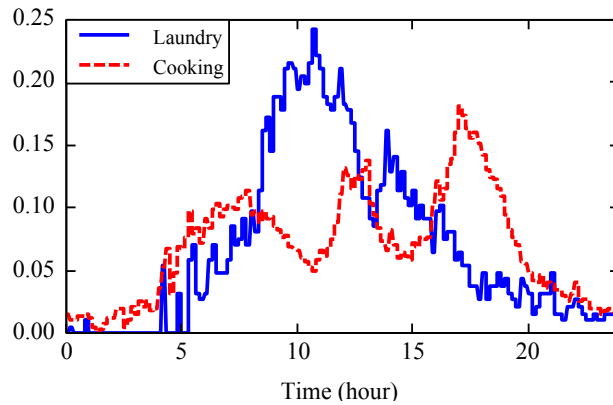


Figure D.3 Example of time-of-use probability curves for household activities



The classification of home appliances according to the activity category is shown in Table D.3. Each of the 27 home appliances in the database belongs to one of the activities. The switch-on event of this home appliance is determined according to the probabilistic curve.

Table D.3 Household activity classification

| <b>Activity</b>   | <b>Related home appliances</b>   |
|-------------------|--|
| Cooking           | Stove, microwave, rice cooker, coffee maker, blender, food processor, dishwasher |
| Breakfast         | Toaster  |
| Laundry           | Washing machine, dryer   |
| Television        | CRT TV, LCD TV   |
| PC                | Desktop + LCD, laptop  |
| Lighting          | CFL, incandescent light, magnetic-ballast lamp, electric-ballast lamp            |
| House cleaning    | Vacuum cleaner   |
| Occasional        | Heater, treadmill  |
| Stove             | Stove, oven  |
| Non-probabilistic | Fridge, freezer, furnace   |

**Input file 3: residential home information** (change by \*.txt file), the format of data file shown in Table D.4.

This classification of data file is reasonable. Input file 1 and Input file 2 are regarded as default data, which are usually kept constant in different studies. However, the users have access to change the default data if they need. They can back up the \*.mat file and make changes to the initial data file in the “Workspace” of Matlab. Input file 3 is changeable data file, which is usually changed in different studies. The user can directly edit this data file in the .txt file according to the format.

Table D.4 Input data file 3 - appliance general information

| HOUSE   | Distance to PCC (km) | Num_app   | Num_people | Working type |            |                        |                        |                    |                                      |
|---|----------------------|-----------|------------|--------------|------------|------------------------|------------------------|--------------------|--------------------------------------|
| HOUSE   | 0.3                  | 15        | 2          | 1            |            |                        |                        |                    |                                      |
| this line represents new behavior probabilities |                      |           |            |              |            |                        |                        |                    |                                      |
| Lighting=                                       | PC=                  | TV=       | Cooking=   | Stove=       | Breakfast= | Laundry=               | Houseclean=            | Occasional=        |                                      |
| Room number                                     | Phase connection     | Appliance | Quantity   | P (W)        | FPF        | Distance to panel (km) | External spectrum file | External prob file | Deterministic turnON instants (hhmm) |
| 1   | A                    | CFL       | 3          | 15           | 0.9        | 0.01                   | CFL_spectr.csv*        |                    |                                      |
| 1   | A                    | LCDTV     | 1          | 300          | 0.99       | 0.015                  |                        |                    |                                      |
| 1   | A                    | CFL       | 6          | 15           | 0.9        | 0.02                   |                        |                    |                                      |
| 1   | A                    | CFL       | 1          | 15           | 0.9        | 0.023                  |                        |                    |                                      |
| 2   | B                    | CFL       | 2          | 15           | 0.9        | 0.005                  |                        |                    | 9:50, 10:37, 20:20 **                |
| 2   | B                    | CFL       | 1          | 15           | 0.9        | 0.01                   |                        |                    |                                      |
| 2   | B                    | CFL       | 4          | 15           | 0.9        | 0.031                  |                        |                    |                                      |
| 2   | B                    | COO       | 1          | 800          | 1          | 0.036                  |                        |                    |                                      |
| 2   | B                    | FUR       | 1          | 500          | 0.84       | 0.042                  |                        |                    |                                      |
| 3   | A                    | CFL       | 2          | 15           | 0.9        | 0.016                  |                        |                    |                                      |
| 3   | A                    | PC        | 1          | 100          | 1          | 0.021                  |                        |                    |                                      |
| 3   | A                    | LCD       | 1          | 40           | 0.96       | 0.021                  |                        |                    |                                      |
| 3   | A                    | CFL       | 1          | 15           | 0.9        | 0.025                  |                        |                    |                                      |
| 4   | AB                   | OVE       | 1          | 1200         | 0.95       | 0.01                   |                        |                    |                                      |
|   |                      |           |            |              |            |                        |                        |                    |                                      |
| HOUSE   | 0.5                  | 12        | 3          | 2            |            |                        |                        |                    |                                      |
| Lighting=                                       | PC=                  | TV=       | Cooking=   | Stove=       | Breakfast= | Laundry=               | Houseclean=            | Occasional=        |                                      |
| 1   | AB                   | OVEN      | 1          | 1200         | 0.95       | 0.01                   |                        |                    |                                      |
| 2   | ...                  | ...       | ...        | ...          | ...        | ...                    |                        |                    |                                      |

\* The users can change the external “harmonic spectrum data” or “probability data” by preparing a \*.csv file of such data and entering the file path.

\*\* The deterministic switch-on time of an appliance should follow the format “hh:mm”.

In “Input file 3”, each home appliance is represented by a code for convenience, as shown in Table D.5.

Table D.5 Checklist of home appliance codes

| <b>Code</b> | <b>Appliance name</b>    |
|-------------|--------------------------|
| CFL         | Compact Fluorescent Lamp |
| EBL         | Electric-Ballast Lamp    |
| MBL         | Magnetic-Ballast Lamp    |
| INC         | Incandescent Lamp        |
| PC          | Desktop PC               |
| LCD         | LCD Computer Monitor     |
| LAP         | Laptop                   |
| LCDTV       | LCD Television           |
| CRTTV       | CRT Television           |
| RFR         | Regular Fridge           |
| FUR         | Furnace                  |
| ASDFR       | ASD-based Fridge         |
| FRE         | Freezer                  |
| WSH         | ASD-based Washer         |
| DRY         | Regular Dryer            |
| OVE         | Electric Oven            |
| MW          | Microwave Oven           |
| TOA         | Toaster                  |
| COF         | Coffee Maker             |
| FOO         | Food Processor           |
| VAC         | Vacuum Cleaner           |
| DSW         | Dishwasher               |

## **Appendix E**

### **Cloud Transient Impact on Distribution Systems with High PV Penetration**

Unlike conventional or other renewable energy generators, PV panels do not have rotating element, and thus have no inertia. This characteristic potentially causes a problem: when the solar irradiance experiences a rapid fluctuation due to the cloud movement over a clear sky, the output power would also fluctuate almost synchronously [66]. The most severe disturbance on the grid would occur when a band of clouds sweep over an area with a large concentration of PV panels. This could result in a fairly large and sudden variation in the PV output [67]. Concerns about the potential of photovoltaic output fluctuations caused by transient clouds were firstly put forward in 1980s [68]. In recent years a lot of researches have been done for investigating the cloud transient patterns and estimating its impact on the distribution system with PV penetration.

In the distribution systems with high PV penetration, large variations of the PV output power induced by cloud transients may result in the following effects [69]:

- At the transmission system level – output power fluctuation require significant back-and-forth throttling of the gas-fired units in order to maintain the balance between generation and load (i.e., frequency regulation).
- At the distribution system level – undesirable voltage fluctuations which may lead to excessive operations of the Load Tap Changers (LTC).

In addition, the sudden reductions in PV output power caused by sudden drops in irradiance may cause undesirable tripping of PV and other generators due to the operation of under-voltage relays [67]. On the other hand, the moving cloud is not large enough to cover the whole city. During a cloud transient event, the solar

irradiance variability might be different at different sites. Therefore, in order to estimate the cloud movement impact, we should at first study the **temporal and spatial** distribution pattern of solar irradiance in cloudy days.

## **E.1 Characteristics of Solar Irradiance Variability – Temporal Distribution**

Generally, the solar irradiance variability is characterized by the irradiance ramp, which is calculated as the difference between the irradiance of two consecutive snapshots, normalized by  $R_{rated} = 1000\text{W/m}^2$  [77].

$$\Delta R(t) = \frac{R(t + \Delta t) - R(t)}{R_{rated}} \quad (\text{E.1})$$

On the other hand, since the PV output is proportional to the solar irradiance when the PV inverter operates in steady state, the irradiance fluctuation ramp also applies to power fluctuation.

$$\Delta P(t) = \frac{P(t + \Delta t) - P(t)}{P_{rated}} \quad (\text{E.2})$$

where  $P_{rated}$  is the rated power of the PV inverter. In this way, a time series of power fluctuation is derived from a time series of power output for a given time interval  $\Delta t$ .

The study of power ramp is significant for estimating the severity of cloud transient impact on the voltage fluctuation. Typically, power fluctuations below 10 minutes are absorbed by the grid as frequency fluctuations, thus affecting power quality; if it is longer than 10 minutes, the network operator can comfortably react by adding (or subtracting) power from other sources [76].

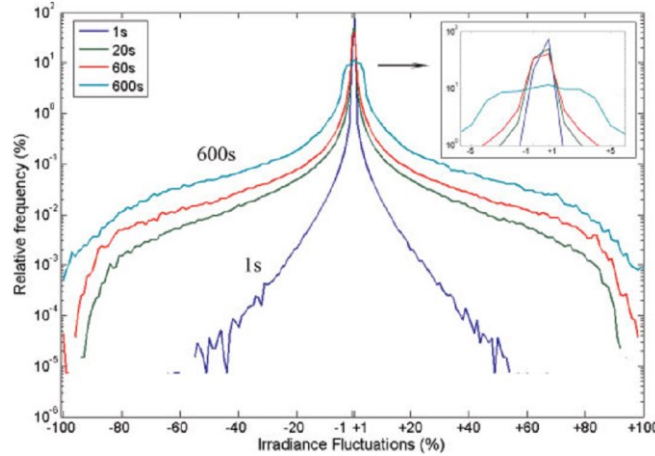


Figure E.1 Distributions of the irradiance fluctuations registered at Cintruenigo site

Figure E.1 shows an example of probability curve derived from 1-year measurement data with different time intervals [77]. It indicates that the curve is highly related to the time interval. With the time interval increasing, the possibility of big power fluctuation ramp between two consecutive snapshots will get much higher.

### 1. Cloud Transient Event

The previous studies on the solar irradiance variability have a drawback in common: no matter which time interval they choose (1-sec, 20-sec, 1-min or 10-min), they only focus on the power fluctuation of “**single-time-interval**”. The result shows that the probability of big power change ( $>50\%$ ) in one time interval is as low as 0.01%. However, when a piece of cloud sweeps over a PV site, the power output drop may last for several time intervals (shown in the dashed blue square frame in Figure E.2). Even if the  $\Delta P$  in each step is below 20%, the total power drop can be as high as 60 ~ 70%. However, this sort of “**multiple-time-interval**” power fluctuation is not included in the previous studies. Therefore they underestimated the probability of big power fluctuation caused by moving cloud.

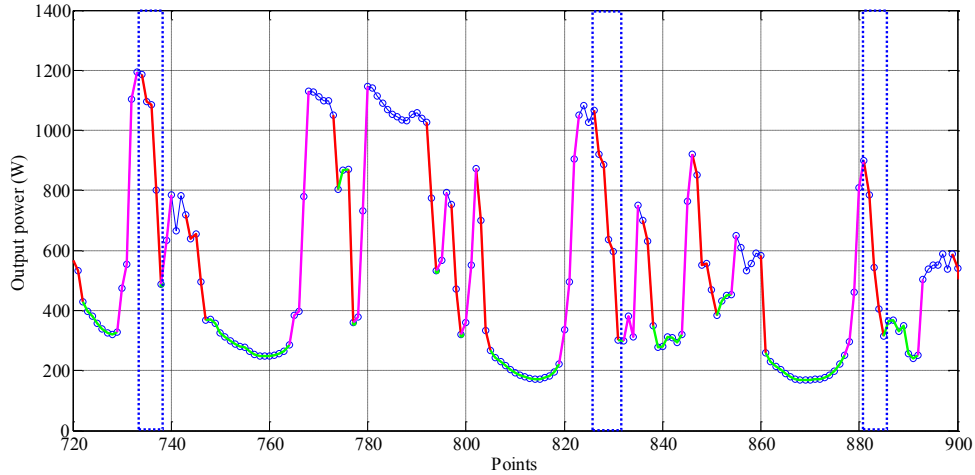


Figure E.2 Power output fluctuation induced by moving cloud

In this project, an event-based solar variability statistic model is proposed for characterizing the cloud transient issue. As shown in Figure E.3, each cloud movement event contains three processes:

- **Cloud approaching:**  $P$  has a big falling ramp (generally  $0.2 \sim 0.8P_{rated}$ ), this process lasts for several second to several minutes.
- **Cloud staying:**  $P$  keeps a low level. This process may last for more than 10 minutes.
- **Cloud leaving:**  $P$  has a big rising ramp ( $0.2 \sim 0.8P_{rated}$ ); this process lasts for several second to several minutes.

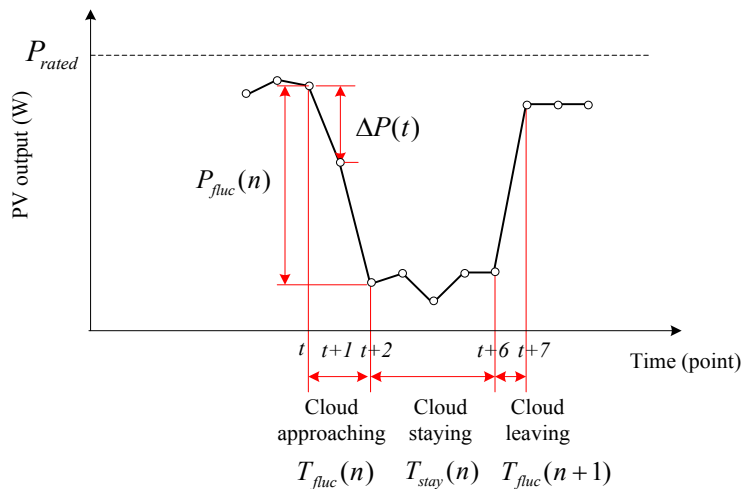


Figure E.3 Cloud transient event

In order to quantify a cloud transient event, we need to count the probability distribution of 3 random factors as shown in Figure E.3:

- Cloud approaching/leaving duration  $T_{fluc}$  (sec.)
- Cloud staying duration  $T_{stay}$  (sec.)
- Power output fluctuation magnitude  $P_{fluc}$  (W) that is caused by cloud approaching/leaving

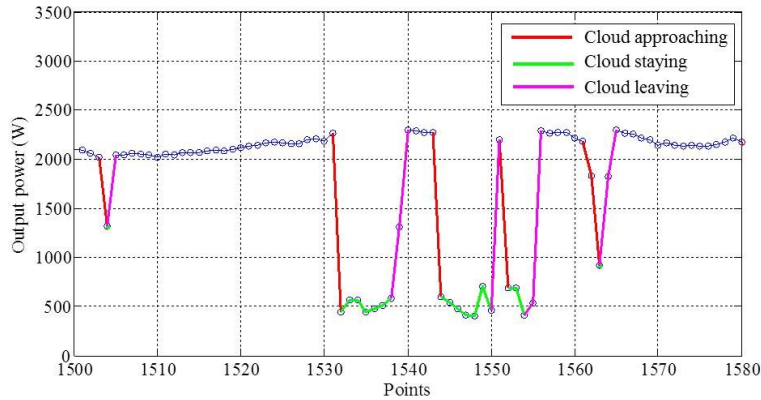
In the example shown in Figure E.3, the values of these three factors are:

$$T_{fluc} = \{2, 1\}$$

$$T_{stay} = 4$$

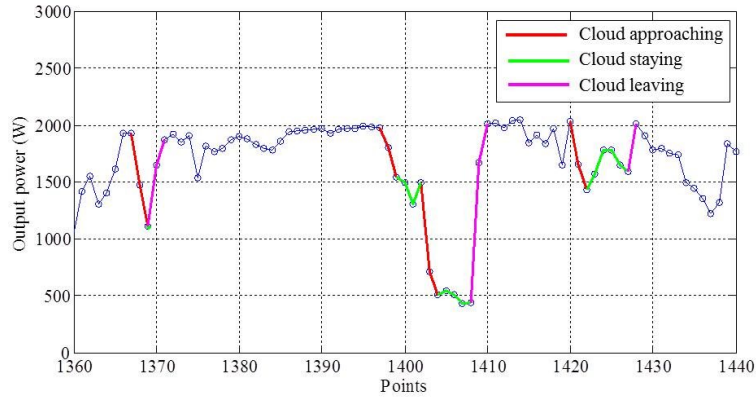
$$P_{fluc} = \{|P(t) - P(t+2)|, |P(t+6) - P(t+7)|\}$$

Some cloud transient events in the field data are labeled in Figure E.4 (a). Furthermore, as is shown in Figure E.4 (b), while a cloud is approaching, there might be a small steady segment in the curve. Therefore we should calculate the power output drop before and after this steady segment separately. When a cloud is leaving, the same situation occurs.



(a) Partial amplitude 1





(b) Partial amplitude 2

Figure E.4 Example of cloud transient event

According to the definition of cloud movement event, a program is developed that can automatically detect the cloud transient events from multiday PV power curve (The detecting method is introduced in Appendix F). There are two sources of data to be analyzed:

- The PV inverter output power data obtained by PDS Lab, University of Alberta. The data covers two periods: February 25<sup>th</sup> ~ March 12<sup>th</sup> and June 17<sup>th</sup> ~ July 2<sup>nd</sup>. 14 cloudy days are selected (five days in period 1 and nine days in period 2) from 31 days. One example day is shown in Figure E. 5.
- The solar irradiance data obtained by National Renewable Energy Laboratory (NREL), United State. The data covers one period: June 1<sup>st</sup> ~ June 30<sup>th</sup>. 19 cloudy days are selected.

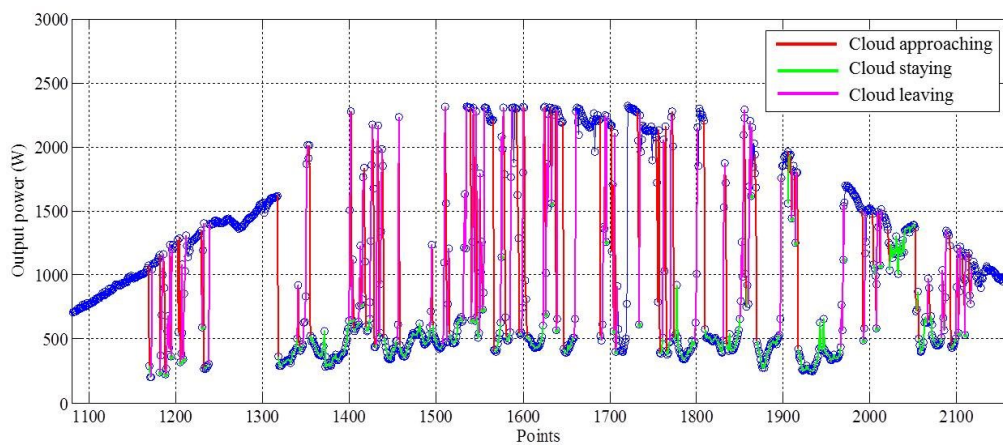


Figure E. 5 Cloud transient event

## 2. Statistics of Cloud Transient Indices

The probability distribution of cloud moving duration, cloud shading duration and relative power variability are presented as follows.

Figure E.6 shows that the cloud approaching/leaving duration is mainly 1~3 seconds. While in two places, the distribution bars are quite different due to different climate.

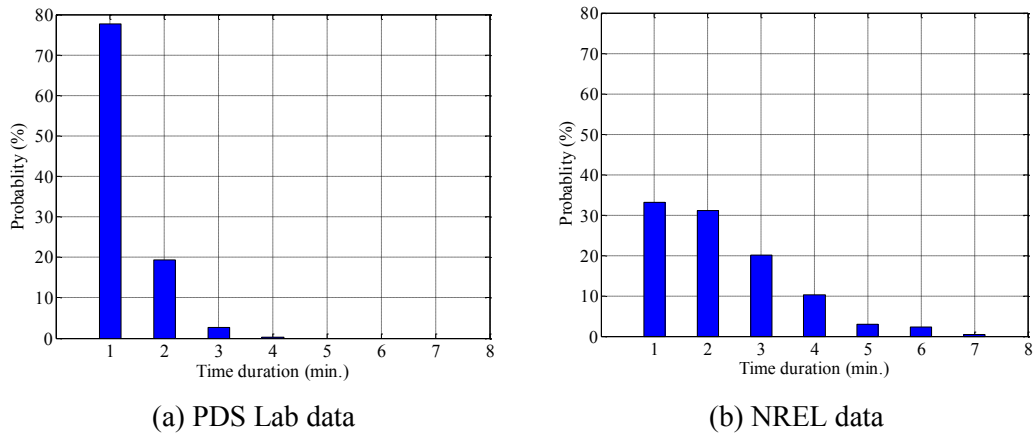
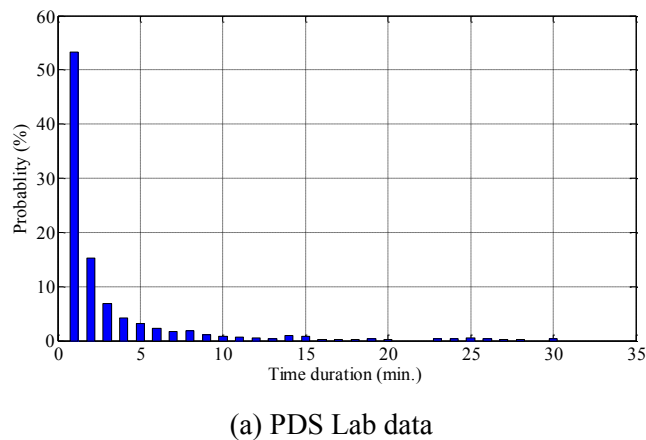
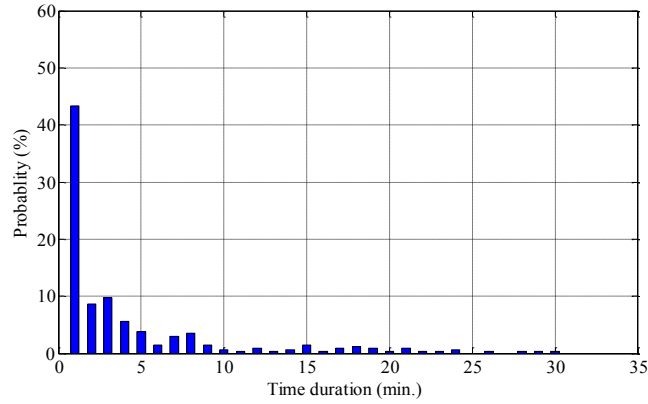


Figure E.6 Probability density of cloud approaching/leaving duration

Figure E. 7 shows that most of the cloud staying duration probability ranges 1~5 minutes. The probability distribution in two places have similar trend.



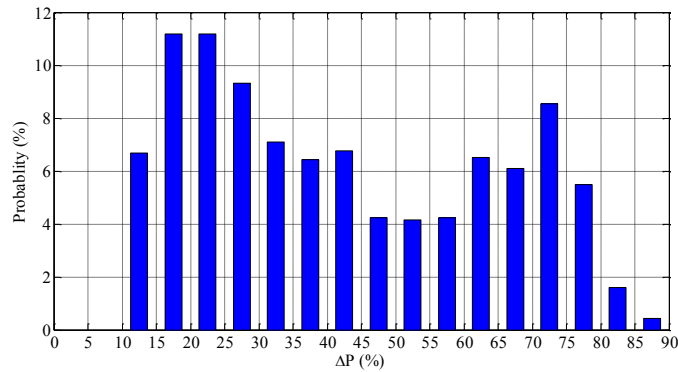
(a) PDS Lab data



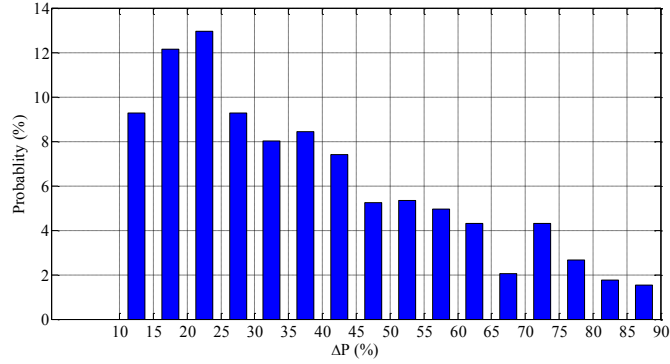
(b) NREL data

Figure E.7 Probability density of cloud staying duration

In Figure E.8, the small power fluctuation ( $\Delta P < 10\%P_{rated}$ ) is not considered as a cloud transient event. The main reason is that we are interested in large solar variability that has considerable impact on the power system. As the figure reveals, the probability decrease slowly with the increasing of PV output fluctuation magnitude. The high fluctuation magnitude ( $\Delta P > 50\%P_{rated}$ ) still has a probability of 20%. The impact of such solar variability on the distribution system voltage should be a concern.



(a) PDS Lab data



(b) NREL data

Figure E.8 Probability density of PV output fluctuation magnitude

## E.2 Characteristics of Solar Irradiance Variability – Spatial Distribution

Generally a distribution feeder can be more than 10 kilometers long and the PV panel can be installed anywhere along the feeder. When we evaluate the power quality impact of cloud transient on this system, one important issue is whether the solar irradiance can be considered identical for different locations. Obviously, during a totally clear day or overcast day, the solar irradiance is almost identical over an area of decades of kilometers. During a cloudy day, this is not necessarily the case due to the random size and shape of the moving cloud cluster. Next is a review of the existing researches on the spatial distribution of cloud transient.

### 1. Concept and Indices

**Dispersion factor  $D$**  is an important index for quantifying the relative distance between two locations [72]:

$$D = \frac{L}{CS \times \Delta t} \quad (\text{E.3})$$

where  $L$  is the distance between two locations (m),  $CS$  is the cloud speed (m/s) and  $\Delta t$  is the time interval of the irradiance data (s).  $D$  is a dimensionless quantity.

As is shown in Figure E.9, the physical meaning of  $D$  is how many time intervals it takes the cloud to move from above one PV site to above another site.

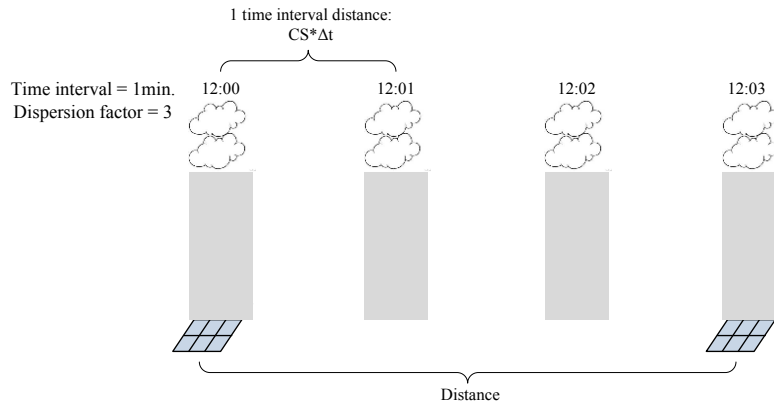


Figure E.9 The moving cloud passing a PV site

**Clear-sky index** is the ratio between transient solar irradiance and clear sky irradiance:

$$\Delta K_{t_{\Delta t}} = \frac{GHI(t)}{GHI_{clear}(t)} \quad (E.4)$$

where  $GHI$  is the global horizontal irradiance ( $W/m^2$ ).  $GHI_{clear}$  is the clear-sky global irradiance (see Figure E. 10).

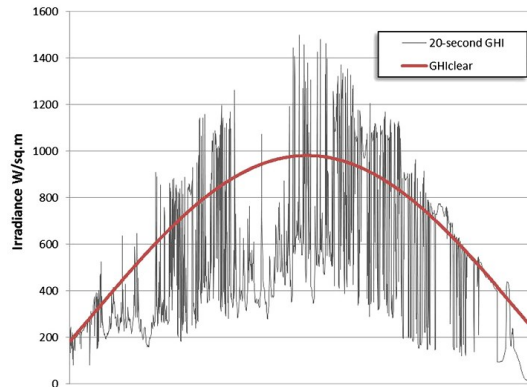


Figure E. 10 Global irradiance ( $GHI$ ) and clear-sky global irradiance

**Correlation coefficient** is the covariance between the clear-sky indices  $\Delta K_{t_{\Delta t}}$  of two sites over a period of time.

$$\rho^{1,2} = \frac{E[\Delta K t_{\Delta t}^1 \times \Delta K t_{\Delta t}^2]}{\sigma_1 \sigma_2} \quad (E.5)$$

where  $\Delta K t_{\Delta t}^1 = \{\Delta K t_{\Delta t}^1(t), \Delta K t_{\Delta t}^1(t + \Delta t), \Delta K t_{\Delta t}^1(t + 2\Delta t), \dots, t + N\Delta t)\}$  and  $\sigma_1$  is the standard deviation of the vector  $\Delta K t_{\Delta t}^1$ .

## 2. Field Measurement Result

Figure E.11 presents a correlation coefficient  $\rho$  in regard to the distance between two sites [73]-[74].

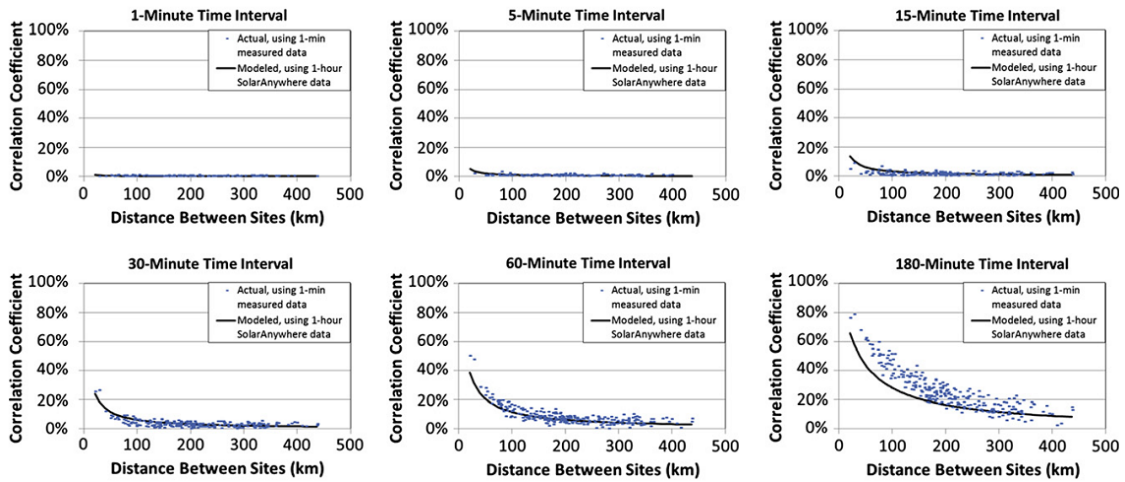


Figure E.11 Comparison of results to geographic diversity study

As the above results indicate, with a specified time interval  $\Delta t$ , the correlation efficient of clear-sky indices in two locations can be damped to zero if they locates far away enough. Reference [75] summarizes the minimal “required” distance to make the solar irradiance in two sites zero-correlated, as is shown in Figure E.12.

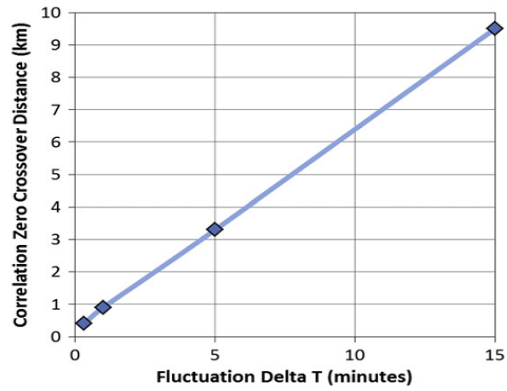


Figure E.12 Zero correlation crossover distance as a function of time scale

This analysis suggests that 20s fluctuations become uncorrelated positively at a distance of less than 500 m. The distances are respectively 1 km, 4 km and 10 km for fluctuation time scales of 1, 5 and 15 min respectively.

## Appendix F

### Method of Detecting the Cloud Transient Event

A cloud transient event consists of three processes: cloud approaching, cloud staying and cloud leaving, as shown in Figure F.1. The aim of detecting cloud transient event is to count the probabilistic distribution of three indices: cloud approaching/leaving duration  $T_{fluc}$ , cloud staying duration  $T_{stay}$  and power output fluctuation magnitude  $P_{fluc}$ . A program is developed to automatically detect these three data segments. The solar irradiance curve or PV output power curve is divided into four data segments, as shown in Figure F.1:

- *High level segment*: equal to the period with clear sky;
- *Falling segment*: the period when cloud is approaching;
- *Low level segment*: the period when cloud is passing and the PV site is fully covered by cloud;
- *Rising segment*: the period when cloud is leaving.

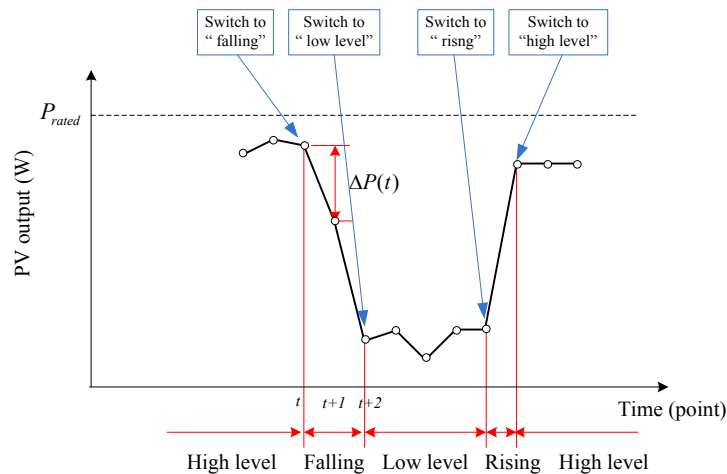


Figure F.1 The recorded data of a cloud transient event

The program is smart enough to detect the starting point and ending point of each segment. Specially, it is critical to define two empirical thresholds for deciding whether we should “switch” to another segment.



Threshold of switching to a falling/rising segment  $|\Delta P_1(t)| = 0.2$  ;

Threshold of continuing a falling/rising segment  $|\Delta P_2(t)| = 0.08$  .

In conclusion, the logical flowchart of detecting the cloud transient event is shown in Figure F.2.

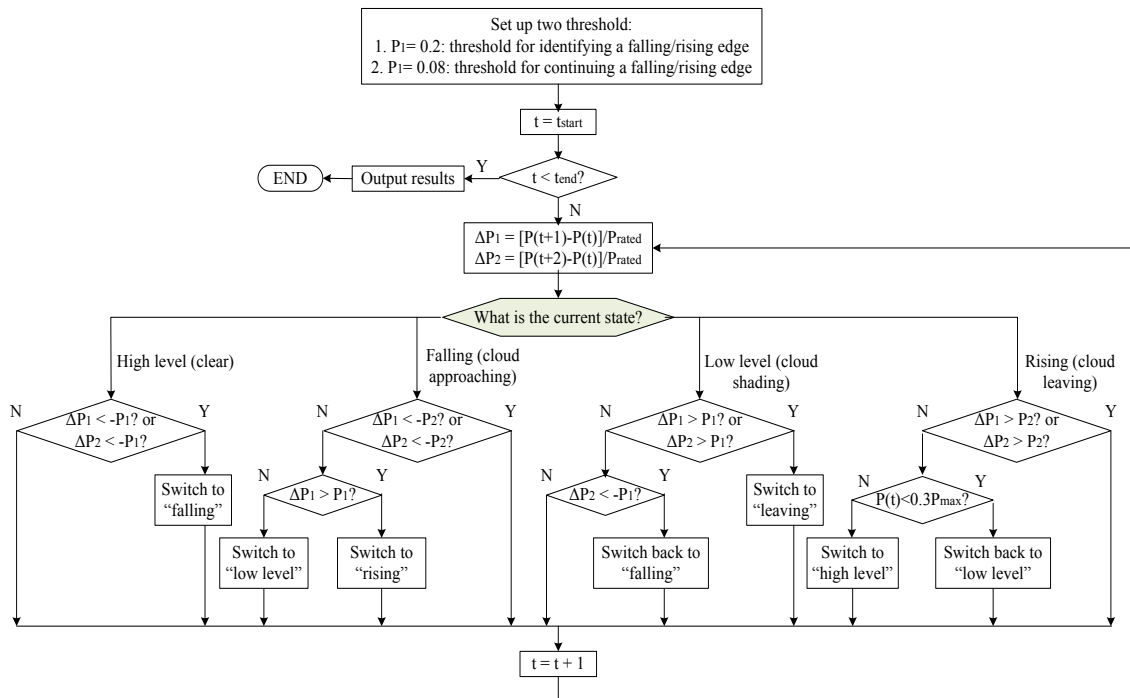


Figure F.2 Flowchart of the detecting method

After the detection, a result table is generated. An example is shown in Table F.1.

Table F.1 An example of detected data segment

| falling/rising segment |           | low level segment |           |
|------------------------|-----------|-------------------|-----------|
| Start point            | End point | Start point       | End point |
| 751                    | 753       | 753               | 758       |
| 758                    | 759       | 765               | 768       |
| ...                    | ...       | ...               | ...       |
| 1074                   | 1079      | 1079              | 1080      |

With the detected start/end point of each segment, the probability distribution of indices  $T_{fluc}$ ,  $T_{stay}$  and  $P_{fluc}$  can be calculated.